Analysis of Low Power,
Low Data Rate Ultra Wideband
Impulse Radio Systems

UNIVERSITÉ DE NEUCHÂTEL
INSTITUT DE MICROTECHNIQUE

Analysis of Low Power, Low Data Rate Ultra Wideband Impulse Radio Systems

THÈSE

PRÉSENTÉE À LA FACULTÉ DES SCIENCES
POUR L'OBTENTION DU GRADE DE DOCTEUR ÈS SCIENCES

PAR

Roman Merz

ACCEPTÉ SUR PROPOSITION DU JURY

Prof. Dr. P.-A. Farine, directeur de thèse
Dr. C. Botteron, rapporteur
Dr. A. Heubi, rapporteur

SOUTENUE LE 20 FÉVRIER 2009

Université de Neuchâtel unine

FACULTE DES SCIENCES
Secrétariat-Décanat de la faculté
- Rue Emile-Argand 11
- CP 158
- CH-2009 Neuchâtel

IMPRIMATUR POUR LA THESE

Analysis of Low Power, Low Data Rate Ultra Wideband Impulse Radio Systems

Roman MERZ

UNIVERSITE DE NEUCHATEL

FACULTE DES SCIENCES

La Faculté des sciences de l'Université de Neuchâtel,
sur le rapport des membres du jury

MM. P.-A. Farine (directeur de thèse), C. Botteron
et A. Heubi (On Semiconductor, Marin CH)

autorise l'impression de la présente thèse.

Neuchâtel, le 26 février 2009

Le doyen :
F. Kessler

UNIVERSITE DE NEUCHATEL
FACULTE DES SCIENCES
Secrétariat - décanat de la faculté
Rue Emile-Argand 11 - CP 158
CH-2009 Neuchâtel
Felix Kessler

■ Téléphone : +41 32 718 21 00 ■ E-mail : secretariat.sciences@unine.ch ■ www.unine.ch/sciences

Denn kein Sonnenaufgang, auch nicht der im Hochgebirge, ist pompös, triumphal, herrschaftlich, sondern jeder geschieht schwach und zaghaft wie die Hoffnung, es könne einmal noch gut werden, und gerade in solcher Unscheinbarkeit des mächtigsten Lichtes liegt das rührend Überwältigende.

Theodor W. Adorno

Keywords—Ultra Wideband, Impulse Radio, Communications, Low Power, Low Data Rate, Performance Analysis.

Abstract

During the last decade, ultra wideband (UWB) systems gained a large interest in the scientific world because of their suitability to realize among others communication systems with tremendous data rates and accurate indoor positioning and location systems. As a differing technology compared to classical narrowband radio transmission systems, UWB requires some novel approaches. Well established methods to develop and analyze narrowband transmission systems remain essentially valid but are not always well tailored or optimal to UWB systems. The need for novel approaches illuminates the reasons why there are still some uncovered topics in the literature, mainly related to the analyses of imperfections and perturbations during an UWB transmission. Consequently, this thesis attempts to cover some of these topics by theoretical studies, numerical simulations, as well as experimental verification.

Contents

List of Acronyms **11**

Nomenclature **13**

1 Introduction **21**
1.1 Motivation for UWB 22
1.2 Ultra Wideband Signals 23
1.3 Historical Interlude 23
1.4 Frequency Allocation 25
1.5 Thesis Outline 27
1.6 Contributions 28
1.7 Summary 29
Bibliography 30

2 An Impulse Radio Primer **33**
2.1 Time Domain Representation 33
2.2 Frequency Domain Representation 41
2.3 Propagation Channels 48
2.4 Noise and Interference 58
2.5 Summary 62
Bibliography 62

3 Architecture Selection **67**
3.1 Communication System 67
3.2 Transmitter Architecture and Implementation 68
3.3 Receiver Architecture and Implementation 75
3.4 RSD Receiver 88

3.5 Summary 95
Bibliography 95

4 Design Considerations **101**
4.1 Analog to Digital Converter 101
4.2 Burst Mode 109
4.3 Link Budget 110
4.4 Summary 112
Bibliography 112

5 Performance Analysis **115**
5.1 Introduction 115
5.2 Bit Error Rate 118
5.3 Duration Limited Acquisition 123
5.4 Pulse Combining 125
5.5 Unmatched Pulse Template 139
5.6 Narrowband Interference 143
5.7 Multiuser Interference 148
5.8 Summary 153
Bibliography 155

6 Synchronization **161**
6.1 Nomenclature 161
6.2 Intentional Frequency Difference 162
6.3 Bin Hopping Algorithm 167
6.4 Synchronization Probability 173
6.5 Summary 187
Bibliography 188

7 Conclusion and Outlook **191**
7.1 Conclusion 191
7.2 Possible Extensions 193
7.3 Future Development for UWB 194

Acknowledgments **195**

Curriculum Vitae **197**

A Modulations **201**
Bibliography 204

List of Acronyms

ADC	analog to digital converter
AH	amplitude modulation (code)
AM	amplitude modulation (data)
AWGN	additive white Gaussian noise
BER	bit error rate
CDMA	code division multiple access
CMOS	complementary metal-oxide-semiconductor
ECC	electronic communications committee (http://www.ero.dk/ecc)
FCC	federal communications commission (http://www.fcc.gov)
FWHM	full width half maximum
IEEE	Institute of Electrical and Electronics Engineers (http://www.ieee.org)
IR	impulse radio
MUI	multiuser interference
OFDM	orthogonal frequency division multiplex
PSD	power spectrum density
RSD	redundant signed digit
SIR	signal to interference ratio
SNR	signal to noise ratio
TH	delay modulation (code)
TM	delay modulation (data)
TOA	time of arrival
UWB	ultra wideband

Nomenclature

Operators and Functions

$*$	convolution operator
$\ominus_N$	subtraction modulo N
$\oplus_N$	addition modulo N
d	differential operator
∂	partial differential operator
$\mathsf{E}[\cdot]$	expectation operator
$\lfloor \cdot \rfloor$	floor operator
$\langle \cdot \rangle$	average operator
$\mathrm{Q}(\alpha)$	Q-function
$\delta(t)$	Dirac distribution
U	uniform distribution

Constant Values

k	Boltzmann constant	$\approx 1.38 \cdot 10^{-23}\mathrm{J/K}$
π	Ludolph's number	≈ 3.14159
e	Euler's number	≈ 2.71828
ς	pulse shape coefficient	$\varsigma = 1/\sqrt{\pi}\,\mathrm{Nm}$
i	imaginary unit	

Time Domain Description

A	multiplicative factor of an amplitude

c_j	jth symbol of the spreading code
d_k	kth symbol of the data sequence
$\hat{d}_k$	kth symbol reconstructed at the receiver
$i(t)$	narrowband interference
M	number of possible values for the code $c_j \in \{0, \ldots, M-1\}$
N_b	number of bits per symbol
N_c	number of chips per frame
N_f	number of frames per symbol
$\hat{N}_\mathrm{f}$	number of received TOAs
N_s	number of symbols per burst
N_u	number of users
$p(t)$	pulse shape
$p_{\mathrm{G}m}(t)$	mth derivative Gaussian pulse
$p_{\mathrm{H}m}(t)$	mth order Hermitian pulse
$\breve{p}(t)$	passband pulse
$q(t)$	received pulse
$\hat{q}_n(t)$	receiver's replica of the received pulse; pulse template
$r(t)$	received signal
$\boldsymbol{r}$	sampled received signal
$\hat{r}_n(t)$	receiver's replica of the received signal; signal template
$r_d(t)$	signal $r(t)$ defined at discrete times
$s(t)$	generated signal
$\boldsymbol{s}$	sampled generated signal
t	time
t_burst	burst duration
t_c	chip duration
$\hat{t}_\mathrm{c}$	receiver's estimation or assumption of the chip duration
t_e	sampling interval
t_f	frame duration
$\hat{t}_\mathrm{f}$	receiver's estimation or assumption of the frame duration
t_s	symbol duration
$\hat{t}_\mathrm{s}$	receiver's estimation or assumption of the symbol duration
$\tilde{t}_\mathrm{s}$	receiver's initial assumption of the symbol duration after startup

t_b	bit duration
t_n	duration of the Gaussian pulse
t_v	duration of the windowing function $v(t)$
t_w	duration of the acquisition window
τ_j	delay of the jth pulse
$\hat{\tau}_j$	receiver's estimation or assumption of the delay τ_j
$v(t)$	duration limiting window function
$\chi(t)$	expected signal

Frequency Domain Description

B_c	coherence bandwidth
B_e	equivalent bandwidth
B_f	fractional bandwidth
B_r	relative bandwidth
$B_{-10\,\mathrm{dB}}$	$-10\,\mathrm{dB}$ bandwidth
f	frequency

f_C	center frequency, geometric mean
f_H	upper frequency bound
f_L	lower frequency bound
f_c	center frequency, arithmetic mean
f_d	maximal Doppler shift
f_m	frequency for which the spectrum is maximal
f_b	average channel data rate or signaling rate
$P(\omega)$	Fourier transform of the pulse shape $p(t)$
$P_{\mathrm{G}m}$	Fourier transform of the mth derivative Gaussian pulse
$\mathrm{PSD}(\omega)$	power spectrum density
$\mathrm{PSD}_\mathrm{max}$	maximum value of the PSD
$Q(\omega)$	Fourier transform the received pulse $q(t)$
$R(\omega)$	Fourier transform of the signal $r(t)$
$R_d(\omega)$	Fourier transform of the signal $r_d(t)$
$S(\omega)$	Fourier transform of the signal $s(t)$
ω	angular frequency

ω_c	angular frequency of a carrier
ω_e	angular sampling frequency
ω_i	angular frequency of a narrowband interference
$V(\omega)$	Fourier transform of the windowing function $v(t)$

Power and Energy

$\mathcal{E}_\mathrm{b}$	energy per bit
$\mathcal{E}_\mathrm{p}$	energy per pulse
$\mathcal{E}_n$	energy of the nth symbol
$\mathcal{N}_0$	noise power density
P_η	noise power
P_i	narrowband interference power
P_r	received power
P_s	signal power
P_t	transmitted power
$P_{\Delta\omega}$	power measured at the output of an ideal filter with bandwidth $\Delta\omega$
S_r	received power per unit area

Propagation and Reception

a_m	amplitude of the mth multipath
A_r	effective area of the receiving antenna
A_t	effective area of the transmitting antenna
B_T	channel bandwidth
$\beta_{m,n}$	amplitudes in a Saleh-Valenzuela model
c	speed of light
d	transmission distance
d_0	reference distance
D	largest extension of an antenna
G_r	gain of the receiving antenna
G_t	gain of the transmitting antenna
γ	path loss exponent

γ	power decay for the paths in the Saleh-Valenzuela model
Γ	power decay for the clusters in the Saleh-Valenzuela model
$h(t)$	channel impulse response
$H(\omega)$	Frequency response of a propagation channel (Fourier transform of the channel impulse response $h(t)$)
λ	Decay in the probability density function for the path time of arrival in the Saleh-Valenzuela model
λ	wavelength
Λ	Decay in the probability density function for the cluster time of arrival in the Saleh-Valenzuela model
σ_τ	root mean square delay spread
T_c	coherence time
τ_m	delay of the mth multipath
τ_n	cluster delays in a Saleh-Valenzuela model
$\tau_{m,n}$	delay of the mth path in the nth cluster in a Saleh-Valenzuela model
v	speed of a mobile transmission device

Acquisition and Processing

α	time error between two clocks accumulated during a frame duration.
$\boldsymbol{b}_k$	intermediate result to minimize in the threshold receiver.
b_i	output signal from the analog to digital converter
$c_{q\hat{q}_n}$	cross-correlation value between q and $\hat{q}_n$. The nth element of the observation vector
$c_{rs}(\tau)$	cross-correlation function between $r(t)$ and $s(t)$
$c_{ss}(\tau)$	autocorrelation function of $s(t)$
$\boldsymbol{C}$	sampled cyclic correlation
$\tilde{\boldsymbol{d}}_k$	noiseless observation vector for the kth symbol
$\boldsymbol{d}_k$	observation vector for the kth symbol
δ_k	delay between transmitter and the receiver at the transmission instant of the kth symbol
ϵ	difference between sampling interval and integer multiple of the pulse repetition interval.

ϵ_j	timing error for the jth frame
G	processing gain
G_{DC}	processing gain due to duty cycle
G_{PC}	processing gain due to pulse combining
$\eta(t)$	noise
$\eta_{\mathrm{sum}}(t)$	summed noise
L	loss of the received energy
N	length of the received signal vector $\boldsymbol{r}$
N	total number of branches in a receiver
N_{r}	number of bits (ADC)
$q_{\mathrm{sum}}(t)$	summed received pulses
$\boldsymbol{q}_{\mathrm{sum}}$	digital summed signal
R	system impedance
T	temperature in Kelvin
$\{T_{j,k}\}$	sequence of transmission times
$\{\hat{T}_j\}$	sequence of arrival times
τ_n	delay in the nth branch of an autocorrelation receiver
u	index identifying the users
v_{in}	input voltage
v_{th}	threshold voltage
v_a	incremental voltage
v_x	voltage stored on a capacitor
ϕ_j	phase for a narrowband interference
$w_{j,k}(t)$	acquisition window
$\boldsymbol{w}_{j,k}$	sampled acquisition window for the jth frame
$w_k(t)$	summed acquisition window
$\boldsymbol{w}_k$	sampled summed acquisition window

Synchronization

$\mathcal{D}$	distinction coefficient
$\varepsilon(n)$	search order
$G_{\varepsilon(n)}(z)$	probability that the synchronization continues after bin n
$H_{\varepsilon(n)}(z)$	probability that the synchronization terminates at bin n

K	consecutive bins leading to a correct synchronization
L	number of tests during the synchronization
N	number of bins (acquisition)
N_{freq}	number of bins due to frequency synchronization
N_{time}	number of bins due to delay synchronization
$p(L)$	probability that the search ends after L bins
P_{sync}	generating function for the expected synchronization time
$\pi_{\varepsilon(n)}$	probability that the synchronization starts with bin n
t_{add}	offset for which pulse combining possible
t_{off}	maximum difference between the symbol durations at the transmitter and the receiver after startup
t_{scan}	scan time
t_{sync}	synchronization time
$\mathcal{W}$	maximum absolute amplitude
$\mathfrak{W}$	maximal number of superposed pulses

Indices and counters with multiple applications

i	index, counting the arrival times
j	index, counting the frames during a symbol period
j	index, counting the transmission times
k	index, counting the symbols
m	index, enumerating the derivative of the Gaussian pulse
m	order of the Hermite pulses
m	index, counting the multipaths
n	index, enumerating the receiver branch
n	index, counting the clusters of a Saleh-Valenzuela model
n	index, counting the elements of a sampled signal
n	undersampling factor

Chapter 1

Introduction

Over the last decade UWB gained a lot of interest from both academical and industrial research and development entities. At the Institute of Microtechnology of the University of Neuchâtel, the promising characteristics of UWB systems for communications and location systems were first analyzed within a project in collaboration with the centre Suisse d'électronique et de microtechnique (http://www.csem.ch), focusing on accurate indoor location systems. Since then, many other related activities helped our laboratory to immerse deeply in the topic of UWB systems. A preliminary study led to a first project financed by the Swiss national science foundation (http://www.snsf.ch), which was later extended. These SNSF projects covered for example an investigation of impulse radio (IR) UWB receiver architectures, a study of appropriate detection and estimation algorithms, a performance analysis of UWB communication systems, and the realization of low-power integrated circuits for UWB transceivers. Later, a mandate from PX Group (http://www.pxgroup.com) supported the development of an indoor location system. In parallel, a project supported by the Swiss commission for technology and innovation (http://www.bbt.admin.ch/kti/) aiming at the commercialization of a low power communication system for medical applications also started.

All these activities were complementary. They included feasibility studies, mathematical modeling of the systems, numerical simulations, prototype realizations, circuit implementations, and laboratory experiments. This thesis collects some results and outcomes of the performance analyses made for

baseband[1] UWB signaling within the different projects.

1.1 Motivation for UWB

UWB is a prospective technology for several technical reasons. The following list of UWB characteristics is supplemented with potential applications that may benefit from UWB signaling. It is noted that the following characteristics may be mutually exclusive and may not all be exploited simultaneously by a single device.

1. Due to the large bandwidth, the absorption or loss of the transmitted signal at some frequency bands, typically narrow compared to the bandwidth of the signal, due to obstructions will not result in an interruption of the communication link. Therefore UWB communication systems can be designed to be reliable in indoor propagation channels.
2. The channel capacity increases linearly with the bandwidth. For this reason high data rate communication systems can be conceived and UWB is a promising approach for applications such as wireless universal serial bus or a wireless transmission of high definition television signals.
3. Due to the large bandwidth, UWB offers a high time resolution. Therefore, an UWB system may isolate the individual multipath signals from the received signal. This ability makes UWB an interesting technology for indoor positioning and location systems.
4. The small scale fading due to multipath propagation is severely reduced compared to narrowband signals. Due to the short duration, the superposition of the signals from the different propagation paths does not result in constructive or destructive interference and hence does not alter the average received energy significantly.
5. For data rates smaller than the signal bandwidth a large processing gain can be obtained. Therefore UWB systems can be designed to be robust against intentional and non-intentional interferences including multiuser access, narrowband and wideband systems, and jammers.
6. UWB has a large potential for building low power communication systems for moderate data rates due to the duty cycle in IR.
7. Being noise-like, an UWB communication is difficult to be detected and intercepted.

[1] The signaling is considered to be baseband if the lower bound of the spectrum is much smaller than the bandwidth of the signal.

1.2 Ultra Wideband Signals

UWB signals are often defined in accordance with the UWB first report and order [FCC02] of the federal communications commission (FCC) of the United States of America. This report and order requires an UWB signal to have a $-10\,\mathrm{dB}$ fractional bandwidth of one fifth of the central frequency or $500\,\mathrm{MHz}$ (see sections 1.4 and 2.2). The FCC does not stipulate any method for generating the UWB signal as long as the emission mask, the minimal bandwidth, and some other characteristics are respected. In this thesis only IR—characterized by the transmission of very short duration pulses—will be considered. However, the term UWB is used throughout the text, even if its validity is restricted to IR.

UWB is one of the oldest methods for radio communication systems (see section 1.3), but it had so many important shortcomings that it disappeared with the invention of narrowband carrier-based communications. However, thanks to the recent progress in fast signal processing and integrated circuit design, novel concepts can be applied to overcome them.

Today, UWB can be applied for communication systems, for radio detection and ranging applications, and for indoor localization devices. Several methods other than IR have been proposed in the literature for UWB systems. An extension to one of the most classical wireless communications, the frequency modulation is proposed in [Ger03]. The modulation index is selected to be extremely large compared to the bandwidth of the signal to be transmitted. For radio detection and ranging, a chirped carrier has also been proposed. Furthermore, code division multiple access (CDMA) schemes with an extremely fast spreading code also result in an UWB signal. Finally, another proposal is orthogonal frequency division multiplex (OFDM), where a large number of subcarriers are used to transmit the data in parallel and to cover a wide bandwidth. OFDM is in particular promising for high data rate communications.

1.3 Historical Interlude

UWB gained tremendous attention from academic research and civilian industrial developments since about one decade. Nevertheless UWB can be considered as the origin of all wireless radio communications. Marconi's first radio communication system, more than a century ago, was based on the creation of short duration pulses using a spark gap transmitter [Sim96], and

hence the signals occupied a large bandwidth compared to the data rate[2]. The first receivers for the spark gap transmitters were based on coherers. This detector consists of a capsule of metal filings between two electrodes. Initially, the metal filling does not form a connection between the electrodes, such that a large resistance is measured across them. Upon the reception of a radio frequency signal, the metal filling may cohere and the resistance drops to low values. To reset the device, normally a mechanical disturbance, e.g., tapping against the coherer, is used. The spark gap communication systems suffered from several shortcomings. The data rate was very restricted, it was not suited for an application like radio broadcast because a continuous reception of analogous signals was not possible and there was no reliable scheme for multiuser access except time interleaving due to the strong emitted power and wide bandwidth. Due to these reasons the spark gap transmission systems were replaced by narrowband radio communication systems. The UWB approach then disappeared for some decades, until it was re-considered in the 1960s, first for military applications. The theoretical background to treat UWB systems started with the description of a linear time-invariant system by its impulse response and the attempt to verify the analytical solution of the transient behavior of microwave networks [Ben78]. The measurement of short duration, repetitive signals became possible in the 1960s by the introduction of sub-nanosecond resolution sampling oscilloscopes by Hewlett-Packard and Tektronix. The basic designs and components for UWB systems were available by the early 1970s [Bar00]. Since then, UWB systems have been continuously developed.

For civilian applications, UWB only gained much attention during the last decade. One driving force was the demand for always higher data transfer rates, e.g., using CDMA or OFDM techniques. Other prospective applications are low data rate systems with low power consumption and localization systems. The latter two applications can be covered by IR. The problems related to the spark gap communication systems can be solved today thanks to the recent progress in fast signal processing and integrated circuit design. Meanwhile, data rates sufficient for the transmission of audio or video signals can be obtained. Multiuser access becomes possible by using individual spreading codes for each user and advanced demodulation algorithms. Attesting the recent civilian interest and progress in UWB systems, figure 1.1 presents the number of publications from the Institute of Electrical and Elec-

[2]The German word *Funken* still bears testimony to that epoch. When used as a noun, it means *spark*, as a verb it stands for *to radio*.

tronics Engineers (IEEE) and patents considering UWB since 1990. There is approximately an exponential increase in both publications and patents between 2000 and 2006. Note that the early contributions to UWB are underestimated in figure 1.1, because they were often published using a different nomenclature than UWB such as baseband or carrier-free communications.

1.4 Frequency Allocation

The emission of electromagnetic waves at radio frequencies is subject to limitations in most countries. A national frequency allocation plan lists the permitted frequency bands for a given application. Due to the introduction of novel applications or novel signaling schemes, the frequency allocation plans need to be updated continuously. However, one of the primary goals of the regulatory authorities is to ensure by the frequency allocation plans that the performance of existing systems is not degraded by the introduction of new systems. By definition, UWB signals cover intentionally a large bandwidth and the protection of existing systems using a division in frequency bands does not apply well. For this reason the adoption of UWB signaling in the frequency allocation plans requires careful examinations. Meanwhile, many countries have performed or are performing studies considering the interference of UWB signals to narrowband systems. The recommendations and the adoptions for UWB communication systems in the frequency allocation plans differ between the countries. There are large efforts to harmonize the national standards, such that UWB devices may be used worldwide. As an international standard is not (yet) available, in the following the frequency allocation plans for Europe, for the United States of America, and for some Asian countries are considered. Considering the currently available regulations, the most promising frequency band for a product that may be used worldwide is between 6.0 GHz and 8.5 GHz.

1.4.1 Regulations in Europe

The limitations of the average transmission power density as a function of the frequency is called an emission mask. The mask that will most probably be applied to devices in Europe is illustrated in figure 1.2 and is labeled as electronic communications committee (ECC) mask. Investigations performed by the conférence Européenne des postes et télécommunications have identified the frequency between 6 GHz and 8.6 GHz to be preferred for UWB applications. The maximum power spectrum density (PSD) in

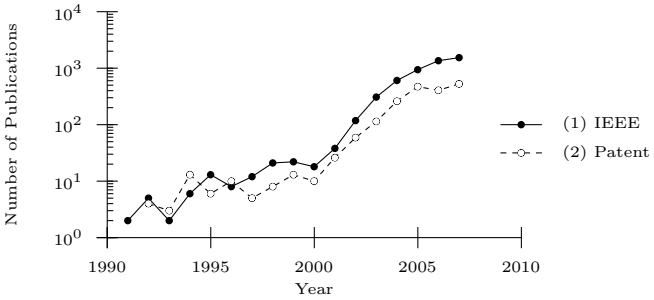

Figure 1.1: Number of publications in (1) IEEE Periodicals and IEEE Conference Proceedings with UWB or ultra wideband in the index terms (2) patents (worldwide) with UWB or ultra wideband in the title or the abstract. Search performed 9 Jan. 2009 using IEEExplore and Espacenet.

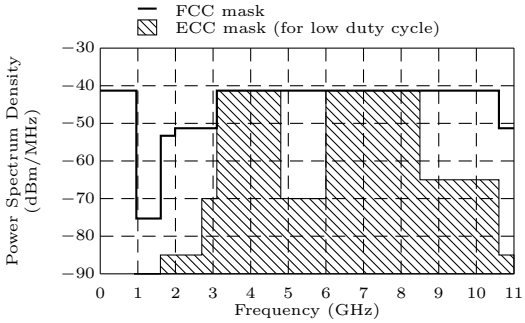

Figure 1.2: The spectrum mask for indoor devices in Europe (ECC) and the United States of America (FCC).

this band is −41.3 dBm/MHz. This has been adopted in March 2006 with decision ECC/DEC/(06)04 [ECC06b]. Further studies were performed concerning the power levels in the bands 2.7 GHz to 4.8 GHz and 8.5 GHz to 9.0 GHz. In December 2006, the band 4.2 GHz to 4.8 GHz was allowed to be used for first generation UWB devices until the end of year 2010. In the ECC/DEC/(06)12 [ECC06a], the use of the band 3.1 GHz to 4.8 GHz was allowed to be used with a low duty cycle mitigation technique[3]. Using detect and avoid mitigation techniques, the bands 3.1 GHz to 4.8 GHz and 8.5 GHz

[3]In the first release it was within the band 3.4 GHz to 4.8 GHz and has been extended in later releases.

to 9.0 GHz are also allowed.

1.4.2 Regulations in the United States of America

For the United States of America, the emission mask is represented in figure 1.2 and labeled as FCC mask. The FCC limits the PSD for indoor UWB communications to −41.3 dBm/MHz between 3.1 GHz and 10.6 GHz. Between 0.96 GHz and 1.61 GHz the allowed PSD is only −75.3 dBm/MHz to avoid any interference to signals for global positioning systems.

1.4.3 Regulations in Asia

Besides the already mentioned regions, emission masks are also available for some Asian countries, i.e., for Japan, Korea, and China. In general, the two frequency bands are allocated: a lower one requiring detect and avoid mitigation techniques and an upper one without such limitations. The lower frequency band covers 4.2 GHz to 4.8 GHz in China, 3.4 GHz to 4.8 GHz in Japan, and 3.1 GHz to 4.8 GHz in Korea. The upper frequency band covers 6.0 GHz to 8.5 GHz in China and 7.25 GHz to 10.25 GHz in Japan and Korea. In all cases, a maximum mean power spectrum density of −41.3 dBm/MHz and a maximum peak power spectrum density of 0 dBm/MHz has to be respected.

There may be restrictions in addition to the maximum power spectrum density. For example in Japan a radio equipment not connected to the AC mains power is only permitted to emit radio waves after having received a signal from another radio equipment connected to the AC mains power. This should ensure that the UWB devices are used indoors only. But it may have implications even for indoor applications, such as a sensor network using distributed, non-coordinated UWB transmitters.

1.5 Thesis Outline

This thesis is structured as follows. A theoretical background of the UWB communication is given in chapter 2. The discussion starts with the time domain representation of the signals and the Fourier transform is used to calculate the frequency domain representation. After a short presentation of the propagation channel models, the models for additive noise and interferences are shown. Chapter 3 considers the architectures and circuits to build an UWB communication system. Some pulse generators are presented

that may be used for a transmitter. The discussion of the receivers start with a matched filter implementation. Using a series of small modifications a simplified architecture with near optimal bit error rate (BER) performance in an additive white Gaussian noise (AWGN) channel is derived. In chapter 4 some aspects to be considered during the implementation of the UWB communication system are illustrated. These aspects include an evaluation of the required performance of the analog to digital converter (ADC), of the burst mode for which the instantaneous data rate may exceed the average data rate, and a link budget. In chapter 5, the performance of a receiver architecture characterized by the coherent addition of limited duration acquisition windows and a correlation with a locally generated template is analyzed. It is assumed that the receiver is already synchronized with the transmitter of interest. The chapter starts with a presentation of potential performance benchmarks. The performance for the matched filter receiver in an AWGN and a multipath propagation channel are presented afterward. The performance is also evaluated in the presence of imperfections or perturbations such as interferences or a mismatch between the pulse template and the received pulse. The assumption that the receiver is synchronized with the transmitter of interest is removed in chapter 6. Possible synchronization procedures and the required synchronization times are considered. Finally, chapter 7 provides some concluding remarks.

1.6 Contributions

As already mentioned, UWB requires a careful examination of the methods known from narrowband communication systems to evaluate and benchmark the performance of UWB systems. Some novel methods have been proposed and published during the elaboration of this thesis. These methods have been used in a large number of performance analysis. Their outcomes help to obtain some insight into the complex interaction between the parameters of an UWB communication system and finally have led to a proposal for a novel receiver architecture. Selected contributions were presented at a conference or published in a journal. The following list of contributions is complemented with citations to the most relevant publications. A complete publication list can be found in the Curriculum Vitae starting at page 197.

- Chapter 2: Conversion table between important time domain characteristics of the Gaussian pulses.

- Chapter 2: Conversion table between the duration and important frequency domain characteristics of the Gaussian pulses.
- Chapter 3: Proposal of the timestamp correlation algorithm for the implementation of a low-complexity incoherent receiver based on time of arrival measurements.
- Chapter 3: Derivation and proposal of a receiver architecture with coherent addition of the pulses and successive digital signal processing, e.g., correlation with a template.
- Chapter 3: Proposal of a low-power implementation of such a receiver using a set of time interleaved, modified redundant signed digit analog to digital converters [Saa08b].
- Chapter 5: Derivation of an average performance loss in a multipath channel compared with the AWGN channel.
- Chapter 5: Time domain analysis of a performance loss in the presence of timing errors, such as a frequency difference and a jitter [Mer04b, Mer07].
- Chapter 5: Analysis of the impact of non-matched templates for the reception of UWB pulses [Mer04a].
- Chapter 5: Analysis of the impact of a narrowband interference to a UWB communication system leading to a bound for which an error-free transmission is possible.
- Chapter 5: Analysis of the impact of multiuser interference to a UWB communication system [Saa08a].
- Chapter 6: Proposal of a synchronization scheme based on a frequency difference between the transmitter's and the receiver's clock. Estimation of the required synchronization time for this scenario.
- Chapter 6: Derivation of a distinction coefficient that indicates the probability that the receiver synchronizes with the transmitter of interest in the presence of interference. Calculations of the distinction coefficients for amplitude and delay modulations [Mer05a, Mer05b].
- Appendix A: Introduction of an alternative, versatile notation of the modulated UWB signaling. Application of the versatile notation to the particular cases of amplitude and delay modulations.

1.7 Summary

UWB has gained a lot of interest for civil applications, in particular during the last decade. It can be used for high data rate communications, for indoor

positioning and location systems, or for low power communication devices. Impulse radio applies mainly for the latter two applications. The spectral masks for Europe, the United States of America, and some Asian countries are settled and the power spectrum density can be up to $-41.3\,\mathrm{dBm/MHz}$ in selected frequency bands.

Bibliography

[Bar00] T. W. Barrett. "History of UltraWideBand (UWB) Radar & Communications: Pioneers and Innovators". *Progress in Electromagnetics Research Symposium*. Cambridge, MA, USA, Jul. 2000.

[Ben78] C. L. Bennett and G. F. Ross. "Time-Domain Electromagnetics and Its Applications". *Proceedings of the IEEE*, 66(3):299–318, Mar. 1978.

[ECC06a] ECC Electronic Communications Committee. "ECC Decision of 1 December 2006 on the harmonised conditions for devices using Ultra-Wideband (UWB) technology with Low Duty Cycle (LDC) in the frequency band 3.4 - 4.8 GHz.", 2006.

[ECC06b] ECC Electronic Communications Committee. "ECC Decision of the 24 March 2006 on the harmonized conditions for devices using Ultra-Wideband (UWB) technology in bands below 10.6 GHz", 2006.

[FCC02] FCC Federal Communications Commission. "First Report and Order". Revision of Part 15 of the Commission's Rules Regarding Ultra-Wideband Transmission Systems, Apr. 2002.

[Ger03] J. F. Gerrits and J. R. Farserotu. "Ultra Wide Band FM: A Straightforward Frequency Domain Approach". *Proceedings of the European Microwave Week*. Munich, Germany, Oct. 2003.

[Mer04a] R. Merz, C. Botteron, and P.-A. Farine. "Characterization of Input Filters in UWB Receivers". *Atelier d'Arc et Senans du Laboratoire Européen Associé en Microtechnique*. Arc et Senans, France, Sep. 2004.

[Mer04b] R. Merz, C. Botteron, P.-A. Farine, and J. Farserotu. "Asymptotical Analysis of Timing Imperfections in UWB Receivers".

IEEE Conference on Circuits and Systems for Communications. Moscow, Russia, Jul. 2004.

[Mer05a] R. Merz, C. Botteron, and P.-A. Farine. "Multiuser Interference during Synchronization Phase in UWB Impulse Radio". *IEEE International Conference on Ultra-Wideband*, pp. 661–666. Zürich, Switzerland, Sep. 2005.

[Mer05b] R. Merz, C. Botteron, and P.-A. Farine. "Multiuser Interference in TH-UWB". Presentation at the Workshop on UWB for Sensor Networks. Lausanne, Switzerland, Nov. 2005.

[Mer07] R. Merz, C. Botteron, and P.-A. Farine. "Performance of an Impulse Radio Communication System in the Presence of Gaussian Jitter". *IEEE International Conference on Ultra-Wideband*. Singapore, Sep. 2007.

[Saa08a] P. Saad, C. Botteron, R. Merz, and P.-A. Farine. "Performance Comparison of UWB Impulse-Based Multiple Access Schemes in Indoor Multipath Channels". *5th Workshop on Positioning, Navigation and Communication*. Hannover, Germany, Mar. 2008.

[Saa08b] P. Saad, R. Merz, F. Chastellain, C. Robert, U. Yodprasit, C. Botteron, P.-A. Farine, R. Caillet, A. Heubi, and N. Senouci. "A Low-Power, Low Data-Rate, Ultra-Wideband Receiver Architecture for Indoor Wireless Systems". Hannover, Germany, Sep. 2008.

[Sim96] R. W. Simons. "Guglielmo Marconi and Early Systems of Wireless Communication". *GEC Review*, 11(1), 1996.

Chapter 2

An Impulse Radio Primer

In this chapter, a theoretical background to UWB communications and an introduction of the models and notations used throughout the rest of the thesis are given. The presentation starts with a time domain representation of the UWB signals. By applying a Fourier transform a frequency domain representation is found. After a short presentation of the propagation channel models, the models for additive noise and interferences are discussed.

2.1 Time Domain Representation

Signals can be represented in the time domain or in the frequency domain. The two representations are complementary as they illustrate and visualize different aspects. But they are also redundant because a single representation contains all information concerning the signal. While the frequency domain representation often allows an intuitive understanding of the phenomena in classical narrowband radio communication systems, both representations are helpful for UWB systems.

2.1.1 Pulse Shape

The pulse shape defines among others the bandwidth of the signal, the correlation property, the sensitivity against multiuser and narrowband interference, and the processing gain[1]. It is therefore a fundamental and important

[1] The processing gain is limited by the ratio between the occupied bandwidth of the signal and the data signaling rate (see section 5.4.1). The occupied bandwidth is mainly a function of the pulse shape (see section 2.2).

design aspect of an UWB system. However, only a relatively low number of pulse shapes have been proposed for UWB in the literature.

GAUSSIAN PULSE: The Gaussian pulse and its derivatives are often used in the theoretical analysis of UWB communications systems. It provides a close approximation to physically generated pulses for commonly used pulse generators. Some measured pulse shaped will be presented in section 3.2.3. The mth derivative Gaussian pulse with a variance t_n^2 is defined as

$$p_{\mathrm{G}_m}(t) = A\frac{\partial^m}{\partial t^m}\exp\left(-\frac{t^2}{2t_n^2}\right), \tag{2.1}$$

where A is selected such that the energy of the pulse is normalized. The zeroth derivative Gaussian pulse is denoted as Gaussian pulse. For normalization, we select the amplitude of the pulses such that the energy is

$$\int_{-\infty}^{\infty}\frac{p_{\mathrm{G}_m}^2(t)}{R}\,\mathrm{d}t = 1\,\mathrm{J}, \tag{2.2}$$

where R is the system impedance. This normalization results in volts as the unit of the signal amplitude. The first four derivative Gaussian pulses are

$$p_{\mathrm{G}_0}(t) = +\sqrt{\frac{\varsigma R}{t_n}} \qquad \exp\left(-\frac{t^2}{2t_n^2}\right) \tag{2.3a}$$

$$p_{\mathrm{G}_1}(t) = -\sqrt{\frac{2\varsigma R}{t_n^3}}\,t \qquad \exp\left(-\frac{t^2}{2t_n^2}\right) \tag{2.3b}$$

$$p_{\mathrm{G}_2}(t) = +\sqrt{\frac{4\varsigma R}{3t_n}}\left(\frac{t^2}{t_n^2}-1\right)\exp\left(-\frac{t^2}{2t_n^2}\right) \tag{2.3c}$$

$$p_{\mathrm{G}_3}(t) = -\sqrt{\frac{8\varsigma R}{15t_n^3}}\left(\frac{t^3}{t_n^2}-3t\right)\exp\left(-\frac{t^2}{2t_n^2}\right) \tag{2.3d}$$

with $\varsigma = 1/\sqrt{\pi}$ Nm. They are represented in figure 2.1 for a pulse duration $t_n = 200\,\mathrm{ps}$, a system with $50\,\Omega$ impedance, and a pulse energy of 1 pJ.

t_n is not the only possible characterization of the pulse duration. Other characteristics may be more closely related to physical properties of the pulse. E.g., the required duration to capture 90 % and 99 % of the pulse energy are denoted $t_{90\,\%}$ and $t_{99\,\%}$ respectively. Another duration characterization is

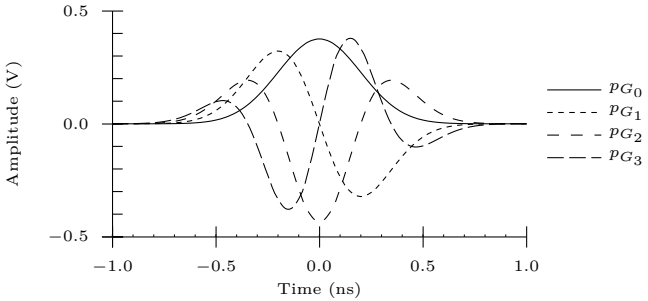

Figure 2.1: Gaussian pulse shapes for 1 pJ energy pulses in a 50 Ω system and $t_n = 200$ ps pulse width.

given by the duration at half the maximum pulse amplitude full width half maximum (FWHM), denoted as t_{FWHM}. While t_{FWHM} is well-defined for the Gaussian pulse, it is ambiguous for the mth derivate Gaussian pulse. In the following, the FWHM is calculated using the envelope of the pulse[2]. Finally, $t_{-10\,\mathrm{dB}}$ is defined as the time corresponding to the −10 dB bandwidth that will be defined in section 2.2. Table 2.1 provides the conversion factors between the above mentioned characteristics and t_n. It is noted, that for the mth derivative Gaussian pulses, the −10 dB bandwidth multiplied by the t_{FWHM} is approximately constant.

The Gaussian pulses are not limited in time. Therefore, all previous and future pulses interfere at the moment when the pulse of interest is received. This is called the inter-pulse interference. To estimate the impact of the

[2]The envelope is defined as the magnitude of the analytic signal; or $\sqrt{p^2(t) + \tilde{p}^2(t)}$, where $\tilde{p}(t)$ is the Hilbert transform of the signal $p(t)$.

Pulse shape	$t_{-10\,\mathrm{dB}}/t_n$	$B_{-10\,\mathrm{dB}}t_n$	$t_{99\,\%}/t_n$	$t_{90\,\%}/t_n$	t_{FWHM}/t_n	$t_{\mathrm{FWHM}} \times B_{-10\,\mathrm{dB}}$
$p_{\mathrm{G}_0}(t)$	4.14	0.242	3.64	2.33	4.19	1.012
$p_{\mathrm{G}_1}(t)$	3.12	0.321	4.76	3.54	3.67	1.177
$p_{\mathrm{G}_2}(t)$	3.02	0.331	5.37	4.01	3.52	1.164
$p_{\mathrm{G}_3}(t)$	2.99	0.334	5.73	2.71	3.46	1.157
$p_{\mathrm{G}_4}(t)$	2.98	0.336	5.71	3.31	3.43	1.153

Table 2.1: Conversion factors between t_n and other characteristics of the pulse duration for the Gaussian pulse shapes.

inter-pulse interference due to the unlimited time duration of the Gaussian pulses, a linear medium is supposed such that all the interfering pulses can be superposed. Furthermore, it is assumed that the received signal consists of an infinite sequence of non-modulated pulses transmitted with a pulse repetition period t_f, i.e., the signal

$$r(t) = \sum_{k=-\infty}^{\infty} p(t - kt_\mathrm{f}) \tag{2.4}$$

is received.

The inter-pulse interference as a function of the frame duration t_f and pulse duration t_n is represented in figure 2.2. It is calculated as follows. The mth derivative Gaussian pulses for even m (2.3a) and (2.3c) are defined such that the pulses are centered at $t = 0$. Without inter-pulse interference the amplitude of the received signal at time $t = 0$ is given by $k = 0$, i.e., $r(0) = p(0)$. The inter-pulse interference IPI is defined as the amplitude due to all the interfering pulses ($k \neq 0$) compared with the amplitude of the pulse for $k = 0$ at the instant $t = 0$,

$$\mathrm{IPI} = \left| \frac{r(0) - p(0)}{p(0)} \right|. \tag{2.5}$$

It is noted, that for $t_\mathrm{f} \gg t_n$ the impact of inter-pulse interference is negligible. Consequently, at typical values for a low data rate communication system such as $t_\mathrm{f} = 100\,\mathrm{ns}$ and $t_n = 0.2\,\mathrm{ns}$, the inter-pulse interference will not need to be considered for the AWGN propagation channel in any performance analysis. For odd derivative Gaussian pulses, the inter-pulse interference is zero for an non-modulated sequence because all the contributions from k negative are compensated by the contributions from k positive.

Hermitian pulse: The Gaussian pulses are not orthogonal. For applications like pulse shape modulation or multiuser access by associating a different pulse shape to each user, orthogonal pulses have been proposed. One example of orthogonal pulses is given by the modified Hermite polynomial functions [Mic01]. The Hermite pulses have the interesting property, that the pulse duration becomes nearly independent of the order [Gha02]. The mth order Hermite pulse is defined as

$$p_{\mathrm{H}_m}(t) = (-1)^m A \exp\left(\frac{t^2}{4t_n^2}\right) \frac{\partial^m}{\partial t^m} \exp\left(-\frac{t^2}{2t_n^2}\right) \tag{2.6}$$

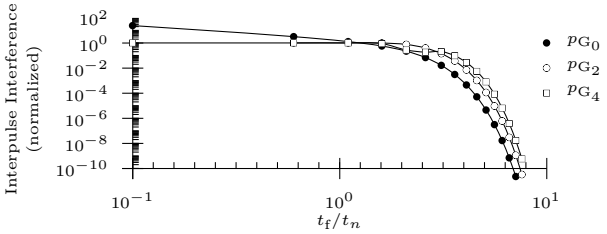

Figure 2.2: Interpulse interference for the mth derivative Gaussian pulse as a function of the frame duration t_f.

where A can be used to normalize the pulse energy. However, the orthogonality property is lost when the two pulses are not received with a zero time delay between them, i.e., when the transmitter of interest and the interferers are not all perfectly synchronized. Independently of the synchronization, the orthogonality is also lost in a multipath propagation channel.

Duration limited sinusoidal pulse: For both the Gaussian pulses (2.1) and the Hermite pulses (2.6), the duration t_n defines the center frequency and the bandwidth. Because of the resulting dependency between the two characteristics it may be difficult to respect the emission mask defined in section 1.4. To respect the emission mask with baseband pulses it may be required to reduce the transmitted power. However, this reduces also the range for a data transmission and the channel capacity. A more promising approach is to fit the spectrum of the pulse to the emission mask. The emitter power can be maximized when the spectrum of the pulse is equal to the emission mask. In [Luo03], the inverse Fourier transform of the emission mask is calculated and presented. However, the resulting pulse shape may be difficult to generate physically. The dependency between the center frequency and the bandwidth can be eliminated by an amplitude modulation of a sinusoidal carrier with a baseband pulse $p(t)$, resulting in

$$\breve{p}(t) = p(t)\cos(\omega_\mathrm{c} t). \tag{2.7}$$

The center frequency depends on the angular frequency ω_c. The bandwidth on the other hand depends on the pulse shape $p(t)$. The two parameters can hence be tuned individually. Commonly used baseband pulses are of rectangular, triangular, or Gaussian shapes. For a rectangular baseband

pulse with duration t_n, the pulse shape is

$$\breve{p}(t) \propto \begin{cases} \cos(\omega_c t) & \text{if } |t| \leq t_n/2 \\ 0 & \text{otherwise.} \end{cases} \tag{2.8}$$

For a triangular baseband pulse with duration t_n, the passband pulse becomes

$$\breve{p}(t) \propto \begin{cases} (t_n/2 - |t|) \cdot \cos(\omega_c t) & \text{if } |t| \leq t_n/2 \\ 0 & \text{otherwise.} \end{cases} \tag{2.9}$$

Finally, for a Gaussian baseband pulse with standard deviation t_n, the passband pulse is

$$\breve{p}(t) \propto \exp\left(-\frac{t^2}{2t_n^2}\right) \cos(\omega_c t). \tag{2.10}$$

The Gaussian pulse has the advantage that the spectrum does not have any side-lobes. As explained in the introduction, this thesis is restricted to baseband impulse radio systems, such that the duration limited sinusoidal pulses are not considered further. However, it is relatively straightforward to extend the theory and the performance estimations presented in this thesis to duration limited sinusoidal pulses.

2.1.2 Composition of a Burst

For a practical communication system we assume that N_s symbols are transmitted using a sequence of pulses as represented in figure 2.3. The entire sequence of pulses is called a burst and has a duration t_{burst}. The burst transmits N_s symbols, each one with a duration t_s. One symbol corresponds to N_b bits (e.g., $N_b = 1$) for a binary data transmission) and is composed of N_f frames. Each frame contains exactly one pulse such that the frame duration t_f is identical to the average interval between two consecutive pulses. The instant when the pulse is generated compared to the beginning of the frame can vary, e.g., as a function of the data or the identification of the transmitter. The frame is decomposed in N_c chips with a duration $t_c = t_f/N_c$, such that the instant of the pulse transmission can be associated with the index of the corresponding chip. Examples of delay and amplitude modulations are shown in the next section.

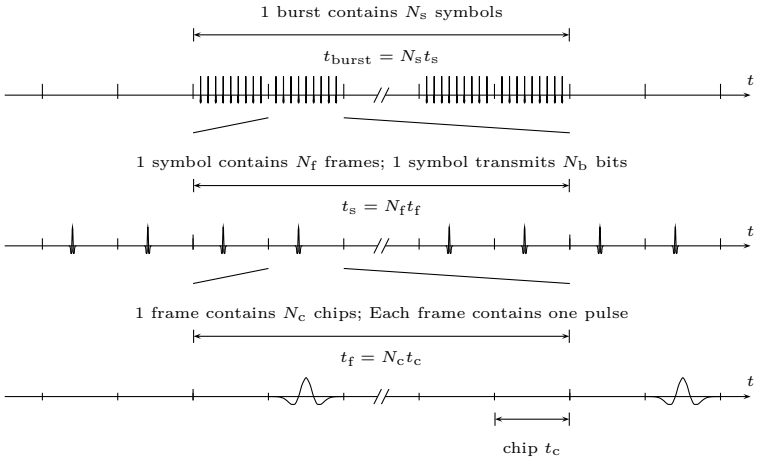

Figure 2.3: Time representation of an impulse radio signal. The burst interval is composed by N_s symbol intervals. Each symbol interval consists of N_f frame intervals and contains N_f pulses. The frame is composed of N_c chips.

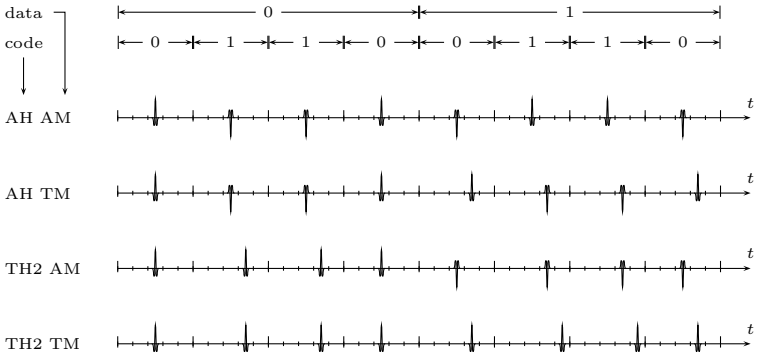

Figure 2.4: Time representation for exemplary modulated signals.

2.1.3 Modulation

The kth data symbol to be transmitted is denoted as d_k and is assumed to be a binary value $d_k \in \{0, 1\}$. The symbol d_k is transmitted by modulating N_f pulses. The modulation is the variation of one or several properties of a signal, such as its amplitude, its central frequency, its shape, or its phase. The detection of the variation of the signal property is called the demodulation. The data symbol is then reconstructed in the receiver and denoted as $\hat{d}_k$. The reception of the data symbol succeeded without error if $\hat{d}_k = d_k$. In this section, some promising modulations for IR are shown. A generic representation of the possible modulations for IR is shown in appendix A. In the generic representation the restriction to binary data $d_k \in \{0, 1\}$ is also eliminated.

For a baseband pulse with a given shape, only two properties can be varied directly: the pulse amplitude and the time of transmission. They result in amplitude modulation (AM) and delay modulation (TM) respectively. It is assumed that each transmitter uses a spreading code sequence $\{c_j\}$ with length N_f that is repeated for the transmission of each data symbol d_k. In the following a selection of four modulations is listed. They are graphically represented in figure 2.4. The used nomenclature describes the code modulation (also called hopping) and the data modulation. For example AH TM describes an amplitude code modulation combined with a delay data modulation. For TH, the integer M denotes the number of admissible values for the elements of the code sequence, i.e., $c_j \in \{0, M-1\}$.

- AH AM: Both the data modulation and the code modulation are made using an antipodal amplitude modulation. It is assumed that the spreading code is a binary sequence $c_j \in \{0, 1\}$. The transmitted signal is given by

$$s(t) = \sum_{k=0}^{N_\mathrm{s}-1} \sum_{j=0}^{N_\mathrm{f}-1} (2d_k - 1)(2c_j - 1)p(t - jt_\mathrm{f} - kt_\mathrm{s}). \tag{2.11}$$

- THM TM: A delay modulation is used for the data symbol d_k and the transmission of the code $c_j \in \{0, M-1\}$. The transmitted signal is written as

$$s(t) = \sum_{k=0}^{N_\mathrm{s}-1} \sum_{j=0}^{N_\mathrm{f}-1} p(t - jt_\mathrm{f} - kt_\mathrm{s} - (d_k + c_j)t_\mathrm{c}). \tag{2.12}$$

- THM AM: The data is transmitted using an antipodal amplitude modulation and the code $c_j \in \{0, M-1\}$ using a delay modulation. The transmitted signal is

$$s(t) = \sum_{k=0}^{N_\mathrm{s}-1} \sum_{j=0}^{N_\mathrm{f}-1} (2d_k - 1)p(t - jt_\mathrm{f} - kt_\mathrm{s} - c_j t_\mathrm{c}). \tag{2.13}$$

- AH TM: The amplitude modulation is applied to the code sequence $c_j \in \{0, 1\}$ and the delay modulation to the data symbol. For the AH TM, the transmitted signal is

$$s(t) = \sum_{k=0}^{N_\mathrm{s}-1} \sum_{j=0}^{N_\mathrm{f}-1} (2c_j - 1)p(t - jt_\mathrm{f} - kt_\mathrm{s} - d_k t_\mathrm{c}). \tag{2.14}$$

It is noted that all the above modulations can be written as

$$s(t) = \sum_{k=0}^{N_\mathrm{s}-1} \sum_{j=0}^{N_\mathrm{f}-1} d_{j,k}^{(\mathrm{a})} p(t - jt_\mathrm{f} - kt_\mathrm{s} - d_{j,k}^{(\mathrm{t})} t_\mathrm{c}), \tag{2.15}$$

where $d_{j,k}^{(\mathrm{a})}$ defines the amplitude and $d_{j,k}^{(\mathrm{t})}$ the delay of the individual pulses. The values $d_{j,k}^{(\mathrm{a})}$ and $d_{j,k}^{(\mathrm{t})}$ are both functions of the data symbol d_k and the elements of the code sequence c_j. For example the THM TM is denoted by (2.15) when $d_{j,k}^{(\mathrm{a})} = 1$ and $d_{j,k}^{(\mathrm{t})} = d_k + c_j$. Other options are shown in appendix A.

2.2 Frequency Domain Representation

Traditionally, the analysis of narrowband communication systems refers to a frequency domain representation of the signals and the constituting elements of the system. The frequency domain representation allows intuitive approaches and deepened understanding of the effects of the modulation and demodulation. It contains an equivalent information concerning the signal and the system as the time domain representation. For the signals and systems of practical interest it is possible to convert between the time representation and the frequency representation using the Fourier transformation[3].

[3]General conditions for the existence of the Fourier transform are complicated to state. Two sufficient but not necessary conditions are the following. The weak Dirichlet condition states that the Fourier transform of $x(t)$ exists if $\int_{-\infty}^{\infty} |x(t)|\,\mathrm{d}t < \infty$. The strong Dirichlet conditions states that the Fourier transform of $x(t)$ exists if the signal has a finite number of discontinuities and a finite number of maxima and minima.

For IR UWB systems, the frequency domain representation is less often used than for narrowband systems. However, as the regulation authorities limit the maximum or the average PSD, the frequency domain representation of the UWB signals still needs to be estimated.

2.2.1 Definitions of the Spectrum

A signal can be characterized by applying it to a bandpass filter and measuring the power at the output of the filter. The larger the filter bandwidth, the more power will pass through the filter. By selecting an infinitely narrowband filter, the previous method provides a mathematical definition of the PSD

$$\mathrm{PSD}(\omega) = \lim_{\Delta\omega \to 0} \frac{P_{\Delta\omega}}{\Delta\omega}, \tag{2.16}$$

where $P_{\Delta\omega}$ is the measured power at the output of an ideal filter with bandwidth $\Delta\omega$. A practical application of (2.16) will face a fundamental problem: The infinitely narrow filter requires an infinite measurement period. In practical applications, such as spectrum analyzers, (2.16) is approximated by selecting a filter with a finite bandwidth, typically between 1 kHz and 5 MHz. The measured power is divided by the resolution bandwidth $\Delta\omega$ to obtain the average PSD. This approximation is valid if the spectrum can be considered constant for the resolution bandwidth.

An alternative approach to obtain the spectrum is to relate the spectrum to the Fourier transform of the signal $s(t)$, i.e.,

$$\mathrm{PSD}(\omega) = \frac{S(\omega)S^*(\omega)}{2\pi}, \tag{2.17}$$

where $S(\omega) = \int_{-\infty}^{\infty} s(t)\mathrm{e}^{-\mathrm{i}\omega t}\,\mathrm{d}t$ is the Fourier transform of the signal $s(t)$ and $S^*(\omega)$ is the complex conjugate of $S(\omega)$. The definition (2.17) requires the Fourier transform to exist. To relax this conditions, it is often more convenient to relate the PSD to the autocorrelation function $c_{ss}(\tau) = \int_{-\infty}^{\infty} s(t+\tau)s(t)\,\mathrm{d}t$ of the signal by

$$\mathrm{PSD}(\omega) = \int_{-\infty}^{\infty} c_{ss}(\tau)\mathrm{e}^{-\mathrm{i}\omega\tau}\,\mathrm{d}\tau. \tag{2.18}$$

The definition (2.18) does only require the signal $s(t)$ to be a wide-sense stationary process and can therefore also be applied to most random signals,

including an UWB signal with an infinite duration. In contrast, a single pulse is a transient signal and not wide-sense stationary. It contains a finite amount of energy, such that the average power is zero. The PSD is therefore also zero. For single pulses, the PSD will be calculated for a finite duration interval of the signal containing the pulse. The outcome may be denoted in form of an energy spectrum density. In the following, the term *spectrum* will be used for both the power and the energy spectrum density.

2.2.2 Characteristics of the Spectrum

Some important characteristics of the signaling can be deduced from the spectrum. For a narrowband communication system, the two most important parameters are the carrier frequency and the bandwidth. The bandwidth can be defined as the difference between an upper frequency and a lower frequency considered to demarcate the spectrum. For narrowband signals, they are often defined as the frequencies for which the spectrum falls permanently 3 dB below the carrier value. For UWB signals, the lower frequency f_{L} is defined as the maximal frequency smaller than the center frequency for which the spectrum is 10 dB below its maximal value. Similarly, the upper frequency f_{H} can be defined as the minimal frequency larger than the center frequency for which the spectrum is 10 dB below its maximum. The difference between the upper and the lower frequency is the -10 dB bandwidth of the signal

$$B_{-10\,\mathrm{dB}} = f_{\mathrm{H}} - f_{\mathrm{L}}. \tag{2.19}$$

Several options are possible for the definition of a characteristic of the UWB signaling corresponding to the carrier frequency of a narrowband signal. Three options are considered in the following. A first definition is to calculate the frequency f_{m} for which the spectrum is maximal,

$$f_{\mathrm{m}} = \frac{1}{2\pi} \arg\max_{\omega} \mathrm{PSD}(\omega). \tag{2.20}$$

Another common approach is the arithmetic mean of the upper and lower frequency

$$f_{\mathrm{c}} = \frac{f_{\mathrm{L}} + f_{\mathrm{H}}}{2}. \tag{2.21}$$

Finally, the geometric mean is defined as

$$f_{\mathrm{C}} = \sqrt{f_{\mathrm{L}} f_{\mathrm{H}}}. \tag{2.22}$$

The geometric mean is proposed to be taken to estimate the propagation path loss or to calculate characteristics of an antenna [Sch05]. In the FCC definition [FCC02], the bandwidth is compared to the arithmetic mean to define the relative bandwidth B_r and the fractional bandwidth B_f related by

$$B_\mathrm{f} = 2B_\mathrm{r} = 2\frac{f_\mathrm{H} - f_\mathrm{L}}{f_\mathrm{H} + f_\mathrm{L}} = \frac{f_\mathrm{H} - f_\mathrm{L}}{f_\mathrm{c}}. \tag{2.23}$$

It is noted that the fractional and the relative bandwidths do not have a unit. They depend on the pulse shape, but they become independent of the pulse duration. For example the fractional bandwidth is 1.34 for a second derivative Gaussian pulse independently of the pulse duration t_n.

Finally, an equivalent bandwidth B_e is introduced. It is defined, such that the average power calculated in the frequency domain is given by the product between the equivalent bandwidth and the maximum value of the spectrum $\langle P_\mathrm{f}\rangle = B_\mathrm{e}\mathrm{PSD}_\mathrm{max}$. The average power calculated in the time domain is given by the pulse energy $\mathcal{E}_\mathrm{p}$ and the frame duration t_f by $\langle P_\mathrm{t}\rangle = \mathcal{E}_\mathrm{p}/t_\mathrm{f}$. Because of Parseval's theorem $\langle P_\mathrm{t}\rangle = \langle P_\mathrm{f}\rangle$ and it follows that the maximum value of the spectrum can be calculated with

$$\mathrm{PSD}_\mathrm{max} = \frac{\mathcal{E}_\mathrm{p}}{t_\mathrm{f} B_\mathrm{e}} \qquad \text{in W/Hz} \tag{2.24}$$

$$\mathrm{PSD}_\mathrm{max} = 90 + 10\log_{10}\left(\frac{\mathcal{E}_\mathrm{p}}{t_\mathrm{f} B_\mathrm{e}}\frac{1\,\mathrm{Hz}}{1\,\mathrm{W}}\right) \qquad \text{in dBm/MHz} \tag{2.25}$$

when the equivalent bandwidth B_e, the frame duration t_f, and the pulse energy $\mathcal{E}_\mathrm{p}$ is known. (2.25) may hence be used to test the compatibility of an UWB signal with the spectral mask. For the Gaussian pulses, the equivalent bandwidths and other characteristics are given in table 2.2.

In the following a numerical example for a second derivative Gaussian pulse with a pulse energy $\mathcal{E}_\mathrm{p} = 1\,\mathrm{pJ}$, a frame duration of 100 ns, and a pulse duration $t_n = 200\,\mathrm{ps}$ is shown. Considering table 2.2 it follows that the equivalent bandwidth is 1.954 GHz. Using (2.25) it follows that the maximum value for the spectrum $\mathrm{PSD}_\mathrm{max} = -53\,\mathrm{dBm/MHz}$. This value is in excellent agreement with the maximum value of the spectrum for the second derivative Gaussian pulse as it can be seen in figure 2.5.

Pulse	$f_{\mathrm{L}} t_n$	$f_{\mathrm{H}} t_n$	$f_{\mathrm{c}} t_n$	$f_{\mathrm{C}} t_n$	$f_{\mathrm{m}} t_n$	$B_{-10\,\mathrm{dB}} t_n$	B_{f}	$B_{\mathrm{e}} t_n$
$p_{\mathrm{G}_0}(t)$	0.0000	0.2415	0.1208	0.0000	0.0000	0.2415	2.0000	0.2821
$p_{\mathrm{G}_1}(t)$	0.0311	0.3519	0.1915	0.1046	0.1592	0.3208	1.6750	0.3834
$p_{\mathrm{G}_2}(t)$	0.0821	0.4128	0.2474	0.1841	0.2251	0.3308	1.3368	0.3908
$p_{\mathrm{G}_3}(t)$	0.1266	0.4609	0.2937	0.2415	0.2757	0.3343	1.1381	0.3935
$p_{\mathrm{G}_4}(t)$	0.1658	0.5019	0.3339	0.2885	0.3183	0.3361	1.0067	0.3948

Table 2.2: Approximate characteristics for Gaussian pulses.

2.2.3 Spectrum of a Single Pulse

The Fourier transform for the first four Gaussian pulses (2.3a) to (2.3d) are

$$P_{\mathrm{G}_0}(\omega) = \sqrt{2 t_n R \sqrt{\pi}}\ \exp\left(-\frac{\omega^2 t_n^2}{2}\right) \tag{2.26a}$$

$$P_{\mathrm{G}_1}(\omega) = +2\mathrm{i}\omega\ \sqrt{t_n^3 R \sqrt{\pi}}\ \exp\left(-\frac{\omega^2 t_n^2}{2}\right) \tag{2.26b}$$

$$P_{\mathrm{G}_2}(\omega) = +2\omega^2 \sqrt{\frac{2}{3} t_n^5 R \sqrt{\pi}}\ \exp\left(-\frac{\omega^2 t_n^2}{2}\right) \tag{2.26c}$$

$$P_{\mathrm{G}_3}(\omega) = -4\mathrm{i}\omega^3 \sqrt{\frac{1}{15} t_n^7 R \sqrt{\pi}} \exp\left(-\frac{\omega^2 t_n^2}{2}\right) \tag{2.26d}$$

It is noted that the Fourier transforms are continuous functions and are either real or purely imaginary functions. In figure 2.5, the spectra for (2.26a) to (2.26d) calculated using (2.17) are traced for the mth derivative Gaussian pulse with $t_n = 200\,\mathrm{ps}$, $\mathcal{E}_{\mathrm{p}} = 1\,\mathrm{pJ}$, and $t_{\mathrm{f}} = 100\,\mathrm{ns}$. Contrary to the Fourier transform, the spectrum is real and non-negative.

2.2.4 Spectrum of a Burst

Infinite duration, non-modulated signal: In the following the spectrum of a non-modulated, repetitive sequence of pulses with infinite duration is calculated. This sequence, denoted as burst, can be written as an infinite sum of pulses

$$s(t) = \sum_{j=\infty}^{\infty} p(t - j t_{\mathrm{f}}). \tag{2.27}$$

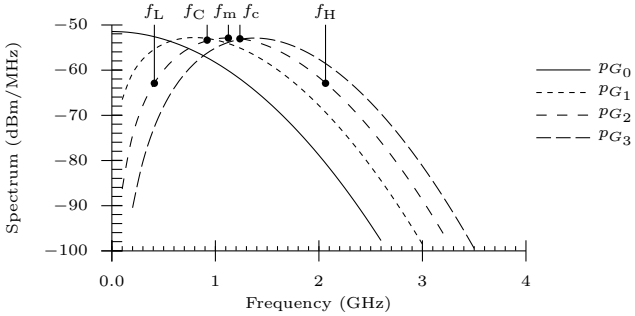

Figure 2.5: Spectrum of single Gaussian pulses with $t_n = 200$ ps and 1 pJ energy. The spectrum is calculated with a frame duration of 100 ns. The characteristics f_m, f_C, f_L, f_H, f_c are shown for the second derivative Gaussian pulse.

Using the convolution operator $*$ and the Dirac distribution $\delta(t)$, the burst can be written as

$$s(t) = p(t) * \sum_{j=\infty}^{\infty} \delta(t - jt_f). \tag{2.28}$$

The Fourier transform $S(\omega)$ of $s(t)$ is

$$S(\omega) = P(\omega) \cdot \frac{2\pi}{t_f} \sum_{j=-\infty}^{\infty} \delta\left(\omega - j\frac{2\pi}{t_f}\right), \tag{2.29}$$

where $P(\omega)$ is the Fourier transform of $p(t)$. It follows immediately from (2.29) that the spectrum for the non-modulated, periodic burst is discrete. The spectrum will hence not comply with any spectrum mask[4].

Duration limited, non-modulated signal: When the transmission is bounded in time, the burst can be written as

$$s(t) = \sum_{j=-N_f/2}^{N_f/2} p(t - jt_f) = \left[p(t) * \sum_{j=-\infty}^{\infty} \delta(t - jt_f) \right] \cdot v(t), \tag{2.30}$$

[4]Except in the trivial case when $P(\omega) \equiv 0$ which means that no pulses are transmitted.

where

$$v(t) = \begin{cases} 1 & \text{if } -t_v/2 < t < t_v/2 \\ 0 & \text{otherwise} \end{cases} \tag{2.31}$$

provides a rectangular shaping with duration t_v. The Fourier transform becomes hence

$$S(\omega) = \frac{1}{2\pi} \left[P(\omega) \cdot \frac{2\pi}{t_\mathrm{f}} \sum_{j=-\infty}^{\infty} \delta\left(\omega - j\frac{2\pi}{t_\mathrm{f}}\right) \right] * V(\omega). \tag{2.32}$$

The bandwidth of $V(\omega)$ is smaller than $2\pi/t_\mathrm{f}$ if the duration of the burst is larger than the frame duration, i.e., more than one pulse is transmitted. Therefore, $S(\omega)$ is a continuous functions, yet is composed of a series of equidistant narrowband contributions. Their amplitudes are given by the spectrum $P(\omega)$. An example of a measured spectrum where these narrowband contributions are clearly visible is given in the next section and illustration in figure 2.6.

Modulated signals: It has been shown, that the spectrum of an non-modulated signal, even when time limited, has peaks. The spectra of modulated signals are given for example in [Rid05, Rom02, Win99, Kis01, Chr03]. An extension to the spectra of the received signals in multipath channels is presented in [Tah03]. In general, the presented spectra contains both discrete and continuous components.

Measured spectrum: The pulse from an Avtech AVM-2-C pulse generator is upconverted using a mixer and a local oscillator at 3 GHz. The measurement results are shown in figure 2.6. The background noise, mainly up to 500 MHz and an interference from a mobile phone base station at about 950 MHz can be seen. By zooming around the frequency of interest for the UWB pulse, the discrete nature of the spectrum becomes visible. The frequency difference between two consecutive narrowband contributions corresponds to the constant pulse repetition frequency, which is 10 MHz in this example.

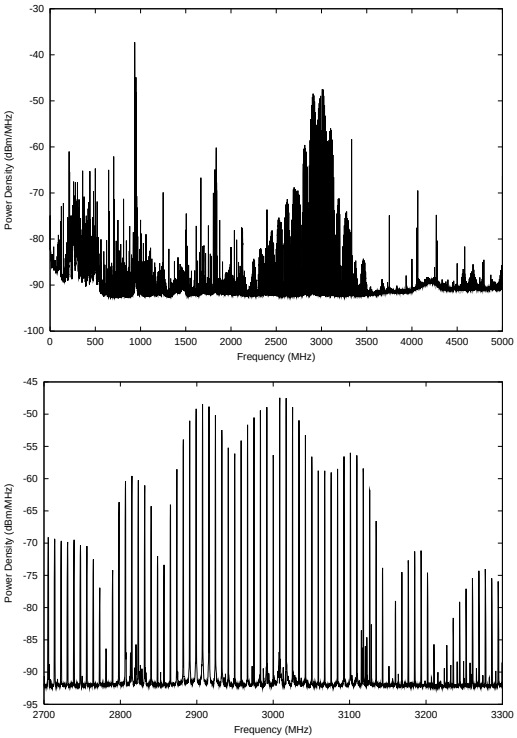

Figure 2.6: Spectrum density seen by an LeCroy SDA6020 Oscilloscope with a complementary flat bicone dipole antenna for the Avtech AVM-2-C pulse generator mixed with a 3 GHz carrier in 3 m distance. The relevant UWB signal is between 2.5 GHz and 3.5 GHz. The signals below 1 GHz and the narrowband signals are due to interferences.

2.3 Propagation Channels

The propagation channel defines the information-theoretic performance limitations for the communication and positioning system. Understanding the channel is thus important for designing and improving UWB systems [Che04]. There exist a large number of different channel models for narrowband and wideband communications. Narrowband channel models normally assume that the channel is not frequency selective. This assumption may not be valid for wideband communications. In this section, theoretical and empir-

ical wideband channel models are presented and discussed. The received pulse shape and its average power will be derived for the selected channel models.

2.3.1 Literature

In the literature several aspects of the wideband propagation channel can be found. There exist theoretical approaches leading to a channel model, such as the geometric theory of the diffraction to explain the propagation [Qiu02], or models based on experimental data. An overview of the experimental measurement methods is given for example in [Bue02, Muq03]. Models for indoor and outdoor propagations can also be found in [Bue04]. A huge number of measurements, performed in the time domain and the frequency domain, are also presented in the same document. In [SJ02], some results including propagations through walls and material characterizations are resumed.

2.3.2 Measurement of the Propagation Channel

The measurements of the propagation channel can be made in the time domain or the frequency domain. When the channel is linear and time-invariant (during the period of interest), then the impulse response $h(t)$ and the frequency response $H(\omega)$ of the channel are related by the Fourier transform.

Time domain measurements: The time domain measurements have traditionally been made using sampling oscilloscopes. During the last years, sampling oscilloscopes have typically been replaced by digital storage oscilloscopes with high bandwidth (up to about 13 GHz) and very fast sampling rates (up to 40 GS/s) for the measurements of propagation channels. A seminal contribution was [Sal87], where a square law detector and a sampling oscilloscope were used to capture the pulses with a center frequency of 1.5 GHz and a duration of approximately 10 ns. The experiments were performed in an office building and were used to propose a novel propagation model (see the Saleh-Valenzuela model in section 2.3.4). Other time domain measurements for UWB in office environments are presented in [Cra02, Win02]. In [Cra02] a CLEAN algorithm is applied to the measurement data to estimate the parameters of a selected channel model. In [Win02] the measurements are used to calculate the performance of a rake receiver in a realistic environment.

In a time domain description of a linear, time-invariant propagation channel, the received signal $r(t)$ is related to the transmitted signal $s(t)$ and the channel impulse response $h(t)$ by

$$r(t) = h(t) * s(t). \tag{2.33}$$

To estimate the channel impulse response (2.33) should be solved for $h(t)$. The solution $r(t) = h(t)$ is found for $s(t) = \delta(t)$. In practical systems, it may be sufficient to generate a sufficiently short duration pulse to measure the channel impulse response directly[5]. Another approach would be to calculate $h(t)$ by inverting (2.33) using the inverse operation of the convolution. This problem is well known in the literature under the name convolution, because it arises in all situations where a signal $s(t)$ should be estimated but only a filtered signal $r(t)$ can be measured. For example in terrestrial space photography, the measured signal (incident light recorded as an image) is filtered by the transmission through the atmosphere and the optical system in the camera. In the context of radio astronomy the CLEAN algorithm has first been proposed for decorrelation [Hög74]. A modified CLEAN algorithm has also been proposed for time of arrival (TOA) estimation in UWB applications [Lee02]. A more generic but numerically unstable solution for the decorrelation is shown in the next section discussing frequency domain measurements.

Frequency domain measurements: These measurements are typically made using a network analyzer. Measurements in an indoor environment are presented in [Hov02]. In [Cho04] the measurements are performed in empty high-rise apartments. In [Gen05, Han03], the measurements are used to calculate the power delay profile. Finally, in [Pah98], the TOA is calculated for a frequency-sweeped signal at frequencies between 900 MHz and 1 100 MHz. Hence, this provides an estimation of the potential of UWB systems for a localization system. However, it would be interesting to compare the outcomes with the ones using signals covering a larger bandwidth.

Converted to the frequency domain, (2.33) becomes

$$R(\omega) = H(\omega)S(\omega). \tag{2.34}$$

[5] E.g., when a multipath propagation channel should be measured, then the duration of the pulse should be shorter than the minimum difference of arrival times from two paths.

The frequency response $H(\omega)$ can now be calculated using $H(\omega) = R(\omega)S(\omega)^{-1}$. Unfortunately, this approach normally does not lead to accurate estimations of the frequency response for wideband signals. It is numerically unstable for frequencies for which $S(\omega)$ and therefore also $R(\omega)$ are small. The result is thus sensitive to interference and noise. To make the estimation more robust, a signal $s(t)$ should be selected, such that $|S(\omega)|$ is non-negligible for all frequencies. For example such that $|S(\omega)|$ is constant. This is the case for $s(t)$ being a Dirac pulse, a white noise, a swept sinusoidal signal, or another wideband signal. The swept sinusoidal signal is used for example in network analyzers. The phase terms in (2.34) can be eliminated by multiplying (2.34) with $S^*(\omega)$. In this case

$$R(\omega)S^*(\omega) = H(\omega)S(\omega)S^*(\omega) \tag{2.35}$$

and the frequency response is

$$H(\omega) = \frac{R(\omega)S^*(\omega)}{|S(\omega)|^2}. \tag{2.36}$$

Also for an estimation using (2.36), $s(t)$ should be a wideband signal, such that $|S(\omega)|^2$ is non-negligible for all frequencies.

Time domain measurements revised: Based on (2.36), the time domain measurements are revised. Using the inverse Fourier transformation

$$c_{rs}(\tau) = h(\tau) * c_{ss}(\tau), \tag{2.37}$$

is obtained, where $c_{rs}(\tau)$ is the cross-correlation between $r(t)$ and $s(t)$ and $c_{ss}(\tau)$ is the autocorrelation of $s(t)$. To measure the channel impulse response, it is sufficient that $c_{ss}(\tau) = \delta(\tau)$. Again, this is the case for $s(t)$ a

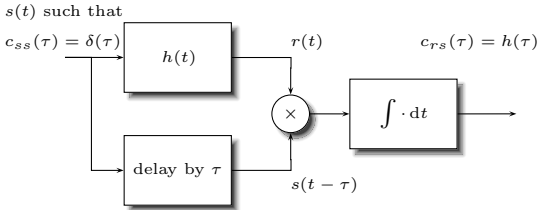

Figure 2.7: Schematic representation of the measurement procedure of the channel impulse response using a sliding correlator.

Dirac pulse, a white noise, a swept sinusoidal signal, or another wideband signal. A possible setup for such a measurement is represented in figure 2.7. The channel impulse response is a function of τ, which can be adjusted accurately. This approach is for example used in [And02] and is called a sliding correlator. At the receiver, the delayed signal $s(t-\tau)$ is correlated with a received signal $r(t)$ and thus the value $c_{rs}(\tau) = h(\tau)$ is obtained.

2.3.3 Free Space Propagation

The propagation of a radio signal from a hypothetical isotropic antenna, which has a unit gain by definition, in the free space is described by a spherical wave. Due to the conservation of the energy, the received power per unit area S_r is

$$S_\mathrm{r} = P_\mathrm{t} \frac{1}{4\pi d^2}, \tag{2.38}$$

where P_t is the transmitted power, and d is the distance between the transmitting and the receiving antenna. Assuming that the distance is much larger than the effective area of the receiving antenna $d \gg A_\mathrm{r}$, the wave front can be approximated by a plane wave and the received power P_r is

$$P_\mathrm{r} = P_\mathrm{t} \frac{A_\mathrm{r}}{4\pi d^2}. \tag{2.39}$$

By definition, the effective area of a hypothetical isotropic antenna with no heat loss is given by

$$A_\mathrm{t} = \frac{\lambda^2}{4\pi}, \tag{2.40}$$

where $\lambda = c/f$ is the wavelength of the radio signal in the propagation medium. Combining (2.39) and (2.40) the Friis free-space transmission formula is obtained [Fri46]

$$\frac{P_\mathrm{r}}{P_\mathrm{t}} = \frac{A_\mathrm{r} A_\mathrm{t}}{d^2 \lambda^2}. \tag{2.41}$$

Today, it is more common to replace the effective areas A_r and A_t with the antenna gains $G_\mathrm{r} = 4\pi\lambda^{-2} A_\mathrm{r}$ and $G_\mathrm{t} = 4\pi\lambda^{-2} A_\mathrm{t}$ such that (2.41) becomes [And03]

$$\frac{P_\mathrm{r}}{P_\mathrm{t}} = G_\mathrm{t} G_\mathrm{r} \left(\frac{\lambda}{4\pi d} \right)^2. \tag{2.42}$$

This model is valid in the far-field or Frauenhofer region of the transmitter antenna. It is noted, that the power loss depends on the frequency of the signal. For an UWB signal the geometric average frequency f_C should be taken as an approximation [Sch05]. Most often, a close distance d_0 is taken as a reference with $2D^2\lambda < d_0 < d$ where D is the largest extension of the antenna. Typically, $d_0 = 1\,\mathrm{m}$ for indoor systems. The received power is given by

$$P_\mathrm{r}(d) = P_\mathrm{r}(d_0)\left(\frac{d_0}{d}\right)^2 \tag{2.43}$$

or

$$P_\mathrm{r}(d)\,[\mathrm{dBm}] = 10\log_{10}\left(\frac{P_\mathrm{r}(d_0)}{1\,\mathrm{mW}}\right) + 20\log_{10}\left(\frac{d_0}{d}\right) \tag{2.44}$$

The Friis transmission formula is valid for free space propagation and does not provide accurate results for frequency selective channels such a multipath propagation channels.

2.3.4 Indoor Propagation

Log-distance path loss model: The log-distance path loss model is an extension of the free space propagation model (2.43) by introducing a path loss exponent γ

$$P_\mathrm{r}(d) = P_\mathrm{r}(d_0)\left(\frac{d_0}{d}\right)^\gamma. \tag{2.45}$$

The path loss exponent characterizes how fast the average received power decreases with an increase in the transmission distance. The log-distance path loss model does not include effects like shadowing or reflection and does hence not provide a mean to calculate the shape of the received signal. Nevertheless, it is useful to establish a link budget for a communication system (see section 4.3). Typical values for path-loss exponents for UWB indoor propagation are between 2.2 and 3.3 [Cra99] compared to 2.0 for free space propagation.

MULTIPATH MODEL: Multipath is a propagation phenomenon which results in signals reaching the receiving antenna by two or more paths [And02]. A geometric interpretation of the multipath propagation is to associate different propagation paths between the emitter and the receiver due to reflection, refraction, diffraction, ducting, and scattering of the electromagnetic wave. The mth path has a real valued gain a_m and a propagation delay τ_m. Assuming that no dispersion occurs within individual pulses and a linear behavior of the propagation medium, the channel impulse response is real and is represented as a superpositions of the multipath components

$$h(t) = \sum_m a_m \delta(t - \tau_m) \tag{2.46}$$

where $\delta(t)$ is the Dirac delta function. As already mentioned, the received signal $r(t)$ is given by the convolution between the transmitted signal $s(t)$ and the channel impulse response $h(t)$. For a time-invariant channel, i.e., a_m and τ_m are independent of the time t, the propagation channel can be considered as a linear, time invariant filter. As a_m and τ_m depend on the environment and in particular on the locations of reflecting objects, the assumption of the time invariance is not in general true for long durations. However, for typical symbol transmission durations (100 ns to 100 µs) the channel can be assumed to be time invariant. The frequency response of the propagation channel is given by the Fourier transform of $h(t)$ and is

$$H(\omega) = \sum_m a_m \mathrm{e}^{-\mathrm{i}\omega\tau_m}. \tag{2.47}$$

The amplitude response $|H(\omega)|$ is in general not constant, but a function of ω. This means that the signal is more attenuated at some frequencies than others because of the multipath propagation. Furthermore the attenuations depend strongly on τ_m, i.e., the positions of the transmitter, receiver and reflectors. At a given frequency, a small variation of the positions may result in an important variation of the received power. This effect is called small-scale fading and appears for narrowband communications. Being wideband, the attenuation of a single frequency does not reduce the average received power of an UWB communication significantly. Hence, the small-scale fading is normally not important for UWB systems.

The channel impulse response $h(t)$ or the frequency response $H(\omega)$ completely describe the propagation channel. Some characteristics can be extracted from the parameters a_m and τ_m. Directly related to the channel

impulse response is the power delay profile, which is defined as [Xu00]

$$\mathrm{PDP} = |h(t)|^2 = \sum_m |a_m|^2 \delta(t - \tau_m). \tag{2.48}$$

The mean excess delay is given by the first moment of the power delay profile

$$\langle \tau \rangle = \frac{\sum_m a_m^2 \tau_m}{\sum_m a_m^2}, \tag{2.49}$$

and the root mean square delay spread by the square root of the second central moment of the power delay profile

$$\sigma_\tau = \sqrt{\langle \tau^2 \rangle - \langle \tau \rangle^2}, \quad \text{where } \langle \tau^2 \rangle = \frac{\sum_m a_m^2 \tau_m^2}{\sum_m a_m^2}. \tag{2.50}$$

The maximum excess delay is either $\max_m(\tau_m)$ or the t_m for which the expected value $\mathsf{E}[a_m^2]$ falls below a given threshold. The maximum excess delay is an important property to characterize the impact of inter-pulse interference.

The coherence bandwidth is the bandwidth over which the frequency correlation function is above a given value. For a value of 0.9, the coherence bandwidth is approximately [Rap02]

$$B_\mathrm{c} \approx \frac{1}{50\sigma_\tau}. \tag{2.51}$$

If we consider the root mean square delay spread to be about 10 ns for a typical indoor propagation channel, the coherence bandwidth is

$$B_\mathrm{c} \approx \frac{1}{500\,\mathrm{ns}} = 2\,\mathrm{MHz}. \tag{2.52}$$

With typical signal bandwidth in excess of 500 MHz, the assumption that the propagation channel should be considered frequency selective is confirmed.

The coherence time is the time for which the channel can be assumed to not change significantly. It is related to the Doppler spread f_d and therefore to the movement of the transmitting and the receiving antennas or other movements in the medium (reflectors). For a large signal bandwidth, the broadening because of the Doppler spread is small. If the bandwidth of the signal is much wider than $2f_\mathrm{d}$, the degrading impact of Doppler spread on

signal reception is negligible [She03]. Two approximations are common. The first one is

$$T_{c1} \approx \frac{1}{f_\mathrm{d}} \tag{2.53}$$

where f_d is the maximum Doppler shift given by $f_\mathrm{d} = v/\lambda$ and v is the radial speed between the transmitter and the receiver. The second approximation

$$T_{c2} \approx \frac{9}{16\pi f_\mathrm{d}} \tag{2.54}$$

describes the coherence time over which the time correlation function is above 0.5. The geometric mean between (2.53) and (2.54) results in

$$T_c \approx \sqrt{\frac{9}{16\pi f_\mathrm{d}^2}} \approx \frac{0.423}{f_\mathrm{d}} \tag{2.55}$$

and is often proposed as rule of thumb to estimate a coherence time [Rap02].

For example for $v = 10\,\mathrm{km/h}$ and $f_\mathrm{C} = 3.5\,\mathrm{GHz}$, the coherence time using this rule of thumb results in $T_c \approx 13\,\mathrm{ms}$. For a data rate faster than about 100 symbols per second, the channel can be assumed slow fading.

Saleh-Valenzuela model: The Saleh-Valenzuela model starts with the physical realization that the signal from different paths arrive in clusters [Sal87]. It assumes that the clusters as well as the paths within each cluster arrive at exponentially distributed inter-arrival times. The impulse response of the Saleh-Valenzuela model is given as

$$h(t) = \sum_{n=0}^{\infty} \sum_{m=0}^{\infty} \beta_{m,n} \delta(t - \tau_n - \tau_{m,n}), \tag{2.56}$$

where m is indexing the paths within a cluster and n the clusters. The delays of the clusters are described by the probability density function

$$p(\tau_n | \tau_{n-1}) = \Lambda \exp\left(-\Lambda(\tau_n - \tau_{n-1})\right), \tag{2.57}$$

and the delays of the paths within a cluster by

$$p(\tau_{m,n} | \tau_{m-1,n}) = \lambda \exp\left(-\lambda(\tau_{m,n} - \tau_{m-1,n})\right). \tag{2.58}$$

The magnitude of the mth path within the nth cluster is denoted by $\beta_{m,n}$. It is Rayleigh distributed with a mean given by [Foe03]

$$\langle \beta_{m,n}^2 \rangle = \langle \beta_{0,0}^2 \rangle \exp\left(-\tau_n/\Gamma\right) \exp\left(-\tau_{m,n}/\gamma\right), \tag{2.59}$$

where $\langle \beta_{0,0}^2 \rangle$ is the average power of the first arrival of the first cluster and γ and Γ are parameters characterizing the attenuation.

IEEE 802.15.3A: The IEEE 802.15.3a tried to develop a common standard for a novel high data rate communication system. It achieved to consolidate 23 individual contributions into two proposals: the Multi-Band Orthogonal Frequency Division Multiplexing (MB-OFDM) supported by the WiMedia Alliance, and the Direct Sequence-UWB (DS-UWB) supported by the UWB Forum. As it was not possible to agree on a common proposal, the standardization process was blocked in 2003. Finally, the members voted to withdraw the project authorization request and hence to dissolve the IEEE 802.15.3a committee.

For the IEEE 802.15.3a, four channel models have been proposed that are based in the Saleh-Valenzuela model. The four models are denoted CM1 to CM4 [Foe03]. The CM1 describes a line-of-sight propagation between 0 m and 4 m. The CM2 models a non line-of-sight channel for the same range. CM3 is a non line-of-sight channel between 4 m and 10 m. Finally, the CM4 models an environment called "extreme non line-of-sight channel". It may be used to describe a communication in a building with a large number of metallic reflectors and an obstructed direct propagation path.

The IEEE 802.15.3a channel model assumes that the rays from the multipath propagation arrive in clusters. The cluster and the rays within the clusters are considered separately and have independent parameters. However, the cluster and the individual rays within the clusters are both modeled by: 1) a delay described by a Poisson process; 2) a decay factor for the exponential decrease of the average power delay profile; 3) a fading described by a log-normal process. The resulting impulse response is normalized. Finally, the total multipath energy is altered by considering a log-normal shadowing. Some characteristics of the IEEE 802.15.3a channel models are resumed in table 2.3 [Foe03]. A representative calculated signal using a CM3 model is shown in figure 2.8. The IEEE 802.15.3a model has been developed for high data rate systems. However, simulated channels using the IEEE 802.15.3a model coincide well with the measurements that were made in our laboratory

Model Characteristic	CM1	CM2	CM3	CM4
Mean excess delay (ns)	5.0	9.9	15.9	30.1
RMS delay spread (ns)	5	8	15	25
NP_{10dB} [1]	12.5	15.3	24.9	41.2
$NP_{85\%}$ [2]	20.8	33.9	64.7	123.3

[1] Number of paths within 10 dB of the strongest path.
[2] Number of paths that capture 85% of channel energy.

Table 2.3: Characteristics of the IEEE 802.15.3a channel models.

for baseband UWB. It will be used for the numerical simulations in chapters 5 and 6.

IEEE 802.15.4A: The IEEE 802.15.4a has developed alternatives for low data rate communications, e.g., for technologies that may complement Zigbee in the future. The channel models to be used for the IEEE 802.15.4a are given in [TG404]. The nine scenarios assumed are: 1) residental line-of-sight; 2) residential non line-of-sight; 3) office line-of-sight; 4) office non light-of-sight; 5) outdoor line-of-sight; 6) outdoor non line-of-sight; 7) industrial line-of-sight; 8) industrial non line-of-sight; and 9) open outdoor environment, such as farm or snow-covered open area [DB07].

2.3.5 Body Area Propagation

Body area networks are one of the proposed applications for UWB communications. The body area propagation has been characterized in [For05, Wel02]. The propagation at the human head in particular is discussed in [Zas06, Zas05]. An application for medical devices that requires transcutaneous transmissions is presented in [Buc04].

2.4 Noise and Interference

The propagation channels in the previous section allow to calculate the average received power or even the shape of the received signal. They do not model any additive noise or interference. However, in practical systems, noise and interferences are always present and limit the achievable performance of any communication system. It is therefore important to model them correctly. In this section common noise and interference models are discussed.

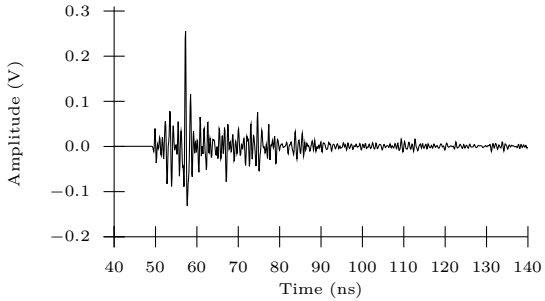

Figure 2.8: Illustration of the resulting signal when a second derivative Gaussian pulse is transmitted over one representative of the IEEE 802.15.3a, CM3 model.

First the difference between noise and interference should be clarified. A noise may arise from natural or human sources and is considered to be random. One example is the thermal noise in resistors present at any receiver with a temperature above 0 K. An interference results from a human source and is deterministic. Of particular interest are interferences that are in the same frequency bands as the signal of interest from the communication system such that it can not be eliminated by simple filtering. Interferences can result from many sources, including narrowband interferences from classical communication systems, wideband interferences from other UWB devices using the same or another signaling, and wideband interferences from brush sparking in electrical motors.

2.4.1 Wideband Noise and Interference

In this section, the AWGN and interferences from other UWB or wideband devices are considered.

Additive white Gaussian noise: The AWGN models noise sources that are white and have a Gaussian distribution of the amplitude. A noise is considered white if the spectrum is flat over the considered frequency bands. The noise source may be external such as the black body radiation from an object or internal such as the thermal (Johnson-Nyquist) noise of the receiver. The AWGN model describes all these noise sources as one external source. The AWGN model is normally combined with a propagation model and potentially with models for interferences. The noise power due to thermal effects

is given by

$$P_\eta = kTB_T \tag{2.60}$$

where k is the Boltzmann constant, T is the effective noise temperature of the receiver in Kelvin, and B_T is the receiver bandwidth in Hertz. For an effective noise temperature of 15 °C, the noise power density $\mathcal{N}_0 = kT$ is $-114\,\mathrm{dBm/MHz}$.

Multiuser interference: Multiuser interference is due to interfering users which are using identical or similar devices. In a network where many identical UWB devices are deployed, the multiuser interference has to be considered. Spreading codes can be used to mitigate it. The BER performance in the presence of multiuser interference will be considered in section 5.7. The synchronization in the presence of multiuser interference will be considered in section 6.4.

Interference from different wideband devices: Wideband interference may also arise from other wideband or UWB devices. There is in general no direct control over these devices. Hence, any UWB system should be able to cope with the interferences that are expected to be present.

Other wideband noise and interference: Other sources of wideband noise and interference are for example brush sparking from electric motors, sparks from plasma cutting, arc welding, or other industrial processes. Also this category of devices may be out of control for the UWB communication system, and may result in severe degradations of its performance if not designed properly.

2.4.2 Narrowband Interference

Due to the omnipresence of radio communications, an interference from a narrowband system may occur. In the most simple case, the narrowband interference can be modeled as a single tone at a angular frequency ω_i and hence is

$$i(t) = \cos(\omega_\mathrm{i} t + \phi_\mathrm{i}). \tag{2.61}$$

The interference is in general not synchronized with the signal from the user of interest, such that the phase ϕ_i is arbitrary and uniformly distributed over

$[0, 2\pi[$. The BER performance in the presence of a narrowband interference is considered in section 5.6. Figure 2.9 shows a measured UWB signal with a strong narrowband interferer. The narrowband signal is due to the downlink channel from a base station for mobile phones in the example. In general, the narrowband interference may have large amplitudes compared to the UWB pulse. For example, a mobile phone at about 900 MHz that emits with 2 W at a distance of 5 m from the UWB receiver will be received with -12.5 dBm when the antenna gain is 1. The associated peak to peak amplitude for a sinusoidal signal measured at 50 Ω is 150 mV. This may even result in non-linearities in the analog front-end of the receiver and hence generate harmonics or force the variable gain amplifier to reduce its sensitivity such that the reception of the UWB pulse becomes more difficult.

2.4.3 Intersymbol and Interpulse Interference

In a frequency selective or a dispersive propagation channel, the received pulse shape is normally altered compared to the transmitted pulse shape[6]. When a broadening of the pulse occurs, it may happen that the duration of the received pulse exceeds the pulse repetition interval. In this case, an interpulse interference occurs. There are at least three options to counteract or limit the interpulse interference. The most simple approach is to ensure that the pulse repetition interval is larger than the maximum excess delay of the propagation channel. This approach limits the maximum data rate, but should be considered whenever the communication system should have a low power consumption, a low complexity, or both. The second option assumes a Nyquist channel, for which it is possible to transmit data without any interpulse interference, given that the pulse repetition interval corresponds with the periodical zeros of the channel impulse response. Unfortunately the wireless communication channel is in general not a Nyquist channel. The third option considers the propagation channel as a linear filter, whose effects can be compensated by an equalization filter at the receiver. The equalization filter needs to be adjusted permanently to match the current propagation channel. The implementation of the equalization filter and the parameter estimation for its tuning increase the complexity of the receiver. The equalization filter provides the best performance and is the best choice for high data rate systems for which the complexity and the power consumption may be less important.

[6] A counter-example are solitons which may exist when the nonlinear and the dispersive effects in the medium are mutually compensated.

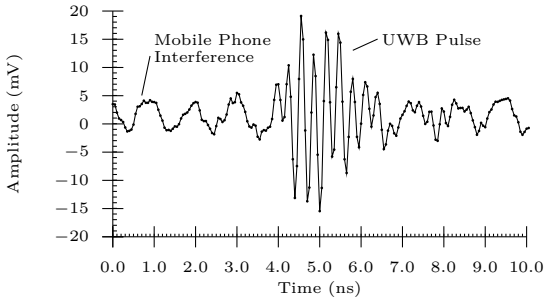

Figure 2.9: Pulse generated by AVM-2-C mixed with 3.5 GHz, 14 dBm carrier. Transmission over 1 m line-of-sight channel. Acquired with SDA6020 with 6 GHz input filter bandwidth, 50 Ω load, and 20 GS/s.

2.5 Summary

Impulse radio UWB relies on the generation and transmission of a signal composed of short duration pulses. Commonly the generated pulses are assumed to be of a Gaussian shape. The occupied bandwidth is mainly defined by the pulse shape. Among others, amplitude and delay modulations can be applied to UWB. A spreading code unique for each user may be used and is repeated for the transmission of each data symbol. The spreading code improves the robustness against multiuser and other interferences. A multipath model combined with an additive white Gaussian noise provides accurate predictions for realistic indoor propagation channels.

Bibliography

[And02] C. R. Anderson. *Design and Implementation of an Ultrabroadband Milimeter-Wavelength Vector Sliding Correlator Channel Sounder and In-Building Multipath Measurements at 2.5 & 60 GHz*. Ph.D. thesis, Virginia Polytechnic Institute and State University, May 2002.

[And03] H. R. Anderson. *Fixed Broadband Wireless: System Design*. John Wiley & Sons, 2003.

[Buc04] T. Buchegger, G. Oßberger, E. Hochmair, U. Folger, A. Reisenzahn, and A. Springer. “An Ultra Low Power Transcutaneous Impulse

Radio Link for Cochlea Implants". *International Workshop on Ultra Wideband Systems Joint with Conference on Ultra Wideband Systems and Technologies*, pp. 356–360. Kyoto, Japan, May 2004.

[Bue02] M. Buehrer, B. Davis, J. Reed, A. Safaai-Jazi, C. Dietrich, S. Riad, and D. Sweeney. "UWB Propagation Measurement and Modeling". Presentation at the DARPA NETEX Meeting, Jul. 2002.

[Bue04] R. M. Buehrer, A. Safaai-Jazo, W. Davis, and D. Sweeney. "Ultra-wideband Propagation Measurements and Modeling—Final Report". DARPA NETEX Program, Jan. 2004.

[Che04] M. S.-W. Chen and R. W. Brodersen. "The Impact of a Wideband Channel on UWB System Design". *Military Communications Conference*. Monterey, CA, USA, Nov. 2004.

[Cho04] C.-C. Chong, Y. Kim, and S.-S. Lee. "UWB Indoor Propagation Channel Measurements and Data Analysis in Various Types of High-Rise Apartments". *IEEE Vehicular Technology Conference*, vol. 1, pp. 150–154. Los Angeles, CA, USA, Sep. 2004.

[Chr03] L. P. B. Christensen. *Signal Processing for Ultra-Wideband Systems*. Master's thesis, Technical University of Denmark, 2003.

[Cra99] R. J.-M. Cramer, R. A. Scholtz, and M. Z. Win. "On the Analysis of UWB Communication Channels". *Military Communications Conference*, vol. 2, pp. 1191–1195. Atlantic City, NJ, USA, Nov. 1999.

[Cra02] R. J.-M. Cramer, R. A. Scholtz, and M. Z. Win. "Evaluation of an Ultra-Wide-Band Propagation Channel". *IEEE Transactions on Antennas and Propagation*, 50(5):561–570, May 2002.

[DB07] M.-G. Di Benedetto, L. De Nardis, G. Giancola, and D. Domenicali. "The Aloha Access (UWB)^2 Protocol Revisited for IEEE 802.15.4a". *ST Journal of Research*, 4(1):131–141, May 2007.

[FCC02] FCC Federal Communications Commission. "First Report and Order". Revision of Part 15 of the Commission's Rules Regarding Ultra-Wideband Transmission Systems, Apr. 2002.

[Foe03] J. R. Foerster, M. Pendergrass, and A. F. Molisch. "A Channel Model for Ultrawideband Indoor Communication". *IEEE Transactions on Wireless Communications*, 10(6):14–21, Dec. 2003.

[For05] A. Fort, C. Desset, J. Ryckaert, P. De Doncker, L. Van Biesen, and P. Wambacq. "Characterization of the Ultra Wideband Body Area Propagation Channel". *IEEE International Conference on Ultra-Wideband*, pp. 22–27. Zürich, Switzerland, Sep. 2005.

[Fri46] H. T. Friis. "A Note on a Simple Transmission Formula". *Proceedings of the IRE*, 34(5):254–256, May 1946.

[Gen05] S. Geng, S. Ranvier, X. Zhao, J. Kivinen, and P. Vainikainen. "Multipath Propagation Characterization of Ultra-wide Band Indoor Radio Channels". *IEEE International Conference on Ultra-Wideband*, pp. 11–15. Zürich, Switzerland, Sep. 2005.

[Gha02] M. Ghavami, L. B. Michael, S. Haruyama, and R. Kohno. "A Novel UWB Pulse Shape Modulation System". *Wireless Personal Communications, Kluwer Academic Publishers*, 23(1):105–120, Oct. 2002.

[Han03] K. Haneda and J. ichi Takada. "UWB Indoor Propagation Channel Measurement Based on Deterministic Approach". *URSI-F Meeting*. Tokyo, Japan, 2003.

[Hög74] J. A. Högbom. "Aperture Synthesis with a Non-Regular Distribution of Interferometer Baselines". *Astronomy and Astrophysics Supplement*, 15:417–426, Jun. 1974.

[Hov02] V. Hovinen and M. Hämäläinen. "Ultra Wideband Radio Channel Modelling for Indoors". *COST 273 Workshop: Opportunities of the Multidimensional Propagation Channel*. Espoo, Finland, May 2002.

[Kis01] W. A. Kissick. "The Temporal and Spectral Characteristics of Ultrawideband Signals". U.S. Departement of Commerce, Jan. 2001.

[Lee02] J.-Y. Lee. *Ultra-Wideband Ranging in Dense Multipath Environments*. Ph.D. thesis, University of Southern California, May 2002.

[Luo03] X. Luo, L. Yang, and G. B. Giannakis. "Designing Optimal Pulse-Shapers for Ultra-Wideband Radios". *Journal of Communications and Networks*, 5(4):344–353, Dec. 2003.

[Mic01] L. B. Michael, M. Ghavami, and R. Kohno. "Effect of Timing Jitter on Hermite Function Based Orthogonal Pulses for Ultra Wideband Communication". *Wireless Personal Multimedia Communications, 4th International Symposium on*. Aalborg, Denmark, 2001.

[Muq03] A. H. Muqaibel. *Characterization of Ultra Wideband Communication Channels*. Ph.D. thesis, Virginia Polytechnic Institute and State University, Mar. 2003.

[Pah98] K. Pahlavan, P. Krishnamurthy, and J. Beneat. "Wideband Radio Propagation Modeling for Indoor Geolocation Applications". *IEEE Communications Magazine*, 36(4):60–65, Apr. 1998.

[Qiu02] R. C. Qiu. "A Study of the Ultra-Wideband Wireless Propagation Channel and Optimum UWB Receiver Design". *IEEE Journal on Selected Areas in Communications*, 20(9):1628–1637, Dec. 2002.

[Rap02] T. Rappaport. *Wireless Communications: Principles and Practice*. Prentice Hall PTR, Pearson Education, Jan. 2002.

[Rid05] A. Ridolfi. *Power Spectra of Random Spikes and Related Complex Signals, with Application to Communications*. Ph.D. thesis, École Polytechnique Fédérale de Lausanne, 2005.

[Rom02] J. Romme and L. Piazzo. "On the Power Spectral Density of Time-Hopping Impulse Radio". *IEEE Conference on Ultra Wideband Systems and Technologies*. Baltimore, MD, USA, May 2002.

[Sal87] A. A. Saleh and R. A. Valenzuela. "A Statistical Model for Inddor Multipath Propagation". SAC-5(2):128–137, Feb. 1987.

[Sch05] H. Schantz. *The Art and Science of Ultra-Wideband Antennas*. Artech House Publishers, Jul. 2005.

[She03] A. U. Sheikh. *Wireless Communications: Theory and Techniques*. Springer, Nov. 2003.

[SJ02] A. Safaai-Jazi, S. M. Riad, A. Muqaibel, and A. Bayram. "Ultra-wideband Propagation Measurements and Channel Modeling, DARPA NETEX Program, Report on Through-the-Wall Propagation and Material Characterization". Virginia Polytechnic Institute and State University, Nov. 2002.

[Tah03] A. Taha. *Performance Considerations of Wireless Multiple-Access Digital Impulse Radio Under Realistic Multipath Channels*. Ph.D. thesis, University of Southern California, May 2003.

[TG404] TG4a channel modeling group. "IEEE 802.15.4a channel model—final report", Sep. 2004.

[Wel02] T. B. Welch, R. L. Musselman, B. A. Emessiene, P. D. Gift, D. K. Choudhury, D. N. Cassadine, and S. M. Yano. "The Effects of the Human Body on UWB Signal Propagation in an Idoor Environment". *IEEE Journal on Selected Areas in Communications*, 20(9):1778–1782, Dec. 2002.

[Win99] M. Z. Win. "Spectral Density of Random Time-Hopping Spread-Spectrum UWB Signals with Uniform Timing Jitter". *Military Communications Conference*, vol. 2, pp. 1196–1200. Atlantic City, NJ, USA, Nov. 1999.

[Win02] M. Z. Win and R. A. Scholtz. "Characterization of Ultra-Wide Bandwidth Channels: A Communication-Theoretic View". *IEEE Journal on Selected Areas in Communications*, 20(9):1613–1627, Dec. 2002.

[Xu00] H. Xu. *Terrestrial Radio Wave Propagation at Millimeter-Wave Frequencies*. Ph.D. thesis, Virginia Polytechnic Institute, May 2000.

[Zas05] T. Zasowksi, G. Meyer, F. Althaus, and A. Wittneben. "Propagation Effects in UWB Body Area Networks". *IEEE International Conference on Ultra-Wideband*. Zürich, Switzerland, Sep. 2005.

[Zas06] T. Zasowksi, G. Meyer, F. Althaus, and A. Wittneben. "UWB Signal Propagation at the Human Head". *IEEE Transactions on Microwave Theory and Techniques*, 54(4):1836–1845, Apr. 2006.

Chapter 3

Architecture Selection

In this chapter, some selected architectures for UWB transmitters and UWB receivers are presented. The transmitter architectures are presented as a literature survey. Due to the large number of proposed architectures for UWB receivers, the discussion has to be restricted to a non exhaustive assortment. The discussion starts with a short presentation of some incoherent receivers. Afterwards some coherent receivers are considered. Their presentation starts with a matched filter receiver. By applying a series of small modifications, a digital receiver using a modified redundant signed digit (RSD) ADC is derived. This receiver architecture is denoted as RSD receiver. Its performance is analyzed in the chapters 5 and 6.

3.1 Communication System

A digital communication system can be decomposed into constituting blocks, as represented in figure 3.1 [Pro01]. The source encoder reduces the redundancy of the data sequence to maximize the data throughput of the communication link. On the other hand, the channel encoder adds intentionally some redundancy to allow a detection or a correction of possible transmission errors. The digital modulator adapts the signal to the properties of the transmission channel. The receiver performs the inverse operations to reconstruct the transmitted data.

For an optimal source encoder, the data sequence $\{d_k\}$ does not contain any redundancy. In this thesis, the source encoder is not considered. Nevertheless it is assumed that the data sequence $\{d_k\}$ at the input of the

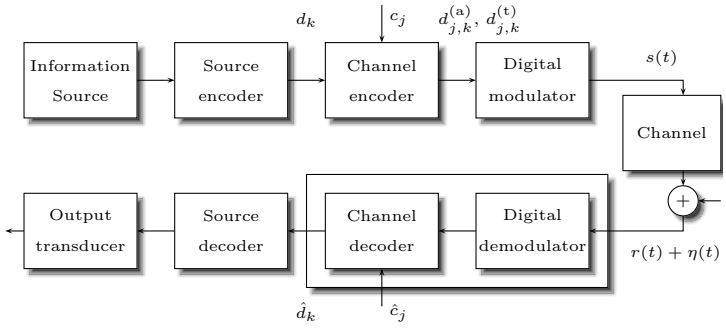

Figure 3.1: Constituting blocks of a digital communication system.

transmission system has maximum entropy, respectively does not contain any redundancy.

As mentioned in the section 2.1.3, the modulated signal (2.15) is entirely defined by the two sequences $\{d^{(a)}_{j,k}\}$ and $\{d^{(t)}_{j,k}\}$. These sequences are functions of the data symbols $\{d_k\}$ and the spreading sequence $\{c_j\}$. The spreading sequence is in general selected to be unique for each user. It reduces the sensitivity against different types of interferences, such as multiuser, wideband, and narrowband interference. Contrary to CDMA systems, where the spreading sequence increases the occupied bandwidth of the signal, the bandwidth is nearly independent of the sequence $\{c_j\}$ in IR, but is mostly defined by the pulse shape. For each couple (j, k) the digital modulator generates one pulse that is radiated by an antenna and propagates through the transmission channel. At the receiver, the electromagnetic wave is captured by an antenna. The antennas are not considered in this text. Theoretical and practical considerations about antennas for UWB applications can be found for example in [Sch05]. The captured signal is then processed by the digital demodulator and the channel decoder. These two blocks will not be considered individually in the following, but are considered as a single unit. This receiving unit outputs an estimation of the received data $\hat{d}_k$.

3.2 Transmitter Architecture and Implementation

A typical implementation of an UWB transmitter is shown in figure 3.2. The clock provides a periodical signal to a microcontroller or another digital con-

trol logic. The microcontroller generates an unmodulated, repetitive trigger signal, and the control signals for the amplitude modulation and the delay modulation of the individual pulses, $d_{j,k}^{(\mathrm{a})}$ and $d_{j,k}^{(\mathrm{t})}$ respectively. The trigger signal is then delayed accordingly to $d_{j,k}^{(\mathrm{t})}$. Finally, the pulse generator provides the radio frequency signal by generating a pulse with an amplitude or polarity that corresponds to $d_{j,k}^{(\mathrm{a})}$. All blocks, except the pulse generator, are standard components widely available on the market. Commercial pulse generators for UWB applications are available but are still relatively expensive devices at the moment. However, the technology for pulse generators is well known from applications such as laser drivers or devices for electromagnetic compatibility testing. In the next sections, some promising approaches to build a pulse generator are considered.

3.2.1 Pulse Generator Specifications

To select an architecture, it is required to define the specifications corresponding to the intended application. For a pulse generator, the basic characteristics are the shape of a pulse (e.g. its duration and amplitude), the pulse repetition frequency, and the output impedance.

Pulse duration: It has been shown in section 2.2, that the bandwidth is inversely proportional to the pulse duration. For a communication system, a short duration pulse compared to the pulse repetition period results in a low duty cycle signal. The low duty cycle may reduce the power consumption as several blocks of the transmitter or the receiver do not need to be enabled all the time. For a location system, the high bandwidth results in a high temporal and spatial resolution capability, important for an accurate location estimation in multipath propagation channels.

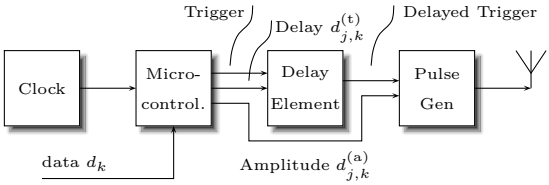

Figure 3.2: Transmitter block representation.

Pulse amplitude: The pulse amplitude is limited by the regulatory authorities as mentioned in section 1.4. For example, the FCC limits the emission of intentional radiators to 500 µV/m measured at a distance of 3 m in a 1 MHz bandwidth for frequencies between 3.1 GHz and 10.6 GHz, which corresponds to an emitted PSD of −41.3 dBm/MHz. For a signal with a bandwidth of 750 MHz and assuming that the spectrum uses the maximum PSD over the whole band, the average power is approximately 56 µW. The maximum power assuming a constant amplitude for 750 ps and zero amplitude for the remaining 99.25 ns is 7.5 mW. For an antenna with 50 Ω impedance, the voltage has to be roughly 0.61 V. While the assumptions used for this estimation do not match a real device, e.g., it is not possible to have a flat spectrum and a constant voltage, the order of magnitude of the pulse voltage provides a useful estimation also for realistic pulse generators.

Pulse repetition frequency: Increasing the pulse repetition frequency results in a higher maximum data rate. Furthermore, the synchronization is faster and the requirements for the clock accuracy are reduced. On the other hand, increasing the pulse repetition frequency results in a shorter inter-pulse interval. If the inter-pulse interval becomes smaller than the maximum excess delay of the propagation channel, inter-pulse interference results. For low data rate systems, the inter-pulse interference can be prevented by selecting a sufficiently low pulse repetition frequency. E.g. for typical indoor environments, a pulse repetition frequency of 10 MHz will lead to negligible amounts of inter-pulse interference.

Output impedance: The pulse generator should be compliant with the laboratory devices for radio frequency. All of them have a 50 Ω impedance.

3.2.2 Pulse Generator Technology

Pulse generators can be divided into power and low-power devices. Development of modern pulse power devices begun in the 1960s, when radiography sources based on Marx generators were built [Sch04]. For applications where pulses with high peak power is required, e.g., in plasma physics, pulsed power[1] is widely used [Mar92, Age98, Sch04]. Pulsed power devices are generating pulses with a rise time in the order of 100 ps and voltages of more

[1] Pulsed power describes the science and technology of accumulating energy over a relatively long period and releasing it quickly.

than 500 kV [Age98]. In general, they are restricted to repetition frequencies in the order of some Hz to kHz, and hence do not apply for short-range, civilian UWB systems. The latter require larger pulse repetition frequencies and lower pulse amplitudes. In the following, some pulse generation techniques proposed for UWB communications are presented. The techniques are classified for the following presentation in three categories. First, the direct generation techniques, where the emitted pulse is directly generated by sufficiently fast components. Second, the signal synthesis, where the pulse is composed by the superposition of several generation functions. Third, the up-conversion approach, where a baseband pulse is mixed with a carrier.

Direct generation: This category covers pulse generators, for which the pulse is generated directly using sufficiently fast components. It may be filtered subsequently to respect the regulatory spectrum restrictions. No local radio frequency oscillator or mixer is used, which allows low complexity implementations with low power consumption. In [Ger02], a second derivative Gaussian pulse generator using the nonlinear tanh transfer function of a bipolar transistor is proposed. In [Kim03], the vertical bipolar transistor available in a complementary metal-oxide-semiconductor (CMOS) process is used to generate a first and second derivative Gaussian pulse. A simulated peak to peak amplitude of less than 10 mV at 50 Ω is reported. In [Mar03b, Mar03a] a design with four CMOS transistors is presented. A two-input NAND gate, for which one input signal is inverted compared with the other one, generates a pulse with a duration given by the delay of the inverter. In [Jun05] the NAND gate is used with a subsequent pulse shaping circuit. It consists of a high pass filter to eliminate the low frequency components of the signal and a common source amplifier with a peaking inductor to improve the exploitation of the FCC spectral mask. In [Sto04], two NAND gates are used to generate two unipolar pulses. One of the pulses is delayed and subtracted from the other to obtain an approximation of a first derivative Gaussian pulse. In [Bag04], a triangular pulse generator generates a short duration signal. This signal is shaped in an active pulse shaping network to generate approximately a first derivative Gaussian pulse. The simulation predicts a minimum pulse width of about 250 ps and a peak to peak voltage of about 200 mV. A well known option for pulse shaping, building step signals, and comb generators, is given by the fast transition time of a step recovery diode [Hew84, Mit03, Han02, Rul04, Han06]. The step recovery diode has also been used in conjunction with avalanche transistors as pulse shaping

networks [Les94, Mia03, Han03]. This technique has been used in the heads of some sampling oscilloscopes, such as the Tektronix S1. Finally, in [Che04] an implementation of a passive UWB filter as irregular structured conductor on a printed circuit board is presented. Further discussions of the non-linear transmission lines can be found in [Cas93].

Signal synthesis: All signals of practical interest for UWB communications can be synthesized by the superposition of generating functions. The generating functions may be selected to be orthogonal or not. Fourier synthesis, i.e., the superposition of sinusoidal generating functions is proposed in [Gil94]. Walsh generating functions are proposed in [Har68,Har69]. In general, generating functions with an infinite duration may not be ideal to form a finite duration pulse by superposition. A large number of generating functions may be required to obtain the requested pulse signal. Furthermore, the generated signal is deterministic. To allow a modulation of non-predictable data, the generating functions may be time duration limited in practice. This can be sinusoidal functions with a limited duration or different functions. For example, in [Mat05] the UWB pulses are described as B-splines. In general, pulse generators based on signal synthesis can provide high pulse peak power, but are complex to implement.

Upconversion: For the generation of a bandpass pulse, the direct synthesis may not be well suited because it may need a pulse shaping with an associated loss of power. An alternative that avoids filtering is to upconvert a baseband pulse using a local radio frequency oscillator and a wideband mixer. This is an implementation corresponding to the mathematical formulation of the duration limited sinusoidal signals in section 2.1.1.

The advantage of this method is that it is possible to control the bandwidth by shaping the baseband signal and to adjust the center frequency by controlling the oscillator's frequency. The disadvantage is the increased power consumption due to the need of a local radio frequency oscillator and a wideband mixer. However the local oscillator is only operated during a short period. Such a pulse generator with 2 mW power consumption for pulses with 1 GHz bandwidth and 40 MHz pulse repetition frequency has been presented by Imec [Ryc05a, Ryc05b]. It was implemented in a 0.18 µm CMOS process. In [Fan06], a pulse generator for the 3.1 GHz to 5.1 GHz band is described. It is implemented in a 0.25 µm SiGe:C BiCMOS process. The pulse repetition interval is locked to the carrier frequency such that all pulses have

a constant phase and the same shape. A pulse generator with 4.5 GHz center frequency and an adjustable bandwidth has been designed in our laboratory and is currently under test.

3.2.3 Tested Pulse Generators

Experiments with laboratory equipment are performed during the execution of this work for the following two reasons.

- The critical issues for a communications system that deserve a deepened theoretical investigation can be identified.
- The developed theory and simulation models can be verified and improved if necessary.

For the time domain measurements a digital storage oscilloscope LeCroy SDA6020 and a fast pulse generator are used. The oscilloscope has a bandwidth of up to 6 GHz and a maximum sampling frequency of 20 GS/s. The advantage of the digital storage oscilloscope compared to a sampling oscilloscope is that transient, non stationary signals can be recorded and processed. The minimal delay between two acquisitions can be significantly reduced (from ms to µs) using a sequence mode. In the sequence mode the available memory is filled with the signals acquired at several successive triggering events before the signal is processed or shown on screen. Two pulse generators are available in our laboratory for the experiments and described below. Both provide approximately a Gaussian pulse to the transmitting antenna.

Bipolar transistor pulse generator: The bipolar transistor pulse generator shown in figure 3.3 is based on a design presented in [Wil91] and implemented in our laboratory. The bipolar transistor works in the avalanche region to discharge a small capacitor in a very short duration. The shape of a generated pulse from the bipolar transistor pulse generator is presented in figure 3.4. Due to the time required to recharge the capacitor, the pulse repetition frequency is limited to about 100 kHz. The pulse duration depends on the transistor and the equivalent series inductance of the capacitor.

Avtech AVM-2-C: The AVM-2-C pulse generator is a commercial device and produces pulses with a minimal rise time of about 100 ps and a pulse duration between 250 ps and 2 ns. The pulse repetition frequency can be as high as 25 MHz. A typical pulse generated by an AVM-2-C is presented in figure 3.5.

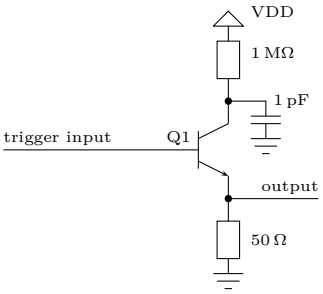

Figure 3.3: Avalanche pulse generator. VDD is typically between 100 V and 300 V. Q1 may be a device specified for avalanche operation or alternatively a low-cost device not specified for avalanche operation such as a 2N2369 or 2N4401.

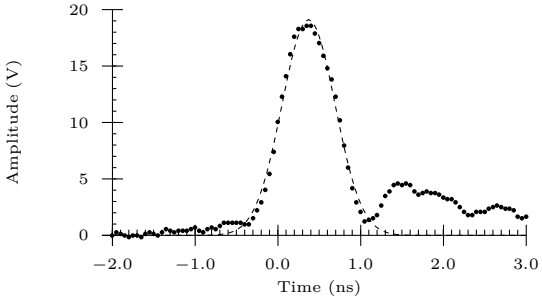

Figure 3.4: A pulse generated by the bipolar pulse generator seen by a 50 Ω charge. Sampled with the SDA6020 with a 6 GHz input filter bandwidth and 20 GS/s. The dashed line represents a Gaussian pulse with $t_n = 321$ ps.

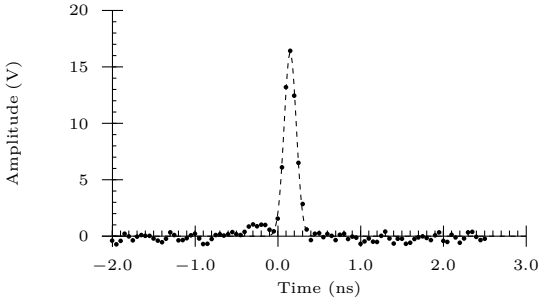

Figure 3.5: Pulse generated by Avtech AVM-2-C sampled with SDA6020 with 6 GHz input filter bandwidth at 20 GS/s. The dashed line represents a Gaussian pulse with $t_n = 73.5$ ps.

3.3 Receiver Architecture and Implementation

All the receiver architectures considered in the next sections can be decomposed into three elements as represented in figure 3.6. The received signal $r(t)$ is obtained at the output of the high frequency circuit, composed of a receiving antenna and an amplifier. A signal demodulator processes the received signal and provides an observation vector $\boldsymbol{d}_k[n]$. Possible implementations of the signal demodulator are considered in the next sections. The detector selects the most probable data symbol $\hat{d}_k$ based on the observation vector. Because of the assumption of the maximum entropy of the data sequence $\{d_k\}$ in section 3.1, all possible data symbols are equiprobable. For a memoryless data transfer in AWGN and a correlation receiver it is shown in [Pro01] that the optimal detector selects the index for which $\boldsymbol{d}_k[n]$ is maximal and $\boldsymbol{d}_k[n]$ is obtained by a correlation receiver as shown in section 3.3.2. In the following, the general block representation of a communication system is applied to incoherent and coherent receivers. The difference between the receivers is the algorithm by which the observation vector $\boldsymbol{d}_k[n]$ is calculated. The definitions of the terms coherent and incoherent are well known for narrowband communications. A receiver is considered coherent, if it requires phase synchronization [Raz98]. More precisely, a coherent receiver determines the phase of the sinusoidal signal carrying the message and uses the phase information to demodulate the message. If the receiver does not require phase synchronization, it is considered to be incoherent. For UWB, there may be no carrier and hence no phase information. The receiver is defined to be coherent, if it needs an a priori information for the data demodulation and it acquires this information during a synchronization phase. This can be an estimation of the received pulse shape, the phase of the spreading sequence, a time delay information between the transmitter and the receiver, or another property. The receiver is considered to be incoherent if it does not require additional information to be estimated during a

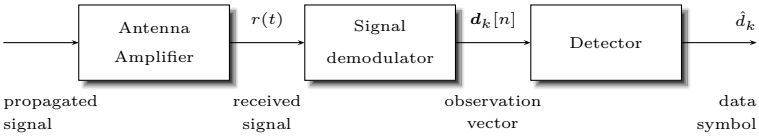

Figure 3.6: Receiver block representation.

synchronization phase.

3.3.1 Incoherent Receiver

In this section, the architectures of selected incoherent receivers are considered: the energy detection receiver, the rectifying receiver, the autocorrelation receiver, and the threshold receiver. For the last one, a novel approach for the data demodulation, called timestamp correlation algorithm, is presented.

Energy detection receiver: The energy detection receiver measures the energy contained in the received signal during a given time interval. It can be applied to delay modulated signals and to non-antipodal amplitude modulated ones. Figure 3.7 shows one of the possible implementations of an energy detection receiver for a delay-modulated signal. The received signal and the noise $r(t)+\eta(t)$ is squared and fed to time domain integrators. Each integrator estimates the received energy over one chip interval. The chip during which the received energy is maximum is assumed to contain the pulse. The number of branches N in the receiver corresponds to the number of values that the data symbol d_k can take, i.e., $d_k \in \{0, \ldots, N-1\}$. To limit the inter-pulse interference, the chip interval should be selected to be larger than the channel excess delay to avoid capturing energy during the following chips. For example, in the IEEE 802.15.4a standard [IEE07], the chip duration has been selected to be half of the frame duration. For the

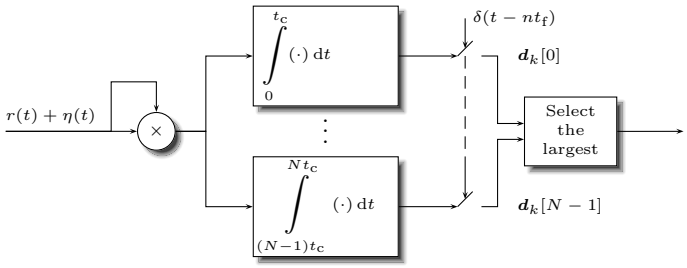

Figure 3.7: Energy detection receiver for pulse delay modulation and equiprobable data symbols.

energy detection receiver the elements of the observation vector are given by

$$\boldsymbol{d}_k[n] = \int_{(n-1)t_c}^{nt_c} \big(r(t) + \eta(t)\big)^2 \,\mathrm{d}t = \int_{(n-1)t_c}^{nt_c} \Big(r^2(t) + 2r(t)\eta(t) + \eta^2(t)\Big) \,\mathrm{d}t, \qquad (3.1)$$

where $n \in \{0, N-1\}$ denotes the receiver branch.

Rectifying receiver: Closely related to the energy detection receiver is the rectifying receiver. It is characterized by a half-wave or a full-wave rectification of the received signal. Rectifying receivers have been proposed using tunnel diodes and back diodes. A comparison of the sensitivity and the power consumption between a rectifying receiver and an energy detection receiver is presented in [Buc05, Buc04]. For the full wave rectifying receiver, the elements of the observation vector are

$$\boldsymbol{d}_k[n] = \int_{(n-1)t_c}^{nt_c} \big|r(t) + \eta(t)\big| \,\mathrm{d}t = \int_{(n-1)t_c}^{nt_c} \sqrt{(r(t) + \eta(t))^2} \,\mathrm{d}t. \qquad (3.2)$$

Autocorrelation receiver: An autocorrelation receiver for UWB communication systems to receive transmitted reference signals was proposed originally in [Hoc02]. Each symbol is transmitted by a pair of pulses. The first pulse is not modulated while the second one is modulated by the data symbol d_k. The delay between the two pulses should be selected to be greater than the channel excess delay and smaller than the channel coherence time. In this case, the distortion of the two pulses can be assumed to be similar and the pulses are correlated. The autocorrelation receiver uses the first pulse as a reference for the demodulation of the second pulse. The signal can be pulse-, delay-, or amplitude-modulated. An example of a receiver for a delay-modulated signal is represented in figure 3.8, where the delays are given by τ_{d_k}. The autocorrelation receiver does not require a channel equalization by adaptive filters or other means. Hence, it has a relatively low implementation complexity. For the receiver shown in figure 3.8, the elements of the observation vector are

$$\boldsymbol{d}_k[n] = \int_{0}^{t_f} [r(t) + \eta(t)] \cdot [r(t - \hat{\tau}_n) + \eta(t - \hat{\tau}_n)] \,\mathrm{d}t. \qquad (3.3)$$

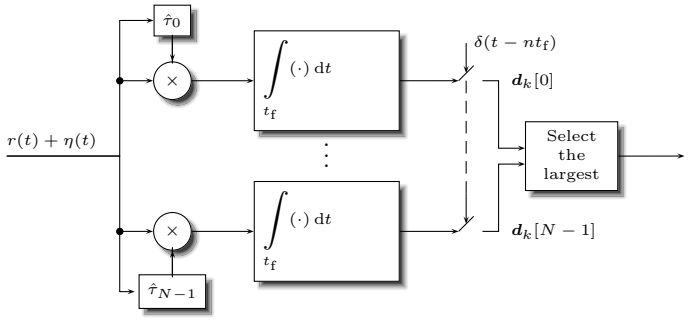

Figure 3.8: Autocorrelation receiver for a delay modulation between reference pulse and data pulse and equiprobable data symbols.

For the transmitted data symbol d_k and an AWGN propagation channel the received signal is $r(t) = p(t) + p(t - \tau_{d_k})$ plus additive noise. The noiseless observation vector is

$$\tilde{\boldsymbol{d}}_k[n] = \int_0^{t_f} (p(t) + p(t - \tau_{d_k}))(p(t - \hat{\tau}_n) + p(t - \hat{\tau}_n - \tau_{d_k}))\,\mathrm{d}t. \tag{3.4}$$

or

$$\begin{aligned}\tilde{\boldsymbol{d}}_k[n] = \int_0^{t_f} &(p(t)p(t - \hat{\tau}_n) + p(t)p(t - \hat{\tau}_n - \tau_{d_k}) + \\ &+ p(t - \tau_{d_k})p(t - \hat{\tau}_n) + p(t - \tau_{d_k})p(t - \tau_{d_k} - \hat{\tau}_n))\,\mathrm{d}t\end{aligned} \tag{3.5}$$

If the delays τ_n are larger than the pulse duration then (3.5) simplifies to

$$\tilde{\boldsymbol{d}}_k[n] = \int_0^{t_f} p(t - \tau_{d_k})p(t - \hat{\tau}_n)\,\mathrm{d}t = \begin{cases} R\mathcal{E}_\mathrm{p} & \text{if } n = d_k \\ 0 & \text{if } n \neq d_k \end{cases}. \tag{3.6}$$

It is noted from (3.6) that it is required that $\tau_{d_k} = \hat{\tau}_n$ for $d_k = n$. This means that the delay elements in the transmitter and the receiver need to be matched. Any mismatch of the delays will deteriorate the performance. The delays may be tuned once during the fabrication of the devices. It follows furthermore from (3.6) that the orthogonality of the elements of $\tilde{\boldsymbol{d}}_k[n]$ is

invariant to a change of the time variable $t \rightarrow t + \delta t$ as long as the pulses are still received during the integration interval. Hence, the autocorrelation receiver does not require an accurate synchronization in the order of the pulse duration (typically $\approx 1\,\text{ns}$), but only a data synchronization such that the pulses are still received during the integration interval (typically $\approx 100\,\text{ns}$).

Presented in the most simple form the autocorrelation receiver has some challenges to face. In the following, some of the them and ideas to improve the characteristics of the autocorrelation receiver are sketched.

- Because of the transmission of two pulses for each data symbol, the throughput is lower than for other receiver architectures. However, a differential signaling can be used with the autocorrelation receiver to increase the throughput. With differential signaling, each pulse transmits a data symbol and serves also as a reference for the consecutive pulse.
- The delays τ_{d_k} and $\hat{\tau}_n$ need to be adjusted accurately and are typically in the range of tens of nanoseconds. As the UWB radio signal is applied to the input of the delay element, they need to have a wide bandwidth. It is a challenging task to develop a delay element with all the above mentioned characteristics in an integrated circuit. A simple solution such as a coaxial cable with a given length is feasible. However this approach leads to a relatively large size of the receiver and an important power consumption because of the need of buffers to drive the cables. To avoid the delay element, alternative signaling schemes for the autocorrelation receiver have been proposed. For example, the reference pulse and the data pulse can be sent at the same time with a small offset of the center frequency [Zha06].
- The BER performance of the autocorrelation receiver in AWGN is suboptimal. This is due to at least two reasons. A noisy template is used for the correlation which increases the noise at the detector compared with a receiver that applies a locally generated template. Due to the non-linear transfer function, the autocorrelation receiver is susceptible to interference in general and intra- and inter-symbol interference specifically [Rom05]. However, it is noted that the autocorrelation receiver has a low implemented complexity and offers a BER performance comparable (in AWGN) or superior (immunity against narrowband interference) to an energy receiver. Further performance improvements are achievable at the cost of an increased complexity, e.g., by splitting the correlation interval to a number of shorter duration correlations,

which are then linearly combined [Leu05].

THRESHOLD RECEIVER: A threshold receiver detects when the received signal exceeds a given threshold voltage and triggers an event. The triggering event may be used to measure the TOA or another characteristic of the received signal. A threshold receiver based on tunnel diodes for UWB communication systems and for radio detection and ranging has been proposed [Fon01, Fon98]. The ambient noise and interference level is monitored and the bias of the tunnel detector adjusted to maintain a constant false alarm rate. The same bias control is also used to time gate the receiver. By adjusting the delay of the bias control with respect of the emission of an impulse, the radio detection and ranging system is only sensitive for echoes resulting from objects at a given distance.

A threshold receiver measuring the TOA can also be used for communication systems. It is assumed that the N_f pulses are coded using time delays, i.e., the transmission times are given by the sequence $\{T_{j,k}(d_k)\}$, with $j \in \{0, \ldots, N_\mathrm{f} - 1\}$ for the transmitter of interest. The receiver stores the TOAs of the received pulses as a sequence $\{\hat{T}_{i,k}\}$, with $i \in \{0, \ldots, \hat{N}_\mathrm{f}\}$ and compares it with the reference sequences $\{T_{j,k}(n)\}$ for all possible values of n to select the most probably received data symbol $\hat{d}_k$. $\hat{N}_\mathrm{f}$ is the number of received pulses and can be different from the number of transmitted pulses N_f. Interference may result in additional TOAs ($\hat{N}_\mathrm{f} > N_\mathrm{f}$) or undetected pulses ($\hat{N}_\mathrm{f} < N_\mathrm{f}$). In the following, two algorithms are presented. The first one uses a least squares estimation, the second one approximates a signal correlation but requires only the TOAs.

The least squares estimation has been proposed in [Mis07]. For the discussion of the least squares estimations it is assumed that $\hat{N}_\mathrm{f} = N_\mathrm{f}$. The least squares estimation compares the sequence of the measured TOAs $\{\hat{T}_{j,k}\}$ with the reference sequences $\{T_{j,k}(n)\}$ for all possible values of n by calculating

$$\boldsymbol{b}_k[n] = \sum_{j=0}^{N_\mathrm{f}-1} (\hat{T}_{j,k} - \Delta T - T_{j,k}(n))^2. \tag{3.7}$$

In a first step, the constant delay offset ΔT is estimated such that $\boldsymbol{b}_k[n]$ is minimal. In a second step, the most probable received symbol $\hat{d}_k$ will be detected. The constant delay offset is obtained with $\partial \boldsymbol{b}_k[n]/\partial \Delta T = 0$, which

results in

$$\Delta T = \frac{1}{N_\mathrm{f}} \sum_{j=0}^{N_\mathrm{f}-1} (\hat{T}_{j,k} - T_{j,k}(n)). \tag{3.8}$$

It is noted that the least squares estimation of the delay offset ΔT is given by an arithmetic average. After inserting (3.8) in (3.7) the most probable received data symbol $\hat{d}_k$ can be estimated using $\hat{d}_k = \arg\min_n \boldsymbol{b}_k[n]$. The least squares approach offers good performance if $\hat{N}_\mathrm{f} = N_\mathrm{f}$ and the error probability for the measurements $\hat{T}_{j,k}$ are Gaussian distributed. In this case, the performance equals to the one of the maximum likelihood estimation. However, both assumptions are not true in general.

In the following, an algorithm is presented that does neither require $\hat{N}_\mathrm{f} = N_\mathrm{f}$ nor assume a Gaussian error probability. Because the algorithm calculates an approximation of a signal correlation and is using the TOA estimations only, it will be called timestamp correlation algorithm. To derive the timestamp correlation algorithm we assume that the reference signals $\boldsymbol{s}[n]$ and the received signal $\boldsymbol{r}[n]$ with length N can be approximated by binary signals

$$\boldsymbol{s}[n] = \begin{cases} 1 & \text{if } n \in \{\lfloor T_{j,k}(d_k)/t_\mathrm{e} \rfloor\} \\ 0 & \text{otherwise} \end{cases}, \quad \boldsymbol{r}[n] = \begin{cases} 1 & \text{if } n \in \{\lfloor \hat{T}_{i,k}/t_\mathrm{e} \rfloor\} \\ 0 & \text{otherwise} \end{cases} \tag{3.9}$$

as illustrated in figure 3.9. The interval t_e is a reference interval to convert the arrival times to integer values and $\lfloor \cdot \rfloor$ is the floor operation. For time discrete systems, t_e is typically set equal to the sampling interval. The cyclic correlation[2] between the received signal and the reference signals is defined as a function of the offset m by

$$\boldsymbol{C}_{sr}[m] = \sum_{n=0}^{N-1} \boldsymbol{s}[n]\boldsymbol{r}[n \ominus_N m], \tag{3.10}$$

where $m \in \{0, \ldots, N-1\}$ and $\ominus_N$ is the subtraction modulo N. The correlation sequences $\boldsymbol{C}_{s_0 r}[m]$ and $\boldsymbol{C}_{s_1 r}[m]$ for two exemplary reference sequences $\boldsymbol{s}_0[n]$ and $\boldsymbol{s}_1[n]$ are also represented in figure 3.9. The elements of the observation vector are then calculated from the correlation sequences using

[2]The cyclic correlation reflects the repetitive nature of the code sequence for each symbol.

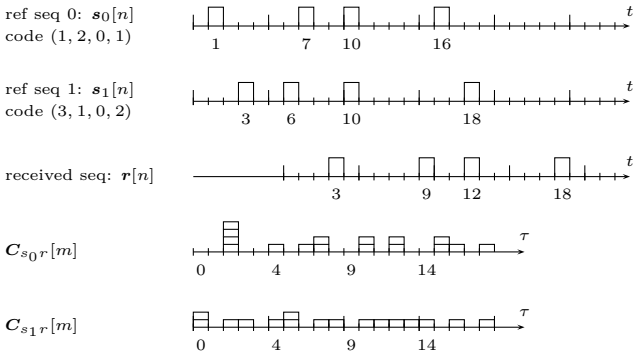

Figure 3.9: Numerical example of the cyclic correlation resulting for signals composed of rectangular pulses.

$\boldsymbol{d}_k[n] = \max_m \boldsymbol{C}_{s_n r}[m]$. Instead of calculating the time domain correlation between the signal $\boldsymbol{r}[n]$ and $\boldsymbol{s}[n]$ using (3.10) the correlation sequence can be obtained directly from the TOAs with the following algorithm.

```
Initialize C_{s_n r} with zero values
for j = 0 to N_f − 1
  for i = 0 to N̂_f − 1
    Calculate m = T̂_{i,k} ⊖_N T_{j,k}(d_k).
    Increment the value at C_{s_n r}[m]
  end i
end j
```

The above algorithm is iterated for each admissible value of n. For the same numerical example as given in the figure 3.9, the outcome of the algorithm is

$$\boldsymbol{C}_{s_0 r}[m] = (0, 0, 4, 0, 0, 1, 0, 1, 2, 0, 0, 2, 0, 2, 0, 0, 2, 1, 0, 1)^t, \quad \boldsymbol{d}[0] = 4 \tag{3.11a}$$

$$\boldsymbol{C}_{s_1 r}[m] = (2, 0, 1, 1, 0, 1, 2, 0, 1, 1, 0, 1, 1, 1, 1, 1, 0, 1, 0, 1)^t, \quad \boldsymbol{d}[1] = 2 \tag{3.11b}$$

as expected. The advantages of the timestamp correlation algorithm compared with the signal correlation are the following.

- The number of operations to calculate $\boldsymbol{C}_{s_n r}[m]$ is proportional to $\hat{N}_\mathrm{f} N_\mathrm{f}$. The required operations are one subtraction, one incrementation, and

one modulo operation. In particular neither multiplications nor divisions are required. The timestamp correlation algorithm can thus be written for efficient execution on microcontrollers, field programmable gate arrays, or integrated circuits.
- The timestamp correlation algorithm is robust against additional or missing pulses due to interference or multipath propagation.
- The timestamp correlation algorithm uses only the TOAs of the pulses. They can be stored and transfered to other devices using a few number of bytes. Therefore, the algorithm applies well to applications where the receiver sends the TOAs to an external device for the remaining signal processing.
- The elimination of the received pulse shape by the approximation by square pulses results in a performance loss in AWGN. In the presence of a strong interference, the timestamp correlation algorithm may be even more robust than a correlation receiver.

The timestamp correlation algorithm can be adjusted to specific situations. For example the robustness against timing jitter can be improved by incrementing not only the value at the position $m = \hat{T}_{i,k} \ominus_N T_{j,k}(d_k)$, but also the neighboring values by an amount smaller than or identical to 1. Finally it is noted that the values $T_{j,k}(d_k)$ and $\hat{T}_{i,k}$ may represent the TOAs of a burst of several pulses. In that case a signal processing resulting in an improvement of the signal to noise ratio (SNR) can be implemented prior to the threshold operation.

3.3.2 Coherent Receiver

A coherent receiver may use a local estimation of the received pulse shape or another property. Such a locally generated pulse shape is called the pulse template. The correlation between the pulse template and the received signal allows that the received signal energy is fully exploited and used for the demodulation. Hence, the pulse template can be considered as a mean to recollect the energy spread due to the multipath propagation channel. An example of a coherent receiver is a rake receiver that estimates the delay and amplitude of each of the multipath propagations using fingers. With error-free estimations, this results in the matched filter receiver. It is well known that the matched filter receiver and the correlation receiver minimize the BER in AWGN [Pro01]. However, the complexity of a coherent receiver, in particular the matched filter receiver, is greater than for the previously

considered incoherent receivers. In this section, we will describe a series of modifications to the correlation receiver leading to receiver with a moderate complexity, a near minimal BER performance in AWGN, and a high potential for a low power consumption implementation. A possible implementation will be presented in section 3.4.

Time reversed communication: The idea of the time reversed communication is to use the properties of the propagation channel to simplify the receiver architecture and implementation. In a first step the impulse response $h(t)$ of the propagation channel is measured. The transmitter then uses a pulse shape $p(t) = h(-t)$ for the communication. Without considering the noise, the received pulse shape is proportional to $p(t) * p(-t)$, which corresponds to the autocorrelation of a real-valued symmetric pulse. When the received signal is sampled at the correct instants, the measured amplitude corresponds directly to one element of the observation vector $\boldsymbol{d}_k[n]$ of a correlation receiver (see next section). Hence, the time reversed communication requires an accurate time synchronization. The use of the propagation channel as a matched filter requires also an accurate measurement of the channel impulse response and a highly accurate generation of arbitrary pulse shapes. Thus, the reduced complexity of the receiver implementation is traded against a more complex transmitter. More details of the time reversed communications can for example by found in [Qiu07].

Correlation receiver: A possible realization of the matched filter receiver, the correlation receiver, is shown in figure 3.10. In this case, the elements of the observation vector are given by

$$\boldsymbol{d}_k[n] = \int_{t_\mathrm{s}} [r(t) + \eta(t)]\hat{r}_n(t)\,\mathrm{d}t - R\mathcal{E}_n \tag{3.12a}$$

$$= \int_{t_\mathrm{s}} r(t)\hat{r}_n(t)\,\mathrm{d}t + \int_{t_\mathrm{s}} \eta(t)\hat{r}_n(t)\,\mathrm{d}t - R\mathcal{E}_n, \tag{3.12b}$$

where $\mathcal{E}_n$ is the energy of the nth data symbol. In the first integral the correlation value between the received signal $r(t)$ and the reference signals $\hat{r}_n(t)$ is calculated for a time delay $\tau = 0$. The correlation value is maximum and equal to $\mathcal{E}_n$ for $r(t) = \hat{r}_n(t)$. Hence, the maximum correlation value is obtained for the receiver branch n that corresponds to the transmitted symbol d_k and for a synchronized system. For all other branches the correlation

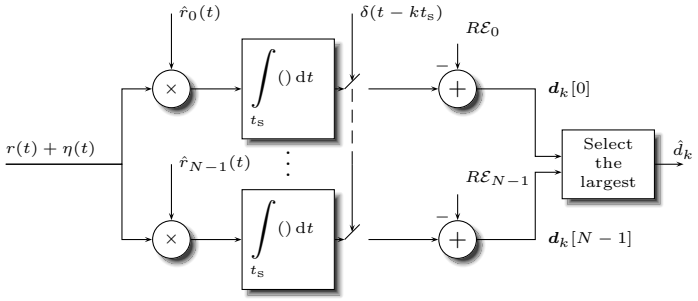

Figure 3.10: Correlation receiver. The received signal is correlated with a symbol duration template.

value is smaller. It may be 0 for orthogonal communications, $-\mathcal{E}_n$ for antipodal communications, or take another value. Often, all the signals $\hat{r}_n(t)$ have the same symbol energy. In that case, the subtraction of the energies $\mathcal{E}_n$ in all branches of the receiver is void. Assuming furthermore a binary modulation $N = 2$ the matched filter receiver can be simplified and is represented in figure 3.11.

In (2.15) it is shown that the considered modulations (AH-AM, AH-TM, THM-AM, THM-TM) can all be written as a sum of pulses. For the kth data symbol, the received signal is

$$r(t) = \sum_{j=0}^{N_\mathrm{f}-1} d_{j,k}^{(\mathrm{a})} q(t - jt_\mathrm{f} - d_{j,k}^{(\mathrm{t})} t_\mathrm{c}). \tag{3.13}$$

The template signal in the nth branch of the receiver can be selected to be

$$\hat{r}_n(t) = \sum_{j=0}^{N_\mathrm{f}-1} \hat{d}_{j,n}^{(\mathrm{a})} \hat{q}_n(t - j\hat{t}_\mathrm{f} - \hat{d}_{j,n}^{(\mathrm{t})} \hat{t}_\mathrm{c}). \tag{3.14}$$

where $\hat{d}_{j,n}^{(\mathrm{a})}$ and $\hat{d}_{j,n}^{(\mathrm{t})}$ are the nth reference sequences and $\hat{t}_\mathrm{f}$ and $\hat{t}_\mathrm{c}$ are the receiver's durations for the frame and the chip respectively. In the following an equivalent, yet novel, architecture is derived. To simplify the notation, the noise term is not written during the development, but only re-introduced

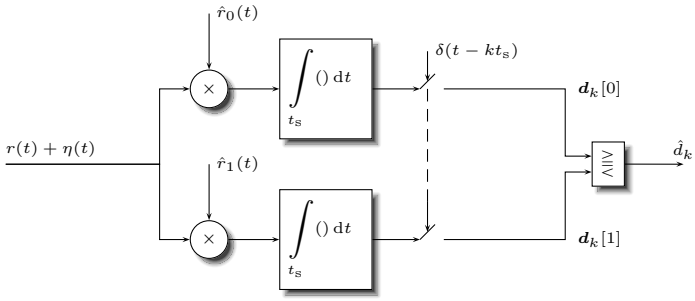

Figure 3.11: Variation of the correlation receiver for equiprobable binary data symbols with equal energy.

at the end. The elements of the noiseless observation vector are

$$\tilde{\boldsymbol{d}}_k[n] = \int_0^{t_\mathrm{s}} \left[r(t)\hat{r}_n(t) \right] \mathrm{d}t \tag{3.15}$$

We assume that the accumulated timing error due to a difference between t_f and $\hat{t}_\mathrm{f}$ is smaller than the frame duration t_f. In this case the result after inserting (3.13) and (3.14) in (3.15) and keeping only the non-zero contributions is given by

$$\tilde{\boldsymbol{d}}_k[n] = \int_0^{t_\mathrm{s}} \left[\sum_{j=0}^{N_\mathrm{f}-1} d_{j,k}^{(\mathrm{a})} \hat{d}_{j,n}^{(\mathrm{a})} q(t - jt_\mathrm{f} - d_{j,k}^{(\mathrm{t})} t_\mathrm{c}) \hat{q}_n(t - j\hat{t}_\mathrm{f} - \hat{d}_{j,n}^{(\mathrm{t})} \hat{t}_\mathrm{c}) \right] \mathrm{d}t \tag{3.16}$$

For a synchronized system the code sequence at the receiver matches the one from the transmitter and the outcome of $d_{j,k}^{(\mathrm{a})} \hat{d}_{j,n}^{(\mathrm{a})}$ is either $+1$ for all j or -1 for all j. We assume without loss of generality that the pulse template $q_n(t)$ is defined such that the multiplied amplitudes are all positive. In that case the multiplied amplitudes $d_{j,k}^{(\mathrm{a})} \hat{d}_{j,n}^{(\mathrm{a})}$ vanish. Because of the finite duration of the pulses, the terms $q(t)\hat{q}(t - \epsilon_j)$ for which the delay ϵ_j is larger than the pulse duration are zero and (3.16) can be written using two summations as

$$\tilde{\boldsymbol{d}}_k[n] = \int_0^{t_\mathrm{s}} \left[\sum_{j=0}^{N_\mathrm{f}-1} q(t - jt_\mathrm{f} - d_{j,k}^{(\mathrm{t})} t_\mathrm{c}) \sum_{j=0}^{N_\mathrm{f}-1} \hat{q}_n(t - j\hat{t}_\mathrm{f} - \hat{d}_{j,n}^{(\mathrm{t})} \hat{t}_\mathrm{c}) \right] \mathrm{d}t. \tag{3.17}$$

When applying a common time shift $j\hat{t}_\mathrm{f} + \hat{d}_{j,n}^{(\mathrm{t})}\hat{t}_c$ to both summations, all the pulses are all located in the first frame. It is sufficient to integrate over the first frame and (3.17) becomes

$$\tilde{\boldsymbol{d}}_k[n] = \int_0^{t_\mathrm{f}} \left[\sum_{j=0}^{N_\mathrm{f}-1} q(t - jt_\mathrm{f} - d_{j,k}^{(\mathrm{t})}t_\mathrm{c} + j\hat{t}_\mathrm{f} + \hat{d}_{j,n}^{(\mathrm{t})}\hat{t}_\mathrm{c}) \sum_{j=0}^{N_\mathrm{f}-1} \hat{q}_n(t) \right] \mathrm{d}t. \tag{3.18}$$

The second sum is $N_\mathrm{f}\hat{q}(t)$ and hence

$$\tilde{\boldsymbol{d}}_k[n] = N_\mathrm{f} \int_0^{t_\mathrm{f}} \hat{q}_n(t) \left[\sum_{j=0}^{N_\mathrm{f}-1} q(t - jt_\mathrm{f} + j\hat{t}_\mathrm{f}) - d_{j,k}^{(\mathrm{t})}t_\mathrm{c} + \hat{d}_{j,n}^{(\mathrm{t})}\hat{t}_\mathrm{c}) \right] \mathrm{d}t. \tag{3.19}$$

Including the noise and using $\tau_j = jt_\mathrm{f} + d_{j,k}^{(\mathrm{t})}t_\mathrm{c}$ and $\hat{\tau}_j = j\hat{t}_\mathrm{f} + \hat{d}_{j,n}^{(\mathrm{t})}$, the result is

$$\boldsymbol{d}_k[n] = \underbrace{N_\mathrm{f} \int_0^{t_\mathrm{f}} \underbrace{\left[\sum_{j=0}^{N_\mathrm{f}-1} q(t - \tau_j + \hat{\tau}_j) \right]}_{\substack{\text{summed signal} \\ q_\mathrm{sum}(t)}} \hat{q}_n(t)\,\mathrm{d}t}_{\text{noisefree correlation value } \tilde{\boldsymbol{d}}[n]} + \underbrace{N_\mathrm{f} \int_0^{t_\mathrm{f}} \underbrace{\left[\sum_{j=0}^{N_\mathrm{f}-1} \eta(t + \hat{\tau}_j) \right]}_{\substack{\text{summed noise} \\ \eta_\mathrm{sum}(t)}} \hat{q}_n(t)\,\mathrm{d}t}_{\text{colored noise}} \tag{3.20}$$

Assuming that $\eta(t)$ is a white Gaussian noise process of zero mean and variance $\mathcal{N}_0/2$, the summed noise $\eta_\mathrm{sum}(t)$ is also a white Gaussian noise process of zero mean and variance $N_\mathrm{f}\mathcal{N}_0/2$.

The block diagram of the receiver architecture described by (3.20) is shown in figure 3.12. The received pulses are first coherently combined and subsequently correlated with the pulse templates $\hat{q}_0(t)$ and $\hat{q}_1(t)$. It is noted that in a practical system it may not be required to implement two independent branches for the two correlations. For antipodal amplitude modulation (AM) where $\hat{q}_1(t) = -\hat{q}_0(t)$ a single branch is sufficient. For orthogonal time modulation (TM) it is sufficient to calculate a single correlation using the template $\hat{q}_0(t) - \hat{q}_1(t)$. In both cases, the sign of the correlation value is used to detect the most probably received symbol. For clarity such optimizations of the implementation are not yet considered. The observation vector is still updated at the symbol frequency. An implementation using

analog circuits is difficult because memory elements are required to store the intermediate results of the coherent addition of the pulses. Possible solutions, such as an analog yet time discrete memory based on a charge coupled device, have a high power consumption and may decrease the SNR.

Digital receiver: The memory elements required for the implementation of a receiver described in (3.20) could be standard digital elements, if the signal is digitized before. The block diagram of the resulting receiver is shown in figure 3.13. However, this implementation requires a fast ADC with a high sampling frequency and a fast memory. The high sampling frequency results in an important power consumption of such a receiver. One approach to lower the sampling frequency consists in combining the coherent addition, the memory element, and the conversion unit into a single element. A modified redundant signed digit (RSD) ADC is a promising candidate to incorporate the coherent addition as a part of the analog to digital conversion algorithm. In the following, a RSD receiver based on modified RSD ADC is shown.

3.4 RSD Receiver

In this section, the architecture and the working principles of the RSD receiver are presented. The RSD receiver is one possible implementation of a receiver that coherently adds the received pulses before correlating the summed signal with a pulse template. The performance of this category of receivers is estimated in the chapters 5 and 6.

3.4.1 Architecture

The block representation of the RSD receiver is shown in figure 3.14. The signal processing, e.g., a correlation with a pulse template and the algorithms for the decision unit, can be implemented on a central processing unit, a digital signal processor, a field programmable gate array, or another digital device. The corresponding block representation is shown in figure 3.15. The element containing the ADC is denoted as the conversion block and will be considered in section 3.4.3. Compared with the analogous correlation receiver, the digital processing unit may provide higher flexibility. For example an arbitrary template for the correlation can be generated. The digital processing unit may even have some reconfigurability, such that it can be used for comparing the performance of different demodulation algorithms.

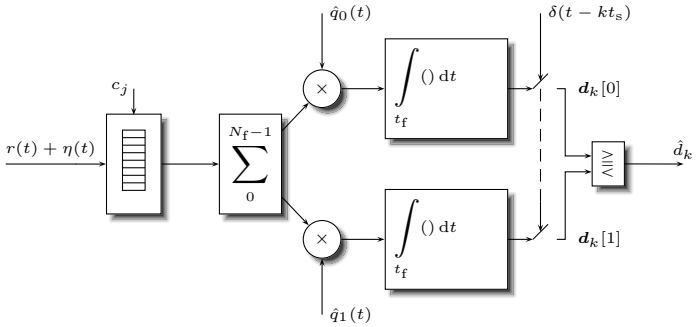

Figure 3.12: Variation of the correlation receiver for equiprobable binary data symbols with equal energy using an analog memory element and coherent pulse combining. The summed signal is correlated with a frame duration template.

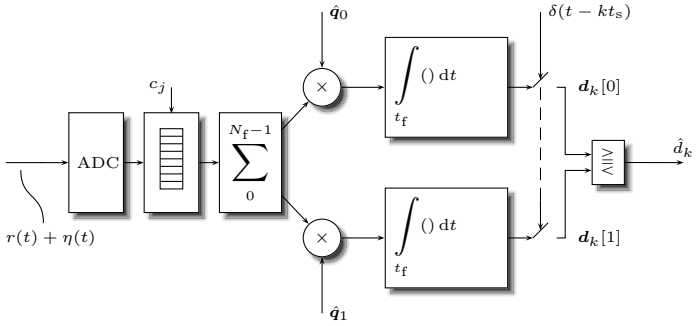

Figure 3.13: Digital implementation of the correlation receiver using a coherent pulse combining.

3.4.2 Coherent Addition

The coherent addition of the pulses in (3.20) is

$$q_{\text{sum}}(t) = \sum_{j=0}^{N_f-1} q(t - \tau_j + \hat{\tau}_j). \tag{3.21}$$

The working principle of a receiver using the coherent addition (3.21) is illustrated in figure 3.16. In this example, the received signal $r(t)$ is composed of four pulses. The receiver is able to acquire and store the signal during a

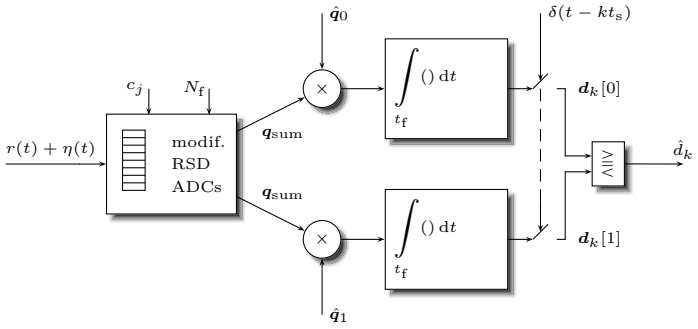

Figure 3.14: A correlation receiver with coherent pulse combining using modified RSD ADCs.

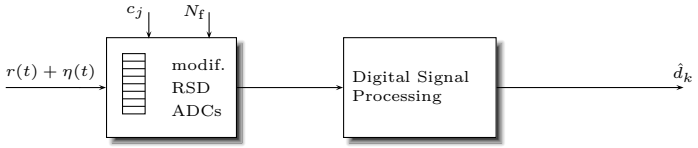

Figure 3.15: Digital implementation of a receiver using modified RSD ADCs.

short period, resulting in the acquisition windows $w_{j,k}(t)$. All the acquisition windows $w_{j,k}(t)$ are then combined to obtain the summed signal

$$w_k(t) = \sum_{j=0}^{N_\mathrm{f}-1} w_{j,k}(t). \tag{3.22}$$

In the RSD receiver, the coherent addition is made as a part of the analog to digital conversion algorithm (see section 3.4.4). For each sample during the acquisition window one dedicated modified RSD ADC is used. During the first acquisition window, the voltage of the input signal at the sampling instant is transferred to a capacitor in the ADC. During the second and all the following acquisition windows, the input voltage at the sampling instant is added to the voltage already stored on the capacitor. Finally, the outcome

of each ADC is one element of the summed signal

$$\boldsymbol{q}_{\mathrm{sum}}[n] = \boldsymbol{w}_k[n] = \sum_{j=0}^{N_\mathrm{f}-1} \boldsymbol{w}_{j,k}[n]. \tag{3.23}$$

Considering (3.21) it is noted that the addition of the acquisition windows is coherent only for $\hat{\tau}_j = \tau_j$. This means that the instant when the acquisition of the signal occurs needs to be accurately controlled. This instant depends among others on the spreading code sequence $\{c_j\}$. A possible implementation of the block containing the modified RSD ADCs is considered in the next section.

3.4.3 Implementation of the conversion block

The conversion block in figure 3.15 receives the signal $r(t)+\eta(t)$ and provides the summed, sampled, digital signal $\boldsymbol{q}_{\mathrm{sum}}[n]$. A possible implementation of this block is shown in figure 3.17. The received signal is transferred to several time interleaved modified RSD ADCs. Each ADC stores and adds a sample with a given delay with respect to the beginning of the acquisition window. At the end of the conversion each ADC contains one element of the summed signal $\boldsymbol{q}_{\mathrm{sum}}[n]$. The sampling interval is given by the delay t_e of the internal clock $\mathrm{CLK}_\mathrm{int}$ between the ADCs. The internal clock provides a trigger signal to mark the beginning of the acquisition window. This task requires an information of the spreading code $\hat{c}_j$ and the chip duration $\hat{t}_\mathrm{c}$. The external clock provides a signal at the frame rate. The external clock is then delayed accordingly to the spreading code.

3.4.4 Implementation of a single converter

As already mentioned, several ADCs in a time-interleaved mode are used for the receiver implementation. Each ADC has a memory element to store one sample of the signal $\boldsymbol{q}_{\mathrm{sum}}[n]$. The memory element is implemented as a capacitor where a charge can be stored. Generally speaking, the RSD ADC is a variant of the algorithmic ADC. The RSD algorithm performs a comparison against two threshold levels and provides a ternary result (-1,0, and 1) as result for each conversion step [Ust03]. The number of times that the thresholds are exceeded is counted and converted in a digital representation of the sampled voltage. In the following, two modes of operation of the modified RSD ADC and their application to UWB are considered more in detail.

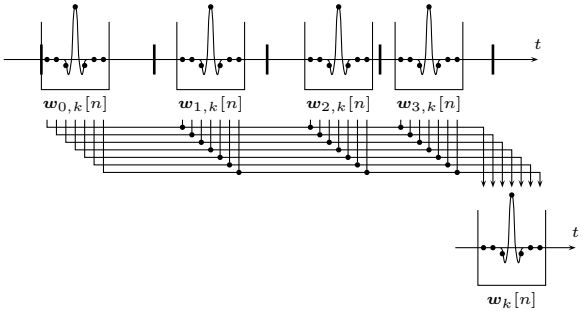

Figure 3.16: Schematic representation of coherent addition of a sampled limited windows of a received signal with a delay modulation.

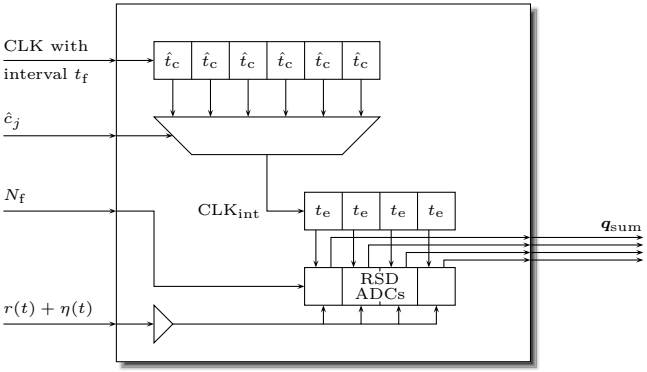

Figure 3.17: Implementation of the code demodulation and the coherent addition in a RSD ADC receiver.

Adding mode: The adding mode is responsible for the coherent addition of the received pulses. A flow diagram of the algorithm used during the adding mode is shown in figure 3.18. For the initialization, the input voltage (after a track and hold circuit) v_in is transferred to the capacitor and stored as v_x. The voltage v_x is then compared to a threshold voltage v_th. When the threshold is exceeded ($v_x/v_\mathrm{th} > 1$) a given voltage v_a is subtracted from v_x and the output of the conversion cell provides a signal $b_i = 1$. When a negative threshold is exceeded ($v_x/v_\mathrm{th} < -1$) a given voltage is added and the output provides a signal $b_i = -1$. If the voltage v_x does not exceed any threshold,

the output is $b_i = 0$. As a next step the counter i is increased and a new input voltage v_{in} is added to the stored voltage v_x. If all the pulses are added the process stops. Otherwise the stored voltage is again compared against the threshold and the acquisition and conversion operations are repeated. The output sequence $\{b_i\}$ is measured for the average input voltage $\langle v_{\text{in}} \rangle$ present during the acquisitions. The average input voltage can be calculated using

$$\langle v_{\text{in}} \rangle = \frac{v_a}{N_{\text{f}}} \sum_{i=0}^{N_{\text{f}}-1} b_i \tag{3.24}$$

if $v_{\text{th}} \leq v_a \leq 2v_{\text{th}}$. It is noted, that the average input voltage is proportional to the average value of b_i. Hence, to increase the resolution of the input voltage measurement by one bit, N_{f} has to be doubled. Hence, for the acquisition of 16 pulses the result is coded on 4 bit. The adding mode alone may require a prohibitively large number of pulses to provide a sufficient resolution. However, the adding mode may be used in combination with the doubling mode described below. It is noted that the coherent addition of the pulses does not require any hardware other then the one already available by the ADC. Furthermore the modified RSD ADC allows to use a small capacitor resulting in a good sensitivity without a reduction of the full scale range.

Doubling mode: The doubling mode can increase the resolution of the resulting digital value without the need to increase the number of pulses per symbol. A flow diagram for the doubling mode algorithm is shown in figure 3.19. It is noted that the algorithm is very similar to the adding mode. It is assumed for the doubling mode that the voltage to be converted is already transferred and stored on the internal capacitor. The main difference compared to the adding mode is that for each cycle the internal voltage is doubled $v_x \Leftarrow 2v_x$. The number of cycles I is independent of the number of pulses per symbols. For each additional cycle the resolution increases by one bit. The reconstruction of the voltage initially stored on the capacitor is given by

$$v_x = v_a \sum_{i=0}^{I-1} b_i 2^{-i}. \tag{3.25}$$

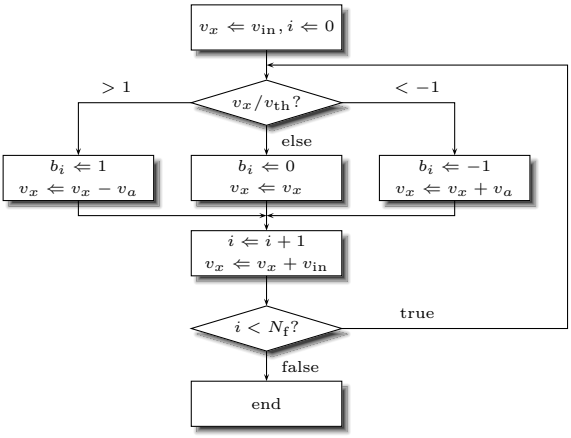

Figure 3.18: Flow diagram for the algorithm used in the RSD ADC during the adding mode.

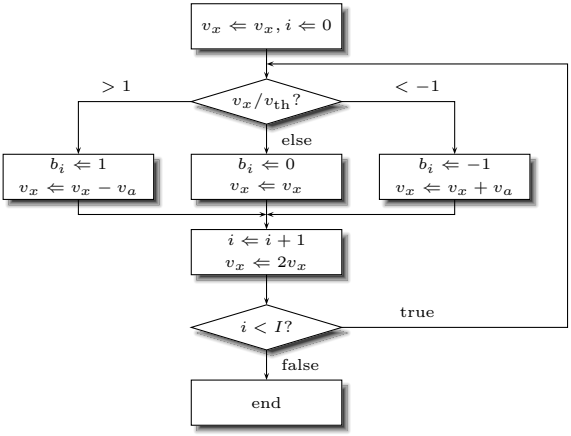

Figure 3.19: Flowchart for the algorithm used in the RSD ADC during the doubling mode.

THROUGHPUT: The best strategy to maximize the throughput for a given N_f is to use the adding mode for the reception of the N_f pulses and to switch to the doubling mode until the required resolution is obtained. Table 3.1 shows the resulting maximum data throughput in kSymbol/s for a given pulse repetition rate. The number of pulses N_f is arranged horizontally, the required resolution in bits vertically.

3.5 Summary

A fast pulse generator is required for the implementation of a transmitter. For typical average output power for UWB communications, a pulse generator may be implemented using a standard CMOS process resulting in low cost and low power devices.

The receiver architectures can be classified into incoherent and coherent ones. An incoherent receiver may result in a simplification of the synchronization and tracking algorithms, but may typically not achieve a bit error rate as low as the one of a coherent receiver. In this chapter, a receiver architecture based on a modified redundant signed digit (RSD) ADC which has a near optimal BER performance has been presented. It is tailored for a low power consumption when implemented in a CMOS process.

Bibliography

[Age98] F. J. Agee, C. E. Baum, W. D. Prather, J. M. Lehr, J. P. O'Laughlin, J. W. Burger, J. S. H. Schoenberg, D. W. Scholfield, R. J. Torres, J. P. Hull, and J. A. Gaudet. "Ultra-Wideband

		Pulses per symbol N_f							
		1	2	4	8	16	32	64	128
ADC Res. (bit)	1	10000	—	—	—	—	—	—	—
	2	5000	5000	—	—	—	—	—	—
	3	3333	3333	2500	—	—	—	—	—
	4	2500	2500	2000	1250	—	—	—	—
	5	2000	2000	1667	1111	625	—	—	—
	6	1667	1667	1429	1000	588	313	—	—
	7	1429	1429	1250	909	556	303	156	—
	8	1250	1250	1111	833	526	294	154	78

Table 3.1: Maximum datarate in kSymbol/s for 10 MPulses/s

Transmitter Research". *IEEE Transactions on Plasma Science*, 26(3):860–873, Jun. 1998.

[Bag04] S. Bagga, W. A. Serdijn, and J. R. Long. "A PPM Gaussian Monocycle Transmitter for Ultra-Wideband Communications". *International Workshop on Ultra Wideband Systems Joint with Conference on Ultra Wideband Systems and Technologies*, pp. 130–134. Kyoto, Japan, May 2004.

[Buc04] T. Buchegger, G. Oßberger, E. Hochmair, U. Folger, A. Reisenzahn, and A. Springer. "An Ultra Low Power Transcutaneous Impulse Radio Link for Cochlea Implants". *International Workshop on Ultra Wideband Systems Joint with Conference on Ultra Wideband Systems and Technologies*, pp. 356–360. Kyoto, Japan, May 2004.

[Buc05] T. Buchegger, G. Oßberger, A. Reisenzahn, E. Hochmair, A. Stelzer, and A. Springer. "Ultra-Wideband Transceivers for Cochlear Implants". *EURASIP Journal on Applied Signal Processing*, 18:3069–3075, 2005.

[Cas93] M. G. Case. *Nonlinear Transmission Lines for Picosecond Pulse, Impulse and Millimeter-Wave Harmonic Generation*. Ph.D. thesis, University of California, Santa Barbara, Jul. 1993.

[Che04] S. L. Chernyshev. "UWB Signals Processing and Forming on Irregular Structures". *IEEE Conference on Circuits and Systems for Communications*. Moscow, Russia, Jul. 2004.

[Fan06] X. Fan, G. Fischer, and B. Dietrich. "An Integrated 3.1-5.1 GHz Pulse Generator for Ultra-Wideband Wireless Localization Systems". *Advances in Radio Science – Kleinheubacher Berichte*, 4:247–250, 2006.

[Fon98] R. J. Fontana, J. F. Larrick, J. E. Cade, and E. Rivers. "An Ultra Wideband Synthetic Vision Sensor for Airborne Wire Detection". *Proceedings of the SPIE Enhanced and Synthetic Vision*. Orlando, FL, USA, Apr. 1998.

[Fon01] R. J. Fontana, F. Larrick, and E. Cade. "UWB Dual Tunnel Diode Detector for Object Detection, Measurement, or Avoidance". United States Patent 6'239'741, May 2001.

[Ger02] J. Gerrits and J. Farserotu. "Wavelet Generation Circuit for UWB Impulse Radio Applications". *Electronics Letters*, 38(25), Dec. 2002.

[Gil94] G. Gill, H. Chiang, and J. Hall. "Waveform Synthesis for Ultra Wideband Radar". *IEEE Conference on Radar*, pp. 240–245, 1994.

[Han02] J. Han and C. Nguyen. "A New Ultra-Wideband, Ultra-Short Monocycle Pulse Generator With Reduced Ringing". *IEEE Microwave and Wireless Components Letters*, 12(6):206–208, Jun. 2002.

[Han03] J.-W. Han, M. Miao, and C. Nguyen. "Recent Development of SRD- and FET-Based Sub-Nanosecond Pulse Generators for Ultra-Wideband Communications". *IEEE Topical Conference on Wireless Communication Technology*. Honolulu, HI, USA, Oct. 2003.

[Han06] J. Han and C. Nguyen. "On the Development of a Compact Sub-Nanosecond Tunable Monocycle Pulse Transmitter for UWB Applications". *IEEE Transactions on Microwave Theory and Techniques*, 54(1):285–293, Jan. 2006.

[Har68] H. F. Harmuth. "A Generalized Concept of Frequency and Some Applications". *IEEE Transactions on Information Theory*, IT-14(3):375–381, May 1968.

[Har69] H. F. Harmuth. "Applications of Walsh Functions in Communications". *IEEE Spectrum*, Nov. 1969.

[Hew84] Hewlett Packard. "Pulse and Waveform Generation with Step Recovery Diodes". Application Note 918, Oct. 1984.

[Hoc02] R. T. Hoctor and H. W. Tomlinson. "An Overview of Delay-Hopped, Transmitted-Reference RF Communications". General Electric Research & Development Center, Jan. 2002.

[IEE07] IEEE Computer Society. "Part 15.4: Wireless Medium Access Control (MAC) and Physical Layer (PHY) Specifications for Low-Rate Wireless Personal Area Networks (WPANs)". IEEE Std 802.15.4a^{TM}-2007, Aug. 2007.

[Jun05] B. Jung, Y.-H. Tseng, J. Harvey, and R. Harjani. "Pulse Generator Design For UWB IR Communication Systems". *IEEE Symposium on Circuits and Systems*, pp. 4381–4384. Kobe, Japan, May 2005.

[Kim03] H. Kim, D. Park, and Y. Joo. "Design of CMOS Scholtz's Monocycle Pulse Generator". *IEEE Conference on Ultra Wideband Systems and Technologies*, pp. 81–85. Reston, VA, USA, Nov. 2003.

[Les94] M. J. Lesha and F. J. Paoloni. "Generation of Balanced Subnanosecond Pulses Using Step-Recovery Diodes". *IEE Electronic Letters*, 31(7):510–511, Mar. 1994.

[Leu05] G. Leus and A.-J. van der Veen. "A Weighted Autocorrelation Receiver for Transmitted Reference Ultra Wideband Communications". *IEEE Workshop on Signal Processing Advances in Wireless Communications*. New York City, NY, USA, Jun. 2005.

[Mar92] J. C. Martin. "Nanosecond Pulse Techniques". *Proceedings of the IEEE*, 80:934–945, Jun. 1992.

[Mar03a] K. Marsden, H.-J. Lee, D. S. Ha, and H.-S. Lee. "Low Power CMOS Re-programmable Pulse Generator for UWB Systems". *IEEE Conference on Ultra Wideband Systems and Technologies*, pp. 443–447. Reston, VA, USA, Nov. 2003.

[Mar03b] K. M. Marsden. *A Study of a Versatile Low Power CMOS Pulse Generator for Ultra Wideband Radios*. Master's thesis, Virginia Polytechnic Institute and State University, Dec. 2003.

[Mat05] M. Matsuo, M. Kamada, and H. Habuchi. "Design of UWB Pulses in Terms of B-Splines". *IEICE Transactions on Fundamentals of Electronics, Communications and Computer Sciences*, E88-A(9):2287–2298, Sep. 2005.

[Mia03] M. Miao and C. Nguyen. "A Uniplanar Picosecond Impulse Generator Based on MESFET and SRD". *Microwave and Optical Technology Letters*, 39(6):470–472, Dec. 2003.

[Mis07] B. Miscopein and J. Schwoerer. "Low Complexity Synchronization Algorithm for Non-Coherent UWB-IR Receivers". *IEEE Vehicular Technology Conference*, pp. 2344–2348. Dublin, Ireland, Apr. 2007.

[Mit03] Miteq Inc. "High Performance Comb Generator Multipliers". *Microwave Journal*, Apr. 2003.

[Pro01] J. G. Proakis. *Digital Communications*. McGraw-Hill Higher Education, 4 ed., 2001.

[Qiu07] R. Qiu, B. Sadler, and Z. Hu. "Time Reversed Transmission with Chirp Signaling for UWB Communications and Its Application in Confined Metal Environments". *IEEE International Conference on Ultra-Wideband*. Singapore, Singapore, Sep. 2007.

[Raz98] B. Razavi. *RF microelectronics*. Prentice-Hall, 1998.

[Rom05] J. Romme and K. Witrisal. "On Transmitted-Reference UWB Systems using Discrete-Time Weighted Autocorrelation". *IEEE Vehicular Technology Conference*. Stockholm, Schweden, May 2005.

[Rul04] P. Rulikowski and J. Barrett. "Truly Balanced Step Recovery Diode Pulse Generator with Single Power Supply". *IEEE Radio and Wireless Conference*, pp. 347–350. Atlanta, GA, USA, Sep. 2004.

[Ryc05a] J. Ryckaert, M. Badaroglu, C. Desset, V. De Heyn, G. Van der Plas, P. Wambacq, B. Van Poucke, and S. Donnay. "Carrier-Based UWB Impulse Radio: Simplicity, Flexibility, and Pulser Implementation in 0.18-micron CMOS". *IEEE International Conference on Ultra-Wideband*, pp. 432–437. Zürich, Switzerland, Sep. 2005.

[Ryc05b] J. Ryckaert, C. Desset, A. Fort, M. Badaroglu, V. De Heyn, P. Wembacq, G. Van der Plas, S. Donnay, B. Van Poucke, and B. Gyselinckx. "Ultra-Wide-Band Transmitter for Low-Power Wireless Body Area Networks: Design and Evaluation". *IEEE Transactions on Circuits and Systems–I: Regular Papers*, 52(12):2515–2525, Dec. 2005.

[Sch04] E. Schamiloglu, R. J. Barker, M. Gundersen, and A. A. Neuber. "Modern Pulsed Power: Charlie Martin and Beyond". *Proceedings of the IEEE*, 92(7):1014–1020, Jul. 2004.

[Sch05] H. Schantz. *The Art and Science of Ultra-Wideband Antennas*. Artech House Publishers, Jul. 2005.

[Sto04] L. Stoica, S. Tiuraniemi, A. Rabbachin, and I. Oppermann. "An Ultra Wideband TAG Circuit Transceiver Architecture". *International Workshop on Ultra Wideband Systems Joint with Conference*

on Ultra Wideband Systems and Technologies, pp. 258–262. Kyoto, Japan, May 2004.

[Ust03] M. Uster. *Current-Mode Analog-to-Digital Converter for Array Implementation*. Ph.D. thesis, Swiss Federal Institute of Technology Zürich, 2003.

[Wil91] J. Williams. "High Speed Amplifier Techniques. A Designer's Companion for Wideband Circuitry". Linear Technology Application Note 47, Aug. 1991.

[Zha06] Q. Zhang. *Slightly Frequency-Shifted Reference Ultra-Wideband Radio*. Ph.D. thesis, University of Massachusetts, Amherst, Sep. 2006.

Chapter 4

Design Considerations

In this chapter, some aspects to be considered during the implementation of the UWB communication system are illustrated. These aspects include an evaluation of the required performance of the ADC, the burst mode for which the instantaneous data rate may exceed the average data rate, and a link budget.

4.1 Analog to Digital Converter

In this section, the impact of the limited sampling rate and the quantization error due to a limited precision of the sample representation are considered.

4.1.1 Sampling Frequency

The sampling frequency should be selected as low as possible for practical reasons. A low sampling frequency simplifies the implementation of the receiver, reduces the required processing power, and decreases the power consumption. In the following, the lower bounds for the sampling frequency are estimated. The criterion for the lower bound is that the non quantized samples should be sufficient to reconstruct the analog signal perfectly. The discussion starts with a sampling at the Nyquist rate, considers the conditions for which undersampling is possible, and finally replaces the notation of the signal bandwidth with the rate of innovation one.

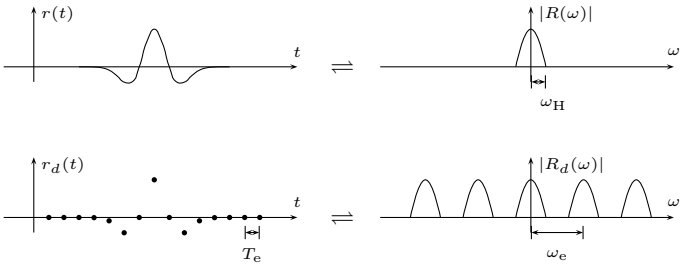

Figure 4.1: Nyquist rate sampling

Sampling at the Nyquist rate: In the original formulation, the well-known sampling theorem[1] applies to signals with an upper frequency bound. In [Sha49] the sampling theorem is stated as:

> "If a function $f(t)$ contains no frequencies higher than W cps [cycles per second], it is completely determined by giving its ordinates at a series of points spaced $1/(2W)$ seconds apart."

It is noted that this statement relates the sampling interval to the maximum frequency contained in the signal and not to its bandwidth. The maximum frequency coincides with the bandwidth only for baseband signals. The sampling theorem can be illustrated in an intuitive manner in the frequency domain, for example with a representation as shown in figure 4.1. Rigorous derivations can be found in the literature, e.g., in [Sha49]. Let the signal $r(t)$ be the signal to be sampled. Its Fourier transform $R(\omega)$ is limited by an upper angular frequency ω_H. We define a continuous signal $r_d(t)$ that is zero everywhere except at the instants nt_e for which $r_d(nt_\mathrm{e}) = r(nt_\mathrm{e})$. As the signal $r_d(t)$ is non-zero only for the sampling instants, it contains the same information as a sampled signal $\boldsymbol{r}[n]$. The signal $r_d(t)$ can be written as a multiplication of the signal $r(t)$ and a train of Dirac pulses

$$r_d(t) = r(t) \cdot \sum_{n=-\infty}^{\infty} \delta(t - nt_\mathrm{e}) \tag{4.1}$$

[1] Named after Nyquist, Whittaker, Shannon, Kotelnikov, or combinations thereof.

The Fourier transform $R_d(\omega)$ of the signal $r_d(t)$ is hence

$$R_d(\omega) = \frac{1}{2\pi}\left[R(\omega) * \frac{2\pi}{t_\mathrm{e}} \sum_{n=-\infty}^{\infty} \delta(\omega - n\frac{2\pi}{t_\mathrm{e}})\right] \tag{4.2a}$$

$$= \frac{1}{t_\mathrm{e}} \sum_{n=-\infty}^{\infty} R(\omega - n\frac{2\pi}{t_\mathrm{e}}) \tag{4.2b}$$

The Fourier transform $R(\omega)$ is repeated around the multiples of the sampling frequency $\omega_\mathrm{e} = 2\pi/t_\mathrm{e}$. These frequency-shifted replicas $R(\omega - n\omega_\mathrm{e})$ are called aliases. If $\omega_\mathrm{e} \geq 2\omega_\mathrm{H}$, then the aliases do not overlap and the original signal $r(t)$ can be reconstructed perfectly from $r_d(t)$. If $\omega_\mathrm{e} < 2\omega_\mathrm{H}$ then the aliases overlap and the signal cannot be reconstructed in general[2]. From the two observations follows that the lowest possible sampling frequency is given by the Nyquist rate.

Sampling at the Nyquist rate with prior signal filtering: To ensure the bandwidth limitation for arbitrary input signal a lowpass filter with an angular cut-off frequency $\omega_\mathrm{e}/2$ may be used prior to the sampling. This avoids aliases but results in a modification of the signal, e.g., a modified pulse shape. In figure 4.2, an UWB pulse is sampled with 1 GS/s and 10 GS/s. The input bandwidth is 3 GHz or 200 MHz. For each configuration 8 acquisitions are superposed. Figure 4.2 (c) may serve as a reference. In figure 4.2 (a) it is noted that sampling at 1 GS/s with an input bandwidth of 3 GHz results in large variations of the acquired signal shape. This configuration will not result in a reliable reception of the pulses. When the input filter bandwidth is reduced to 200 MHz as in figure 4.2 (b) and (d) the signal is reliably received. However a part of the signal energy is lost. The pulse has a reduced amplitude and an increased duration.

Undersampling of bandpass signals: A signal is denoted as bandpass, if the lower frequency ω_L is larger than zero and a finite upper frequency ω_H exists. In this case, sampling at the Nyquist rate is still sufficient but not necessarily required. For a bandpass signal, the condition is that a positive n exists such that its Fourier transform $R(\omega)$ is zero for all ω outside of the

[2] There exist however signals for which a perfect reconstruction is nevertheless possible. One class of such signals is considered later in this section.

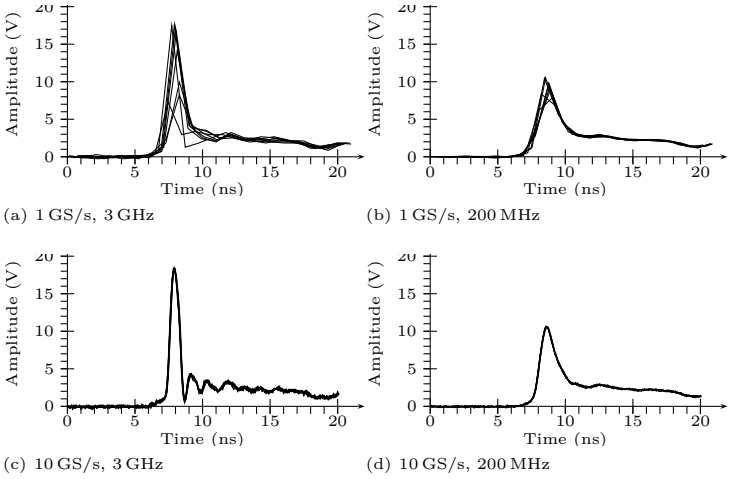

(a) 1 GS/s, 3 GHz (b) 1 GS/s, 200 MHz

(c) 10 GS/s, 3 GHz (d) 10 GS/s, 200 MHz

Figure 4.2: Impulse generated by a pulse generator using a bipolar transistor sampled with SDA6020 with 3 GHz and 200 MHz input bandwidth with 1 GS/s and 10 GS/s.

band

$$\left(-\frac{n}{2}\omega_{\mathrm{e}}, -\frac{n-1}{2}\omega_{\mathrm{e}}\right) \cup \left(\frac{n-1}{2}\omega_{\mathrm{e}}, \frac{n}{2}\omega_{\mathrm{e}}\right). \tag{4.3}$$

The corresponding reconstruction filter is then given by

$$n\,\mathrm{sinc}\left(\frac{nt}{t_{\mathrm{e}}}\right) - (n-1)\,\mathrm{sinc}\left(\frac{(n-1)t}{t_{\mathrm{e}}}\right). \tag{4.4}$$

When $n = 1$, the criterion for baseband signal is found. For $n > 1$, the sampling is below the Nyquist rate and is called undersampling. The effects of the undersampling of passband signals are schematically represented in figure 4.3. Undersampling architectures have also been proposed for UWB receivers. For example, one design with subsequent analytical signal processing is proposed in [Che03, Che04]. One of the issues of undersampling is that the noise density increases. UWB signals occupy a large bandwidth and the maximal undersampling factor is in general small [Che04].

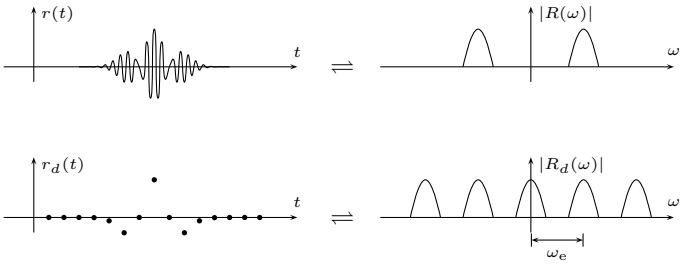

Figure 4.3: Undersampling of bandpass signals.

Figure 4.4: Undersampling of periodic signals

Undersampling of periodic signals: For particular baseband signals undersampling may also be possible without loosing any information contained in the signal. One element of that class of signals is a periodic signal[3]. An example of a periodic signal is the non-modulated signal from an UWB communication

$$r(t) = \sum_{j=-\infty}^{\infty} q(t - jt_f). \tag{4.5}$$

The undersampling of these signals is considered in the time domain and illustrated in figure 4.4. With the sampling interval t_e, the samples are given by

$$\boldsymbol{r}[n] = \sum_{j=-\infty}^{\infty} q(nt_e - jt_f). \tag{4.6}$$

[3]For a constant sampling rate. An extension to modulated (non-periodic but repetitive) signals is feasible assuming a non-constant sampling rate.

The sampling interval is selected to be close (but not equal) to a multiple of the pulse repetition interval t_f, i.e.,

$$t_\mathrm{e} = mt_\mathrm{f} + \epsilon, \tag{4.7}$$

where $\epsilon \ll t_\mathrm{f}$ and m is a positive integer. Without loss of generality the case $m = 1$ is considered. The samples are obtained by

$$\boldsymbol{r}[n] = \sum_{j=-\infty}^{\infty} q(nt_\mathrm{f} + n\epsilon - jt_\mathrm{f}) = \sum_{j=-\infty}^{\infty} q((n-j)t_\mathrm{f} + n\epsilon). \tag{4.8}$$

Due to the limited duration of the pulse it is required that $(n-j)t_\mathrm{f} + n\epsilon \approx 0$ for the summand to be non-zero. For $n < t_\mathrm{f}/\epsilon$, the term $n\epsilon$ is smaller than t_f and the only solution is obtained for $n - j = 0$. Hence, the nth sample is

$$\boldsymbol{r}[n] = q(n\epsilon) = q(n(t_\mathrm{e} - t_\mathrm{f})). \tag{4.9}$$

The vector $\boldsymbol{r}[n]$ represents hence accurately the sampled pulse shape. The time scale changes from t to $t_\mathrm{e} - t_\mathrm{f}$.

To illustrate this result, some acquisitions using a SDA6020 oscilloscope in the undersampling mode are shown in figure 4.5. The pulse seems to last for about 100 µs instead of 500 ps. This is due to an intentional misalignment of the frequency of the pulse generator and the one of the oscilloscope of 5.56 ppm. Figure 4.5 (b) shows the result for 10 MS/s or $m = 1$. The acquired pulse shape has a lot of noise. This results from the fact, that between two samples (100 ns) the time shift is only 0.556 ps. Hence a typical timing jitter of some picoseconds results in a large variation of the acquired amplitude. In figure 4.5 (c), the sampling frequency is 500 kS/s and hence $m = 20$ and the time shift between two acquisitions is 11.1 ps. This is in the same range as the typical timing jitter, such that additional noise can still be perceived, but is largely reduced. In figure 4.5 (d), the sampling frequency is 100 kS/s and $m = 100$. The time shift between two samples is 55.6 ps and hence larger than the typical jitter, such that the noise due to jitter is negligible.

Sampling at the rate of innovation: It is noted from the previous sections that the sampling frequency is decreased when more information concerning the analogous signal is available. For the sampling at the Nyquist frequency the knowledge of an upper bound of the covered spectrum is sufficient. It is shown that sampling at a lower rate, or undersampling, may

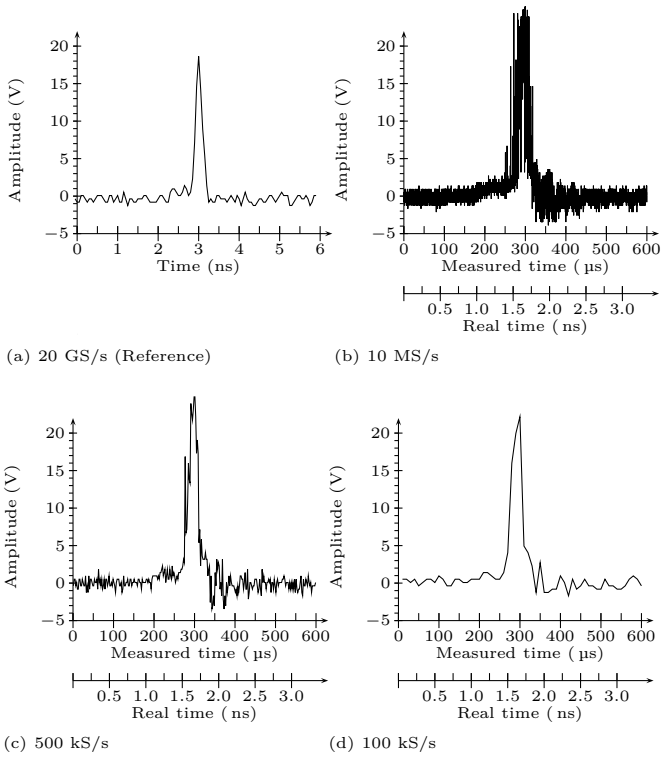

Figure 4.5: Impulse generated by AVM-2-C sampled with SDA6020 with (a) 20 GS/s (b) 10 MS/s (c) 500 kS/s (d) 100 kS/s. The PRR is 10 MHz, the frequency offset between transmitter and receiver is 5.56 ppm. A 100 µs measured duration in the undersampled signals (b) to (d) corresponds to 556 ps in real time.

become possible if an upper and a lower bound of the spectrum are known. The undersampling is also shown for periodic signals with known periodicity. In the following, a lower bound for the sampling rate is presented based on the entropy of the signal. Let's assume an UWB signal (2.15) for the symbol

$k = 0$,

$$s(t) = \sum_{j=0}^{N_\mathrm{f}-1} d_{j,0}^{(\mathrm{a})} p(t - j t_\mathrm{f} - d_{j,0}^{(\mathrm{t})} t_\mathrm{c}). \tag{4.10}$$

When the pulse shape $p(t)$ and the frame duration t_f are known, then the signal $s(t)$ is completely described by the $2N_\mathrm{f}$ parameters $d_{j,0}^{(\mathrm{a})}$ and $d_{j,0}^{(\mathrm{t})}$ for $j \in \{0, \ldots, N_\mathrm{f} - 1\}$. This means that the signal $s(t)$ can be reconstructed unambiguously from $2N_\mathrm{f}$ parameters independently of the occupied bandwidth, upper frequency bound, or signal duration. Thus, at minimum $2N_\mathrm{f}$ measurements are required for the extraction of the $2N_\mathrm{f}$ parameters. In [Vet02, Kus02, Kus03, Mar03, Mar04] the acquisition at this minimal sampling rate is considered. The number of parameters to be estimated is called the degree of freedom and the degree of freedom per unit of time is called the rate of innovation. The minimal sampling rate is then given by the rate of innovation. Sampling at the rate of innovation requires an appropriate selection of the sampling kernel, i.e., the signal must be filtered appropriately before the $2N_\mathrm{f}$ measurements are taken. The estimation of the parameters may be degraded in the presence of noise. In practical situations an oversampling compared to the rate of innovation may be applied to increase the robustness against the noise.

4.1.2 Quantization Error

The ADC provides a numerical representation of the signal amplitude at its input. The numerical representation uses a given number of bits N_r. The constraining of the continuous amplitude to the discrete set of numbers is called quantization. For this operation, the range of the possible amplitude values is first divided into 2^{N_r} slots, the nth slot is selected for input voltages between v_n and v_{n+1}. For the reconstruction of the signal, the index n is associated with an exact amplitude, e.g., $(v_{n+1} + v_n)/2$. The difference between the input amplitude and the reconstructed amplitude is called the quantization error. The quantization error can be considered as an additional noise. The SNR due to the quantization of given by the number of bits N_r. For a uniform distribution of the limits v_n the resulting SNR is

$$\mathrm{SNR\,(dB)} = 1.76 + 6.02 N_\mathrm{r}. \tag{4.11}$$

for a sinusoidal input and

$$\mathrm{SNR\,(dB)} = 6.02 N_\mathrm{r}. \tag{4.12}$$

for triangular and sawtooth signals. For example for $N_\mathrm{r} = 8$, the quantization noise results in SNR $\approx$ 50 dB for a sinusoidal signal. As other noises the quantization noise can be reduced by the processing gain. For example, when the received pulses are coherently added in the digital domain, the SNR can be increased, i.e., the effective number of bits is increased. Another approach to reduce the quantization noise is to select the limits v_n non-uniformly. An algorithm to calculate the limits v_n to minimize the quantization noise is for example presented in [Pro01].

4.2 Burst Mode

For a continuous transmission, the average channel data rate f_b is related to the pulse repetition duration t_f, the number of bits transmitter per symbol N_b and the number of frames per symbol N_f

$$f_b = \frac{1}{t_\mathrm{f}} \frac{N_\mathrm{b}}{N_\mathrm{f}}. \tag{4.13}$$

For a numerical application, we assume that one symbol equals one bit ($N_\mathrm{b} = 1$) and that four pulses are transmitted per symbol ($N_\mathrm{f} = 4$). For a frame duration of $t_\mathrm{f} = 100$ ns, the average channel data is 2.5 Mbit/s and may exceed the required useful bit rate for a low data rate communication system. The options to obtain the required useful bit rate are the following.

1. The pulse repetition frequency is lowered. A low pulse repetition frequency results in a more complex initial synchronization and a need of higher accuracy for the clocks used in the transmitter and the receiver.
2. The number of pulses per symbol is increased. This increases the complexity during the initial synchronization. The processing gain increases.
3. Some symbols are used for the channel coding by increasing the redundancy of the transmitted message. The probability of a transmission error is lowered.
4. The transmission is not at a constant data rate. Bursts containing the data are sent periodically with the maximum data rate. Between the bursts, the transmission is interrupted and the devices may be disabled.

The proposals 2. and 3. increase the processing gain but do not reduce the average power consumption. The average power consumption is reduced for proposals 1. and 4. In approach 4. it may be possible to disable some blocks of the transmitter and the receiver between the bursts. Furthermore, approach 4. does not require an increased accuracy of the clocks because the coherent addition is still made using a 100 ns interval between the pulses. However, it may be required to re-synchronize the receiver for each burst.

4.3 Link Budget

A link budget for a UWB communication is derived in this section. It is presented using the signal energy $\mathcal{E}_\mathrm{b}$ and the noise power density $\mathcal{N}_0$. The channel bandwidth does not appear contrary to a link budget based on the radio of the averaged signal power to the average noise power. In the latter the channel bandwidth will once appear in the calculation of the average noise power and a second time in a processing gain. These two effects will mutually compensate.

The link budget is presented in table 4.1. It is divided into four sections. In the first section, the system specifications are given. These are independent parameters, which need to be defined depending on the application scenarios. In the shown link budget, a data rate of 100 kbit/s and a signal bandwidth of 1 GHz is assumed. For a second derivative Gaussian pulse, this bandwidth corresponds to a pulse duration of $t_n \approx 0.33$ ns. The limitation for the maximum value of the power spectrum density (PSD) is given by the regulations. It is assumed that the spectrum should not exceed -41.3 dBm/MHz.

In the second section, the noise power density is calculated. It consists of the captured thermal noise and a increase of the noise power primarily due to noise figure of the first amplifier.

In the third section, the signal energy per bit captured by the receiver is derived. Therefore, all the losses during the transmission are considered and subtracted from the transmitted energy. In the example, both antennas are assumed to have a loss of 3 dB each. However, depending on the application, directional antennas with a gain instead of a loss may be used. The energy per bit at a reference distance (typically 1 m for indoor systems) is then calculated. This value is compared to the expected noise power density to obtain the SNR at the reference distance. In the example, the SNR is 75.1 dB at 1 m.

Parameter	Equation	Typical Value	
System Specifications			
Channel data rate	f_b	100 kbps	
Channel and signal bandwidth	B_T	1 GHz	
Center frequency (arithmetic mean)	f_c	0.5 GHz	
Maximum PSD	$\mathrm{PSD}_{\max}$	−41.3 dBm/MHz	
Noise Power Density			
Noise power density at antenna	kT	−173.8 dBm/Hz	
RX Amplifier Noise Figure	NF	5 dB	
Noise power density at detector	$\mathcal{N}_0 = kT + \mathrm{NF}$	−168.8 dBm/Hz	
Signal Energy per bit			
Average Transmit Power	$P_t = \mathrm{PSD}_{\max} \cdot B_T$	−11.3 dBm	
TX Antenna Gain	G_t	−3 dBm	
Path Loss at 1 m	$L_1 = 20\log_{10}(4\pi f_c/c)$	26.4 dB	
RX Antenna Gain	G_r	−3 dBm	
RX Power at 1 m	$P_r = P_t + G_\mathrm{t} + G_\mathrm{r} - L_1$	−43.7 dBm	
RX Energy per bit at 1 m	$\mathcal{E}_\mathrm{b}(1) = P_r - 10\log_{10}(f_b)$	−93.7 dBm/Hz	
$\mathcal{E}_\mathrm{b}/\mathcal{N}_0$ at 1 m	$\mathcal{E}_\mathrm{b}(1) - \mathcal{N}_0$	75.1 dB	
SNR per bit			
Path Loss at d m	$L_2(d) = 10\gamma\log_{10}(d)$	$\gamma = 2.0$	$\gamma = 3.3$
$\mathcal{E}_\mathrm{b}/\mathcal{N}_0$ at 2 m	$\mathcal{E}_\mathrm{b}(1) - \mathcal{N}_0 - L_2(2)$	69.1 dB	65.2 dB
$\mathcal{E}_\mathrm{b}/\mathcal{N}_0$ at 5 m	$\mathcal{E}_\mathrm{b}(1) - \mathcal{N}_0 - L_2(5)$	61.1 dB	52.0 dB
$\mathcal{E}_\mathrm{b}/\mathcal{N}_0$ at 10 m	$\mathcal{E}_\mathrm{b}(1) - \mathcal{N}_0 - L_2(10)$	55.1 dB	42.1 dB
$\mathcal{E}_\mathrm{b}/\mathcal{N}_0$ at 20 m	$\mathcal{E}_\mathrm{b}(1) - \mathcal{N}_0 - L_2(20)$	49.1 dB	32.2 dB
$\mathcal{E}_\mathrm{b}/\mathcal{N}_0$ at 50 m	$\mathcal{E}_\mathrm{b}(1) - \mathcal{N}_0 - L_2(50)$	41.1 dB	19.0 dB
$\mathcal{E}_\mathrm{b}/\mathcal{N}_0$ at 100 m	$\mathcal{E}_\mathrm{b}(1) - \mathcal{N}_0 - L_2(100)$	35.1 dB	9.1 dB

Table 4.1: Link Budget (Approach using signal energy and noise power density).

In the forth section, the SNR is considered for some communication ranges. The loss due to the communication range is considered using a log-distance path loss model. Path loss exponents of $\gamma = 3.3$ and $\gamma = 2.0$ are assumed. A path loss exponent of 2 correspond to a free space propagation and a path loss exponent of 3.3 corresponds to a worst case assumption for an indoor propagation channel as discussed in section 2.3.4. This assumption may be overly pessimistic in particular for a line-of-sight propagation.

This SNR is related to the BER. For an AWGN channel the relation is given by the Q-function (see section 5.2.1). For antipodal modulations, the approximate BERs are $7.7 \cdot 10^{-3}$ and $3.9 \cdot 10^{-6}$ for 7 dB and 10 dB SNR per bit, respectively. For orthogonal modulations, they are $1.3 \cdot 10^{-2}$ and $7.7 \cdot 10^{-3}$ for the same respective SNRs.

To obtain the same BER in a CM3 transmission channel, the same SNR as for AWGN is required[4]. However, the receiver may not be able to process the entire bit energy due to imperfections. It will be shown in section 5.2.2, that without any channel estimation – resulting in an unmatched correlation template – an SNR margin of 9 dB may be required for a CM3 channel. Furthermore, it is shown in section 5.3, that a limited duration acquisition window may also lower the amount of the processed bit energy as compared to the total received bit energy, e.g., by about 3 dB for a 10 ns acquisition window and a CM3 channel.

4.4 Summary

For baseband signals with limited bandwidth the sampling at the Nyquist rate is shown to be sufficient. Undersampling is shown to be possible for passband signals with limited bandwidth and also for repetitive signals when the repetition period is known. Finally, a lower bound on the sampling frequency is shown to be related to the rate of innovation and not to the bandwidth of the signal. A typical link budget for UWB communications shows the feasibility of a data communication for ranges up to 100 m for an AWGN channel and about 50 m for a typical indoor NLOS channel.

Bibliography

[Che03] M. S.-W. Chen and R. W. Brodersen. "A Subsampling Radio Architecture for 3-10 GHz UWB". Presentation at the Berkeley Wireless Research Center Summer Retreat. Berkeley, CA, USA, Jun. 2003.

[Che04] M. S.-W. Chen and R. W. Brodersen. "A Subsampling UWB Radio Architecture by Analytic Signaling". *IEEE Conference on Acoustics, Speech, and Signal Processing*. Montreal, QC, Canada, May 2004.

[Kus02] J. Kusuma, A. Ridolfi, and M. Vetterli. "Sampling of Communication Systems with Bandwidth Expansion". *IEEE Conference on Communications*, vol. 3, pp. 1601–1605. New York City, NY, USA, May 2002.

[4] For a multipath channel, the same SNR may be obtained for a shorter or larger communication range than for an free space propagation. A larger communication range may occur, because for sufficiently short pulses the energy received from the individual multipaths may be summed, yielding to a path loss exponent smaller than 2.

[Kus03] J. Kusuma, I. Maravić, and M. Vetterli. "Sampling with Finite Rate of Innovation: Channel and Timing Estimation for UWB and GPS". *IEEE Conference on Communications*, vol. 5, pp. 3540–3544. Anchorage, AK, USA, May 2003.

[Mar03] I. Maravić, J. Kusuma, and M. Vetterli. "Low-Sampling Rate UWB Channel Characterization and Synchronization". *Korean Journal of Communications and Networks, Special Issue on UWB Systems*, 5(4):319–327, Dec. 2003.

[Mar04] I. Maravić, M. Vetterli, and K. Ramchandran. "Channel Estimation and Synchronization with Sub-Nyquist Sampling And Application to Ultra-Wideband Systems". *IEEE Symposium on Circuits and Systems*, vol. 5, pp. 381–384. Vancouver, BC, Canada, May 2004.

[Pro01] J. G. Proakis. *Digital Communications*. McGraw-Hill Higher Education, 4 ed., 2001.

[Sha49] C. E. Shannon. "Communication in the Presence of Noise". *Proceedings of the Institute of Radio Engineers*, 37(1):10–21, Jan. 1949.

[Vet02] M. Vetterli, P. Marziliano, and T. Blu. "Sampling Signals With Finite Rate of Innovation". *IEEE Transactions on Signal Processing*, 50(6):1417–1428, Jun. 2002.

Chapter 5

Performance Analysis

In this chapter, the performance of a receiver architecture characterized by the coherent addition of limited duration acquisition windows and a correlation with a locally generated template is analyzed. It is assumed that the receiver is already synchronized with the transmitter of interest. This assumption is valid during the communication but not during the synchronization phase. The latter will be considered in chapter 6. The current chapter starts with a presentation of potential performance benchmarks. The BER for the matched filter receiver in an AWGN and a multipath propagation channel are estimated afterward. Finally, performances are evaluated in the presence of imperfections or perturbations such as interferences or a mismatch between the pulse template and the received pulse.

5.1 Introduction

5.1.1 Assumptions

Except otherwise noted, the following assumptions are made throughout the chapter to obtain commensurable performance estimations and simulation results.

1. The receiver architecture is characterized by a coherent addition of limited duration acquisition windows and by a correlation between the summed signal and a locally generated template. The template is not necessarily matched to the received signal. One possible implementation is the RSD receiver presented in section 3.4.

2. The receiver is assumed to be synchronized with the transmitter of interest. The synchronization phase will be considered in chapter 6.
3. The transmitted pulse shape is a second derivative Gaussian with duration $t_n = 200\,\text{ps}$.
4. The transmission channel is AWGN for free space communications and the IEEE 802.15.3a CM3 (see section 2.3) for indoor communications. The CM3 is selected because the theoretical signals using this model predict accurately received signals measured at our laboratories.
5. The frame duration is 100 ns. The associated pulse repetition frequency is sufficient for a typical low data rate system for example used in sensor applications, yet low enough to prevent inter symbol interference in indoor propagation channels.
6. A binary data modulation is used and results in a delay (TM) or a reversal of the amplitude (AM) of all the N_f pulses transmitted per symbol. A spreading code with length N_f exists and is applied to modulate each one of the N_f pulses per symbol. The same spreading code is repeated for each symbol. The code modulation results in a delay (TH) or a variation of the pulse amplitude (AH). The TH may be M-ary with $M \in \{2, 4, 8\}$ and is denoted as THM. Only binary code amplitude modulation is considered. The resulting combinations are denoted as TH2 TM, TH2 AM, TH4 TM, TH4 AM, TH8 TM, TH8 AM, AH TM, and AH AM. The chip duration, i.e., the delay applied for a delay modulation, is 2 ns.

5.1.2 Performance Benchmarks

Various performance evaluations are feasible and several benchmarks exist. There is no universal or univocal benchmark and an appropriate one should be selected depending on the property to be characterized. In the following some benchmarks that will be used in this and the next chapter are introduced.

Bit error rate: The BER indicates the probability that an error occurs during the transmission of one bit. For an AWGN transmission channel, a memoryless transmission, and a matched filter receiver, the BER is entirely defined by the signal to noise ratio per bit $\mathcal{E}_\text{b}/\mathcal{N}_0$. For other scenarios, some mathematical derivations of the BER and a comparison with outcomes of numerical simulations are provided in this chapter. To obtain the BER by measurements or simulations, in general a large number of random, equiprob-

able data is transmitted and the number of errors is counted. For simulations, this approach can for example be implemented using a Monte Carlo method.

SIGNAL TO NOISE RATIO: Two definitions of signal to noise ratios will be used. The first one is the carrier to noise ratio P_s/P_η. The second one is the signal to noise ratio per bit $\mathcal{E}_\mathrm{b}/\mathcal{N}_0$.

The carrier to noise ratio is calculated with the averaged signal power P_s and the average noise power P_η at the antenna. For a thermal noise and a channel bandwidth B_T, the noise power is $P_\eta = kTB_T$, where k is the Boltzmann constant and T is the temperature in Kelvin. To calculate the average signal power the time average over one symbol duration is used. The signal power may also depend on the transmitted symbol such that the ensemble average over all admissible data symbols has to be considered and the carrier to noise ratio becomes

$$\frac{P_\mathrm{s}}{P_\eta} = \frac{1}{kTB_T}\,\mathsf{E}\left[\frac{1}{t_\mathrm{s}}\int_0^{t_\mathrm{s}} r^2(t)\,\mathrm{d}t\right]. \tag{5.1}$$

If the average signal power is independent on the transmitted symbol, it is given by the product of the energy per bit $\mathcal{E}_\mathrm{b}$ and the data signaling rate f_b in bits per second,

$$P_\mathrm{s} = \mathcal{E}_\mathrm{b} f_b. \tag{5.2}$$

Introducing a noise power density $\mathcal{N}_0$ as the noise power normalized by the channel bandwidth,

$$\mathcal{N}_0 = P_\eta/B_T = kT, \tag{5.3}$$

the signal to noise ratio per bit $\mathcal{E}_\mathrm{b}/\mathcal{N}_0$ becomes

$$\frac{\mathcal{E}_\mathrm{b}}{\mathcal{N}_0} = \frac{P_\mathrm{s}}{f_b}\frac{1}{kT} = \frac{P_\mathrm{s}}{f_b}\frac{1}{kT}\frac{B_T}{B_T} = \frac{B_T}{f_b}\frac{P_\mathrm{s}}{P_\eta}. \tag{5.4}$$

The proportionality factor B_T/f_b between the carrier to noise ratio P_s/P_η and the signal to noise ratio per bit $\mathcal{E}_\mathrm{b}/\mathcal{N}_0$ is known as the processing gain. It is considered more in detail in section 5.4.

Noiseless observation vector: The signal to noise ratio per bit $\mathcal{E}_\mathrm{b}/\mathcal{N}_0$ is shown in (5.4) to be related to the average power ratio by the processing gain. For a memoryless transmission and a matched filter demodulator, the signal to noise ratio at the input of the symbol detector (see also figure 3.6) is also $\mathcal{E}_\mathrm{b}/\mathcal{N}_0$ and the noise distribution remains Gaussian. For other scenarios the signal to noise ratio per bit can be calculated from the elements of the observation vector $\boldsymbol{d}_k[n]$. Using a normalized correlation template, the noise power density remains constant and it is sufficient to consider the noiseless elements of the observation vector $\tilde{\boldsymbol{d}}_k[n]$.

Maximum of the signal: The noiseless elements of the observation vector scale linearly with the received signal amplitude if the pulse shape does not change. It may be sufficient to estimate the signal amplitude, e.g., considering the maximum absolute amplitude of a signal $w_k(t)$ by

$$\mathcal{W} = \max_t |w_k(t)| \tag{5.5}$$

Distinction coefficient: The maximum amplitude of the signal for a scenario (a) is written as $\mathcal{W}_{(\mathrm{a})}$. The ratio between $\mathcal{W}_{(\mathrm{a})}$ and $\mathcal{W}_{(\mathrm{b})}$ relates the signals from scenario (a) and scenario (b). It is denoted as a distinction coefficient

$$\mathcal{D} = \mathcal{W}_{(\mathrm{a})}/\mathcal{W}_{(\mathrm{b})}. \tag{5.6}$$

The distinction coefficient characterizes among others the probability that the receiver will detect a signal from scenario (a) and reject a signal from scenario (b). It is therefore useful to estimate the performance during the synchronization phase and will be used in chapter 6.

5.2 Bit Error Rate

The BER is estimated for an AWGN channel in section 5.2.1 and for a multipath channel in section 5.2.2.

5.2.1 BER in AWGN

The theoretical BER for AWGN, a memoryless transmission, and a matched filter receiver is well known and can be found in most textbooks about digital communication systems, e.g., in [Pro01]. It is

$$\mathrm{BER}_{\mathrm{antipodal}} = \mathrm{Q}\left(\sqrt{\frac{2\mathcal{E}_\mathrm{b}}{\mathcal{N}_0}}\right), \quad \mathrm{BER}_{\mathrm{orthogonal}} = \mathrm{Q}\left(\sqrt{\frac{\mathcal{E}_\mathrm{b}}{\mathcal{N}_0}}\right) \tag{5.7}$$

for antipodal and orthogonal binary modulations, respectively. The Q function is defined as

$$\mathrm{Q}(\alpha) \stackrel{\mathrm{def}}{=} \frac{1}{\sqrt{2\pi}} \int_\alpha^\infty \exp\left(-\frac{x^2}{2}\right) \mathrm{d}x = \frac{1}{2} - \frac{1}{2}\,\mathrm{erf}\left(\frac{\alpha}{2}\right). \tag{5.8}$$

The theoretical BERs for antipodal and orthogonal modulations are shown in figure 5.1, where they are compared to the outcomes of numerical Monte Carlo simulations for an UWB transmission with matched templates and antipodal AM or orthogonal TM modulation, respectively. The outcomes of the numerical simulation are in excellent agreement with the theoretical BERs.

For the TM, a chip duration $t_\mathrm{c} = 2\,\mathrm{ns}$ larger than the pulse duration has been selected and the performance is orthogonal as expected. For shorter chip durations, the BER may not correspond to the one of an orthogonal modulation.

The optimal chip duration $t_{\mathrm{c,opt}}$ that results in a minimum BER in an AWGN transmission channel is calculated in the following. The noiseless observation vector (3.19) is for a single pulse

$$\tilde{\boldsymbol{d}}_k[n] = \int_0^{t_\mathrm{f}} q(t)\hat{q}_n(t)\,\mathrm{d}t, \quad n \in \{0, 1\}. \tag{5.9}$$

For the delay modulation the transmitted signal is $p(t - d_k t_\mathrm{c})$ and the template is $\hat{q}_n(t) = p(t - nt_\mathrm{c})$. Because of the AWGN assumption, the noiseless received signal is proportional to the transmitted one, i.e., it has the same shape. Writing the autocorrelation of the $p(t)$ as $c_{pp}(\tau)$ and assuming that

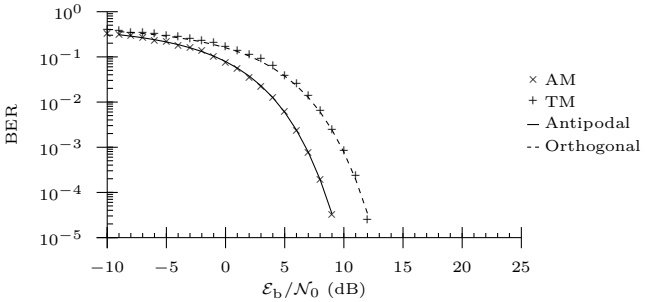

Figure 5.1: BER in an AWGN transmission channel. The BER for orthogonal and antipodal modulation and simulation results for AM and TM are represented.

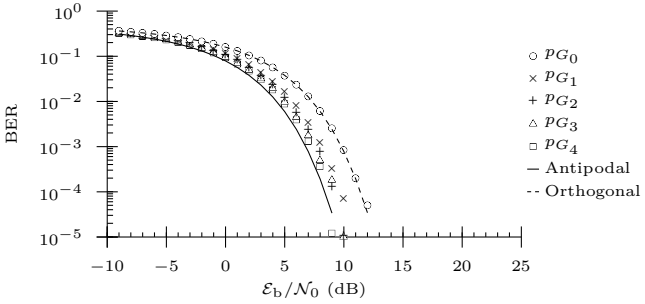

Figure 5.2: BER in an AWGN transmission channel for TM with optimized chip duration $t_{c,opt}$. The BER is in between the ones for orthogonal and antipodal modulations.

the pulses are received entirely within the acquisition windows, the different outcomes of the noiseless observation vector are thus

$$\tilde{\boldsymbol{d}}_k[n] = \int_{-\infty}^{\infty} p(t - d_k t_c) p(t - n t_c)\,\mathrm{d}t = \begin{cases} c_{pp}(0) & \text{if } n = d_k, \\ c_{pp}(t_c) & \text{if } n = 0,\ d_k = 1, \\ c_{pp}(-t_c) & \text{if } n = 1,\ d_k = 0. \end{cases} \quad (5.10)$$

The autocorrelation is symmetric $c_{pp}(-t_c) = c_{pp}(t_c)$ and independent of the transmitted data symbol. The two outputs of the receiver branches are given by $c_{pp}(0)$ and $c_{pp}(t_c)$. To minimize the BER, the distance between these outcomes should be maximized. The chip duration that minimizes the

BER is thus

$$t_{\mathrm{c,opt}} = \arg\max_{t_\mathrm{c}} \left(c_{pp}(0) - c_{pp}(t_\mathrm{c}) \right). \tag{5.11}$$

It is known that $c_{pp}(0) = \mathcal{E}_\mathrm{b}$ is constant. The optimal chip duration is hence given by

$$t_{\mathrm{c,opt}} = \arg\min_{t_\mathrm{c}} \left(c_{pp}(t_\mathrm{c}) \right). \tag{5.12}$$

The optimal chip duration depends thus on the pulse shape. For the Gaussian pulses, the optimal chip durations normalized by the pulse duration t_n are listed in table 5.1. The BER when using TM with the optimal chip duration is shown in figure 5.2. It is noted, that the resulting BER is in between the ones for the antipodal and the orthogonal modulations and improves with increasing order of the Gaussian pulse. In general $t_{\mathrm{c,opt}}$ will not result in a minimal BER for a multipath propagation channel.

5.2.2 Multipath Propagation

The BERs for antipodal and orthogonal modulation in AWGN are compared with the BER in a multipath propagation channel considering the IEEE 802.15.3a CM3 model.

In AWGN, the received pulse is not distorted by the transmission channel and hence can be assumed to be known. The receiver can apply a locally generated template which is perfectly matched to the received pulse. For a multipath propagation channel, the received pulse shape is in general not known a priori. It can however be estimated during the reception of the pulses. In this section, the discussion is limited to two cases. First, it is assumed that the receiver has a perfect knowledge of the transmission channel. Second, it is assumed that the receiver applies a replica of the transmitted pulse shape as template.

Pulse shape	$t_{\mathrm{c,opt}}/t_n$	cross-correlation $c_{pp}(t_{\mathrm{c,opt}})$
$p_{\mathrm{G}_0}(t)$	∞	0
$p_{\mathrm{G}_1}(t)$	2.45	−0.4463
$p_{\mathrm{G}_2}(t)$	1.92	−0.6183
$p_{\mathrm{G}_3}(t)$	1.63	−0.7086
$p_{\mathrm{G}_4}(t)$	1.45	−0.7644

Table 5.1: Minima of the autocorrelation functions of Gaussian pulses.

	TM ($d_k = 0$)		AM	
Channel Model	Median	Average	Median	Average
CM1	6.27	6.94	6.33	6.26
CM2	7.79	8.21	7.45	7.26
CM3	8.52	9.17	8.89	8.82
CM4	9.69	10.37	10.44	10.45

Table 5.2: Median and average performance losses (dB) due to a correlation with the AWGN template for the reception over a multipath channel.

When the receiver has perfect knowledge of the transmission channel all the energy received from the UWB signal is "collected" by the correlation with the matched template. By definition the total energy per bit is $\mathcal{E}_\mathrm{b}$. It is therefore expected that the BER is identical to the AWGN one. The outcomes of a numerical simulation are shown in figure 5.3 and are in excellent agreement.

It is noted that the energy per bit does not necessarily correspond to the same transmission distance in AWGN and for a CM3 channel. Indeed, if present, the energy received from a line-of-sight propagation may correspond to the received energy in an AWGN channel. The contributions from the multipaths may increase the received energy. Therefore, at the same transmission distance a multipath propagation may even result in a higher received energy per bit than an AWGN channel. The relation between the transmission distance and the energy per bit is considered for the link budget. The calculations presented in this chapter are independent of the transmission distance.

In the second scenario, the receiver does not have any knowledge about the propagation channel and uses the transmitted pulse shape as template. Because this minimizes the BER in an AWGN transmission channel, this template is denoted as AWGN template. The application of the AWGN template does not require any channel estimation and may hence result in low complexity architectures. When the AWGN template is applied to a CM3 transmission channel, the elements of the observation vector change. In particular the element $n = d_k$ is reduced. The reduction of the received energy (compared to the energy contained in the received signal including all the multipath) is evaluated for 100 representatives of the CM3 channel and the resulting cumulative distribution function for the SNR loss is illustrated in figure 5.4. It is noted that the average performance loss is similar for AM and TM. The variation of the received energy is smaller for AM. The aver-

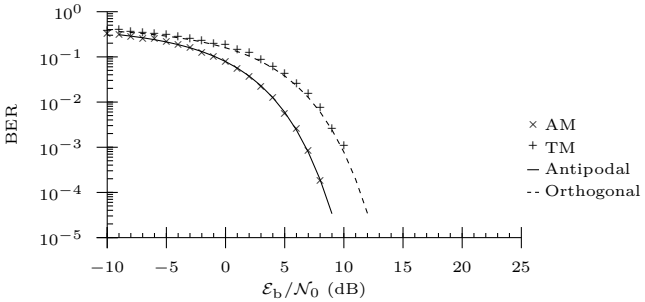

Figure 5.3: BER for CM3 transmission channels for different modulations, and perfectly matched pulse template. The performance is identical to the result for a matched filter receiver in AWGN.

age performance losses are listed in table 5.2. For a numerical estimation of the BER performance, a single transmission channel is selected to limit the simulation time. The channel 91 has been identified as a typical representative with close to average loss. The energy loss for this channel is 8.18 dB for AM and 8.31 dB for TM when the data symbol $d_k = 0$ is transmitted. In figure 5.5, the outcomes of a numerical simulation of the BER for the channel number 91 are compared to the expected performance. It is noted that the results are in excellent agreement for AM. For TM the results are accurate for the transmitted data symbol 0 as expected. For the transmitted data symbol 1, the performance is slightly different. This effect is due to an asymmetry of the cross-correlation function between the template and the received signal, i.e., the transmission of a given symbol may have a different influence to symbols modulated with a positive delay than to symbols with a negative delay.

The two considered cases—perfect channel estimation and no channel estimation—result in an upper and a lower bound for the BERs to be expected for realistic communication systems. Typically a receiver may have partial knowledge of the transmission channel characteristics.

5.3 Duration Limited Acquisition

A receiver may benefit from the low duty cycle signaling by acquiring the signal only for the short duration during which a pulse is supposed to be received. The RSD receiver in section 3.4 for example acquires the signal during a short duration acquisition window instead of continuously. This re-

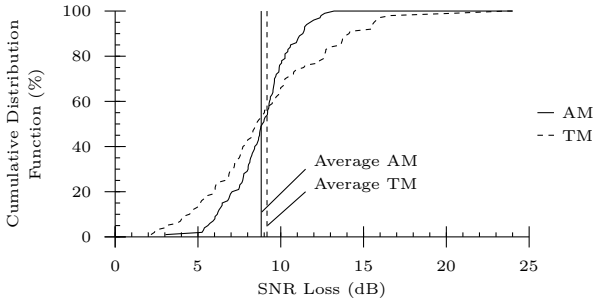

Figure 5.4: Cumulative distribution function for the energy reduction calculated for 100 CM3 transmission channels.

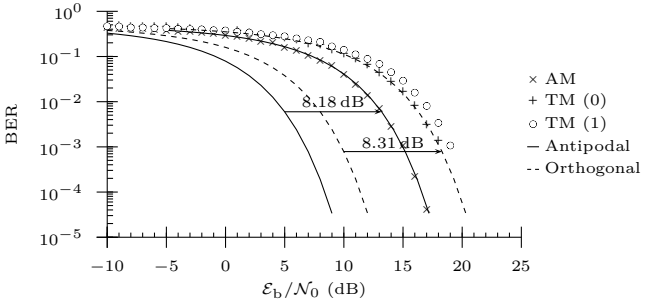

Figure 5.5: BER in a CM3 transmission channel (number 91) for AM and TM modulation calculated using the AWGN template.

sults in a substantial reduction of the power consumption. However, the short acquisition window durations may result in a performance loss for positioning or communications. In the following a loss relevant for communications is considered: the expected loss of signal energy acquired during the limited duration. For positioning systems other characteristics such as the potential to detect the direct propagation path even when the receiver is synchronized with a multipath may be more relevant. The loss of signal energy is directly related to the signal to noise ratio per bit $\mathcal{E}_b/\mathcal{N}_0$ because the noise power density $\mathcal{N}_0$ does not depend on the acquisition duration. It is hence sufficient to consider the loss in the acquired bit energy $\mathcal{E}_b$.

For an AWGN transmission channel and synchronized systems, the reduction of the received energy becomes important only when the acquisition

window duration t_w becomes smaller than the duration of the received pulse. The loss of the received energy,

$$L = \frac{1}{R\mathcal{E}_\mathrm{b}} \int_{-t_\mathrm{w}/2}^{t_\mathrm{w}/2} q^2(t)\,\mathrm{d}t. \tag{5.13}$$

is presented in figure 5.6. The window duration t_w is normalized with the pulse duration t_n. It can be seen, that the loss in the received energy is in general more important for higher derivatives Gaussian pulses. In typical systems $t_\mathrm{w} \gg t_n$ and the losses due to the limited acquisition window duration are not relevant for an AWGN channel.

For a multipath propagation channel, where the energy is spread over a much longer period, it is expected that the losses may become significant. The results averaged over 100 implementations of CM3 propagation channels are presented in figure 5.7. The acquisition window duration is normalized with the pulse duration (in this example $t_n = 200\,\mathrm{ps}$), because the outcomes do not depend on the pulse duration but only on the delay spread of the propagation channel. The time instant to place the acquisition window has been selected to maximize the received energy, and the loss is obtained with

$$L = \frac{1}{R\mathcal{E}_\mathrm{b}} \max_{\tau} \int_{\tau-t_\mathrm{w}/2}^{\tau+t_\mathrm{w}/2} q^2(t)\,\mathrm{d}t. \tag{5.14}$$

For example, for an acquisition window duration of 6 ns, the expected performance loss in a CM3 channel is about 3.77 dB. This performance loss cannot be compensated by other means than by increasing the acquisition window duration.

5.4 Pulse Combining

The coherent addition of several received pulses is one of the options to increase the SNR and hence obtain a processing gain. The discussion of the coherent addition is divided into an introduction to the processing gain in section 5.4.1, a calculation of the processing gain with experimental verification for perfectly synchronized systems in section 5.4.2, and an estimation of the processing gain in the presence of timing errors in section 5.4.3.

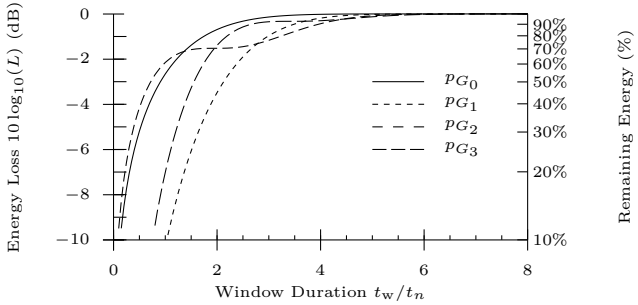

Figure 5.6: Energy loss due to a limited duration of the acquisition window in AWGN.

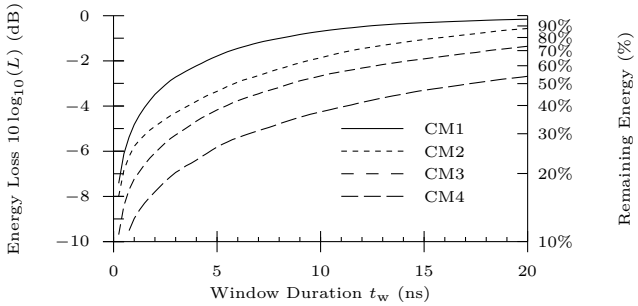

Figure 5.7: Energy loss due to a limited duration of the acquisition window in multipath channels.

5.4.1 Processing Gain

In a spread-spectrum communications system, the processing gain G is an improvement of the signal to noise ratio due to the de-spreading of the received signal. It results from the increased occupied bandwidth of the transmitted signal compared to the required bandwidth given by the data signaling rate f_b. The maximal processing gain (5.4) is given by the channel bandwidth B_T and the data signaling rate f_b as

$$G = \frac{B_T}{f_b}. \tag{5.15}$$

If the channel bandwidth B_T is identical to the signal bandwidth, B_T is inversely proportional to the pulse duration t_{FWHM} and the data signaling rate f_b is also inversely proportional to the bit duration $t_b = t_\mathrm{s}/N_\mathrm{b}$. The bit duration depends on the number of bits per symbol N_b and the symbol duration t_s. The processing gain can also be written in the time domain as

$$G = \frac{t_b}{t_{\mathrm{FWHM}}}, \tag{5.16}$$

and can be decomposed into two terms, i.e., as

$$G = \underbrace{\frac{t_b}{t_{\mathrm{FWHM}}} \frac{N_\mathrm{b}}{N_\mathrm{f}}}_{G_\mathrm{DC}} \times \underbrace{\frac{N_\mathrm{f}}{N_\mathrm{b}}}_{G_\mathrm{PC}} . \tag{5.17}$$

The first contribution, G_DC, is due to the duty cycling of the communication, i.e., the transmitted signal is non-zero only for a duration $N_\mathrm{f} t_{\mathrm{FWHM}}$ for the transmission of one data symbol. The second contribution is due to the coherent addition of N_f pulses for each symbol. It can be seen, that the overall processing gain G is independent of the number of pulses per symbol (as long as $\mathcal{E}_\mathrm{b}$ and t_s are not altered together with N_f). Changing the number of pulses per symbol N_f trades the duty cycle gain against the pulse combining gain. However, in the non-ideal case, one of the processing gains may be limited or be non-proportional to N_f. In this case, the total processing gain may be improved by a careful selection of N_f. The ratio of the processing gains and the resulting BER is discussed in [Fis02, Opp04]. In [Gez03], the trade-off between the processing gains is considered in presence of timing jitter. The selection of N_f depends on many additional criteria. In the following, the impact for a variation of N_f is considered under the assumption that the symbol energy $\mathcal{E}_\mathrm{s}$ and the symbol duration t_s are constant. The arguments in favor of an increase of N_f or an increase of the number of pulses per symbol are:

- The regulatory authority may decide to limit the peak power in addition to the maximum average power. It may become necessary to distribute the symbol energy to several pulses.
- The peak power may be limited due to the implementation of the pulse generator. For example by the maximum voltages that can be handled by the selected technology.
- The increase of the number of pulses per symbol increase the length of the spreading code and hence improves the robustness against interferences.

- The duration between the pulses is reduced for a constant symbol rate. A given frequency difference between the clocks at the transmitter and the receiver results in a smaller timing error accumulated between two pulses. Therefore, an increase of N_f results in a system that is less sensitive against a clock frequency difference.

The arguments to decrease N_f are:

- Inter-pulse interference may be reduced or avoided for a given symbol rate.
- The data synchronization is simplified due to a shorter spreading code.
- The spectrum (2.29) of the non-modulated signal is shown to be composed of narrowband contributions that are separated by an angular frequency $2\pi/t_\mathrm{f}$. The amplitudes of these contributions also scale with $2\pi/t_\mathrm{f}$. A decrease of N_f increases the frame duration t_f for a constant symbol duration. The narrowband contributions are therefore more closely spaced and reduced in amplitude. Therefore less spreading by the code modulation is required to respect the regulatory emission masks.
- The exploitation of the duty cycle gain instead of the pulse combining gain may result in simplified receiver architectures. E.g., an incoherent threshold receiver may be sufficient to estimate accurately the arrival times of the pulses.

5.4.2 Synchronized Systems

In this section, the theoretical pulse combining gain is estimated and compared with the measured gain using an experimental platform. The summed, received signal (3.21) is

$$q_\mathrm{sum}(t) = \sum_{j=0}^{N_\mathrm{f}-1} q(t+\epsilon_j), \tag{5.18}$$

where $\epsilon_j = \hat{\tau}_j - \tau_j$. For a perfect synchronization the delay is $\epsilon_j = 0$ for all j. In that case, the summed signal is $q_\mathrm{sum}(t) = N_\mathrm{f} q(t)$ and the received signal energy is proportional to N_f^2. The noise power for AWGN increases proportionally to N_f such that a pulse combining gain proportional to N_f remains as expected. In figure 5.8, the theoretical G_PC is compared to a measured gain by using a pulse generator and an oscilloscope LeCroy SDA6020. Up to several thousands of combined pulses the measured pulse combining gain

is in excellent agreement with the theoretical prediction. For high values of N_f the measured pulse combining gain is limited due to the quantization and deterministic noise correlated with the pulses. The deterministic noise correlated with the pulses is not attenuated by the coherent addition. To calculate the impact of the quantization noise, the representation of the digital values in the oscilloscope is considered. For the LeCroy SDA6020, the input voltages are sampled with 8 bit and the internal mathematical functions use a 16 bit representation. The noise standard deviation of the input signal is approximately given by the three least significant bits[1]. For an approximation of the maximum gain it is assumed that the noise is reduced until the noise standard deviation corresponds to the least significant bit of the 16 bit signal or $\sqrt{N_\mathrm{f}} = 2^{16}/2^6$. This results in an upper limit of the pulse combining gain of approximately 60 dB.

Both above mentioned noise contributions result in an upper bound for the pulse combining gain. The bound is asymptotically approached for large numbers of combined pulses. Other limitations of the pulse combining gain, for example due to timing jitter, are negligible compared to the mentioned phenomena.

5.4.3 Plesiochronous Systems

In a realistic system, the synchronization between the transmitter and the receiver will not be perfect. There may be long term variations between the clocks (wander, drift) or short term variations (jitter). In this section, we consider the influence of the jitter and a frequency difference on the pulse combining gain and the resulting BER. The jitter may be random or deterministic.

In previous work, the effect of timing errors on the spectral density has been studied in [Win99] and [Win02]. A comparison between the BER of different UWB modulation schemes has been performed in the presence of a uniform timing error in static and Rayleigh fading channels in [Güv03b]. The BER performance has been studied in correlated random timing error in [Lin03]. Jitter models in delay locked loop and phase locked loop have been used to evaluate the sensitivity of sampling and correlation in an UWB digital receiver in [Pel03]. The BERs for several modulation schemes and various conditions (multipath, multiple-access interference, narrowband interference,

[1] The measured standard deviations are 40 mV for 10 V full scale range, 4 mV for 1 V full scale range, 480 µV for 100 mV full scale range. For lower full scale ranges, the noise remains at 480 µV.

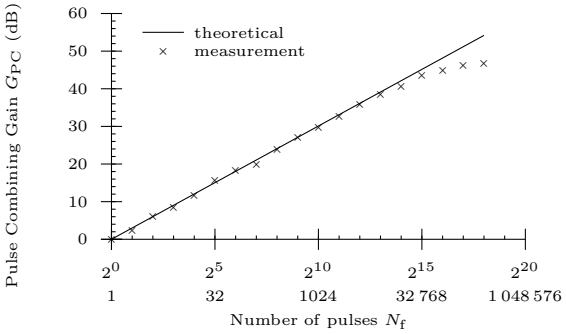

Figure 5.8: Pulse combining gain as a function of the number of coherently added pulses. The measurements are very close to the theoretical results up to several thousands of added pulses.

and timing errors) have been evaluated in [Güv03a]. The influence of timing errors on BER in the case of orthogonal Hermite pulse shapes has been studied in [Mic01] and [For03]. Finally, using computer simulations, the performance of UWB impulse radio in terms of throughput has been shown sensitive to timing errors and tracking in [Lov02].

In contrast to the above literature, we investigate in the following the influence on the received signal of the jitter and a frequency difference by assuming that the received pulses are combined to increase the SNR. With this approach, we can take into account the effect of the timing errors on the coherent combining of the pulses. Based on this time domain analysis, the BER performance is deduced in a second step. This alternative approach complements the existing performance evaluations available in the literature. In addition, lower bounds for the BER for a finite number of combined pulses are derived. Some of the following results are published in [Mer04b] and [Mer07].

Expected received signal: Again, the summed signal (3.21) is considered

$$q_{\text{sum}}(t) = \sum_{j=0}^{N_f-1} q(t + \epsilon_j) \tag{5.19}$$

where the time difference term is $\epsilon_j = \hat{\tau}_j - \tau_j$. The error term ϵ_j can be used to model different imperfections. In the following, a mathematical model is

first established to calculate an expected received signal. Based on this signal, the expected received energy is then calculated. The model is applied for a frequency difference and Gaussian jitter. Finally, the results are compared with outcomes of numerical simulations.

The delayed pulses in (5.19) can be written using the convolution integral as

$$q(t+\epsilon_j) = \int_{-\infty}^{\infty} q(\tau)\delta(t+\epsilon_j-\tau)\,d\tau = q(t) * \delta(t+\epsilon_j). \tag{5.20}$$

Using the linearity properties of the convolution, the summed signal can thus be written as

$$q_{\text{sum}}(t) = \sum_{j=0}^{N_\text{f}-1} \Big[q(t) * \delta(t+\epsilon_j)\Big] = q(t) * \sum_{j=0}^{N_\text{f}-1} \delta(t+\epsilon_j). \tag{5.21}$$

At the limit $N_\text{f} \to \infty$, and assuming that ϵ_j is mean ergodic[2], we thus obtain the expected, normalized, summed signal

$$\chi(t) \stackrel{\text{def}}{=} \lim_{N_\text{f}\to\infty} \mathsf{E}\left[\frac{q_{\text{sum}}(t)}{N_\text{f}}\right] = q(t) * \mathsf{E}\left[\frac{1}{N_\text{f}} \sum_{j=0}^{N_\text{f}} \delta(t+\epsilon_j)\right] \tag{5.22a}$$

$$\chi(t) = q(t) * \left[\int_{-\infty}^{\infty} \delta(t+\epsilon_j) f_\epsilon(\epsilon_j)\ \mathrm{d}\epsilon_j\right] \tag{5.22b}$$

$$\chi(t) = q(t) * f_\epsilon(-t) \tag{5.22c}$$

where $\mathsf{E}[\cdot]$ denotes statistical expectation and $f_\epsilon(t)$ is the probability density function for ϵ_j. For sufficiently large N_f and $f_\epsilon(t)$ an even function, we can thus approximate $q_{\text{sum}}(t)$ as

$$q_{\text{sum}}(t) \approx N_\text{f}\chi(t) = N_\text{f} q(t) * f_\epsilon(t). \tag{5.23}$$

[2]Note that assuming ϵ_j to be mean ergodic is not a very restrictive assumption, as it can be shown that a sufficient condition for a discrete-time white-sense stationary random process ϵ_j to be mean ergodic is $C_\epsilon(0) < \infty$ and $\lim_{n\to\infty} C_\epsilon(n) = 0$ where $C_\epsilon(n)$ is the covariance of ϵ_j [Vin97].

Based on the summed signal $\chi(t)$, we approximate the energy of the summed signal as

$$\mathcal{E}_{\text{sum}} = \frac{1}{R}\int_{-\infty}^{\infty} q_{\text{sum}}^2(t)\,\mathrm{d}t \approx \frac{N_\text{f}^2}{R}\int_{-\infty}^{\infty}\chi^2(t)\,\mathrm{d}t \stackrel{\text{def}}{=} \mathcal{E}_\chi \tag{5.24}$$

It is also interesting to consider the pulse combining gain due to the acquisition of N_f pulses. It is given by the ratio between the SNR per bit measured using the received signal $\mathcal{E}_\text{b}/\mathcal{N}_0$ and the one at the detector. The energy of the summed signal is $\mathcal{E}_{\text{sum}}$ and the noise power density increases proportionally with N_f. The resulting pulse combining gain is

$$G_\text{PC} = \frac{\mathcal{E}_{\text{sum}}}{N_\text{f}\mathcal{N}_0}\frac{\mathcal{N}_0}{\mathcal{E}_\text{b}} \approx \frac{\mathcal{E}_\chi}{N_\text{f}\mathcal{E}_\text{b}} = \frac{N_\text{f}}{R\mathcal{E}_\text{b}}\int_{-\infty}^{\infty}\chi^2(t)\,\mathrm{d}t \tag{5.25}$$

For perfectly synchronized systems, $\int_{-\infty}^{\infty}\chi^2(t)\,\mathrm{d}t = R\mathcal{E}_\text{b}$ and the gain due to the pulse combining is $G_\text{PC} = N_\text{f}$ as expected. In the next section, analytical results for $\chi(t)$ and G_PC are given and compared with numerical results for finite N_f.

5.4.4 Application to Gaussian distributed jitter

Expected received signal: In this paragraph, we assume that there is no deterministic jitter but only a random one. Furthermore, it is assumed that it is composed of several uncorrelated noise sources, such that by applying the central limit theorem, the resulting random jitter has a Gaussian distribution. When the variance of the Gaussian distributed jitter is σ^2, the jitter distribution becomes

$$\epsilon_j \sim f_\epsilon^{(\text{G})}(t) = \frac{1}{\sigma\sqrt{2\pi}}\exp\left(-\frac{t^2}{2\sigma^2}\right). \tag{5.26}$$

The influence of the Gaussian jitter on the pulse combining gain is considered for the second derivative Gaussian pulse (2.3c)

$$p_{\text{G}_2}(t) = +\sqrt{\frac{4\varsigma R}{3t_n}}\left(\frac{t^2}{t_n^2}-1\right)\exp\left(-\frac{t^2}{2t_n^2}\right). \tag{5.27}$$

Using (5.22c), the expected summed signal for $N_\mathrm{f} \to \infty$ is a second derivative Gaussian pulse with duration $\sqrt{t_n^2 + \sigma^2}$, i.e.,

$$\chi(t) = \sqrt{\frac{4R\varsigma}{3}\left(\frac{t_n}{t_n^2+\sigma^2}\right)^5}\left(t^2 - t_n^2 - \sigma^2\right)\exp\left(-\frac{1}{2}\frac{t^2}{\sigma^2+t_n^2}\right). \tag{5.28}$$

Finally, the pulse combining gain (5.25) is proportional to the number of combined pulses

$$G_\mathrm{PC}^{(\mathrm{G})} \approx \left(\frac{t_n}{\sqrt{\sigma^2+t_n^2}}\right)^5 N_\mathrm{f}. \tag{5.29}$$

The pulse combining gain is not bounded, but increases proportionally to the number of combined pulses. We define a proportionality factor κ between the pulse combining gain and the number of summed pulses as

$$\kappa \stackrel{\mathrm{def}}{=} \frac{G_\mathrm{PC}^{(\mathrm{G})}}{N_\mathrm{f}} \approx \left(\frac{t_n}{\sqrt{\sigma^2+t_n^2}}\right)^5. \tag{5.30}$$

The factor κ depends on the pulse duration and the variance of the jitter and is between 0 and 1. In the absence of jitter ($\sigma = 0$), the proportionality factor κ is independent of the pulse width and is 1. Pulses with a long duration are more robust in the presence of a Gaussian jitter. Figure 5.9 represents the proportionality factor κ as a function of the jitter standard deviation for four values of the pulse duration t_n. For example, the proportionality factor κ is $-2.42\,\mathrm{dB}$ for $t_n = 0.2\,\mathrm{ns}$ and $\sigma = 0.1\,\mathrm{ns}$.

Bit error rate for Gaussian jitter: The probability of an error during a binary data transmission in a communication system using orthogonal modulation in an AWGN transmission channel is given by the Marcum Q function

$$P(c_{q\hat{q}_n}(\epsilon_0,\ldots,\epsilon_{N_\mathrm{f}-1}),\mathcal{N}_0) = \mathrm{Q}\left(\sqrt{\frac{c_{q\hat{q}_n}(\epsilon_0,\ldots,\epsilon_{N_\mathrm{f}-1})}{\mathcal{N}_0}}\right). \tag{5.31}$$

where $c_{q\hat{q}_n}$ is the cross-correlation value between $q(t)$ and $\hat{q}_n(t)$ and depends on all the timing errors $\{\epsilon_j\}$. The BER of the data transmission with timing

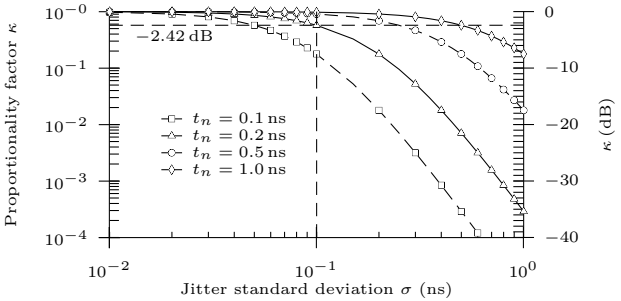

Figure 5.9: Theoretical proportionality factor κ for a second derivative Gaussian pulse with duration t_n and a Gaussian distributed timing jitter with standard deviation σ.

error is therefore given by

$$\mathrm{BER} = \int_{-\infty}^{\infty} \cdots \int_{-\infty}^{\infty} P(c_{q\hat{q}_n}(\epsilon_0, \ldots, \epsilon_{N_\mathrm{f}-1}), \mathcal{N}_0) \prod_{j=0}^{N_\mathrm{f}-1} f(\epsilon_j)\, \mathrm{d}\epsilon_j \tag{5.32}$$

where $f(\epsilon_j)$ is the distribution of the random variable ϵ_j. In the following, (5.32) is solved for a Gaussian jitter.

Large number of pulses: As the locally generated template $\hat{q}(t)$ is matched to the expected received signal $\chi(t)$, we expect that the BER for orthogonal modulations is given by

$$\mathrm{BER} = \mathrm{Q}\left(\sqrt{\frac{\mathcal{E}_\chi}{\mathcal{N}_0}}\right). \tag{5.33}$$

To prove (5.33), we consider that the expected correlation value becomes independent of the individual timing errors and is identical to the expected energy per bit $\mathcal{E}_\chi$. Therefore, (5.32) can be expressed as

$$\mathrm{BER} = P(\mathcal{E}_\chi, \mathcal{N}_0) \int_{-\infty}^{\infty} \cdots \int_{-\infty}^{\infty} \prod_{j=0}^{N_\mathrm{f}-1} f(\epsilon_j)\, \mathrm{d}\epsilon_j. \tag{5.34}$$

If furthermore all the ϵ_j are statistically independent, the BER is

$$\mathrm{BER} = P(\mathcal{E}_\chi, \mathcal{N}_0) \prod_{j=0}^{N_\mathrm{f}-1} \int_{-\infty}^{\infty} f(\epsilon_j)\, \mathrm{d}\epsilon_j \tag{5.35}$$

and because of the normalization of the probability density function

$$\mathrm{BER} = P(\mathcal{E}_\chi, \mathcal{N}_0). \tag{5.36}$$

Combining (5.36) and (5.31), the proposal (5.33) is shown to be correct.

As a consequence, the BER performance depends on the expected energy $\mathcal{E}_\chi$. By the definition of κ, the expected energy $\mathcal{E}_\chi$ is related to the bit energy by $\kappa\mathcal{E}_\mathrm{b}$. In a logarithmic representation of the BER as a function of the SNR, the factor κ appears as a shift toward the right side of the BER. For the above scenario, the shift is illustrated in figure 5.10, where the theoretical BER using (5.33) and (5.24) is represented and compared with numerical results obtained by Monte-Carlo simulations for $N_\mathrm{f} = 50$. The numerical results are in excellent agreement with the analytical equations. For example, the BER for $\sigma = 0.1\,\mathrm{ns}$ is shifted toward the right side by 2.42 dB as expected. We note, that the BER is not bounded for high SNR but tends toward 0.

Small number of combined pulses: For a small number of combined pulses the behavior of the BER performance for high SNR is considered in the following. The SNR is high if the BER is dominated by the timing errors and the AWGN becomes negligible. The discussion leads to a lower bound for the BER performance.

The probability that an error occurs during the transmission of one bit is given in (5.31). For a noiseless transmission, (5.31) simplifies to the sign of the correlation value and is

$$P(c_{q\hat{q}_n}(\epsilon_0, \ldots, \epsilon_{N_\mathrm{f}-1})) = \frac{1}{2}\left[1 - \mathrm{sign}\{c_{q\hat{q}_n}(\epsilon_0, \ldots, \epsilon_{N_\mathrm{f}-1})\}\right]. \tag{5.37}$$

It is noted that under the influence of the timing errors ϵ_j, it is possible that the cross correlation $c_{q\hat{q}_n}$ changes its sign even at high SNR. This result is in contrast to the case of a high number of combined pulse, where the BER tends towards 0 for high SNR. To calculate the BER we assume the locally generated templates to be $\hat{q}_n(t) = \chi(t - nt_\mathrm{c})$. In the absence of timing errors these templates are identical to the templates $\hat{q}_n(t) = q(t - nt_\mathrm{c})$

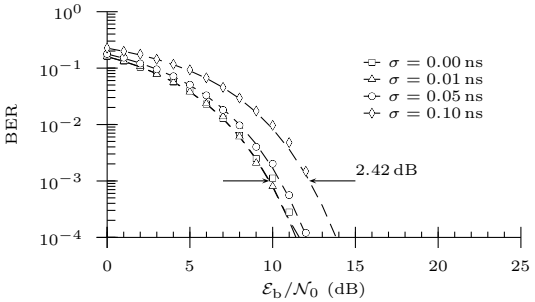

Figure 5.10: BER as a function of the SNR in AWGN transmission channel for TM in the presence of Gaussian jitter with standard deviation σ. The dashed lines represent the theoretical results. The dots represent the outcomes of Monte-Carlo simulations for $N_f = 50$.

optimal for AWGN. In the presence of timing errors, the proposed templates are matched for $N_f \to \infty$. We have observed that the proposed template $\chi(t - nt_c)$ outperforms the AWGN template in the presence of a Gaussian jitter also for limited N_f.

The results of an estimation of (5.37) introduced to (5.32) are represented in figure 5.11 for $1 \leq N_f \leq 5$. For example, for a single pulse ($N_f = 1$) and a Gaussian jitter with standard deviation 0.1 ns, the BER is $2.44 \cdot 10^{-2}$ even for a noiseless transmission. For $N_f = 2$, the BER is reduced to $2.50 \cdot 10^{-3}$.

Comparison with numerical simulations: The outcomes of Monte-Carlo simulations are compared to the bound for high SNR. Figures 5.12, 5.13, and 5.14 represent the results for $N_f = 1$, $N_f = 2$, and $N_f = 10$, respectively. As expected, the BER converges asymptotically to the lower bound for high SNR provided in figure 5.11. For low SNR it is observed that the performance estimation (5.33) provides an accurate prediction of the performance even for limited N_f.

5.4.5 Application to Frequency Difference

A frequency difference occurs if the clock frequency at the transmitter is different than the one at the receiver. The received pulses change their position inside the acquisition windows. The addition of the pulses is hence not coherent. It is uncoherent for a large frequency difference and partially coherent for a sufficiently small frequency difference. The frequency difference

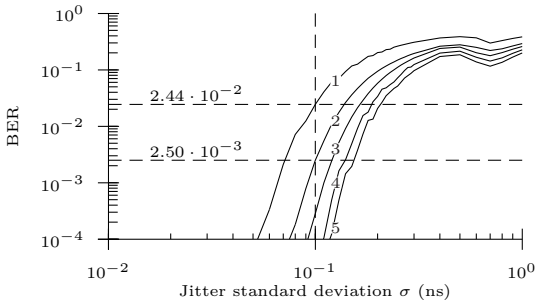

Figure 5.11: BER as a function of the jitter standard deviation σ in a noiseless transmission for a second derivative Gaussian pulse with $t_n = 200\,\text{ps}$ and $\delta = 2\,\text{ns}$. The results are shown for 1 to 5 pulses ($N_\text{f} = 1, \ldots, 5$).

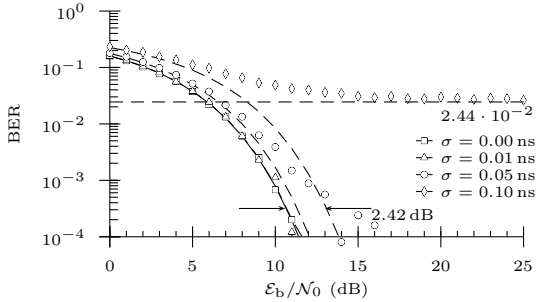

Figure 5.12: BER as a function of the SNR in an AWGN transmission channel for TM in the presence of Gaussian jitter with standard deviation σ. Numerical results obtained for $N_\text{f} = 1$. The dashed lines represent the bounds for high SNR and the theoretical performance for $N_\text{f} \to \infty$.

is modeled with a linear error term $\epsilon_j = (\hat{t}_\text{f} - t_\text{f})j$. The time difference after N_f additions is

$$N_\text{f}\alpha = N_\text{f}(\hat{t}_\text{f} - t_\text{f}) \tag{5.38}$$

where α is the time difference between the two clocks accumulated during one frame interval. The timing error can be defined by a probability density function. An asymmetry in the probability density function does not influence the power spectral density of the signal [Win02]. According to Parseval's theorem the energy is also independant of an asymmetry. We can

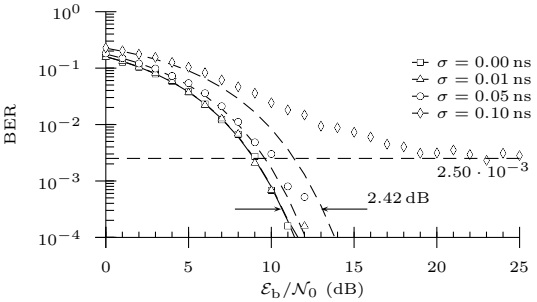

Figure 5.13: BER as a function of the SNR in an AWGN transmission channel for TM in the presence of Gaussian jitter with standard deviation σ. Numerical results obtained for $N_\mathrm{f} = 2$. The dashed lines represent the bounds for high SNR and the theoretical performance for $N_\mathrm{f} \to \infty$.

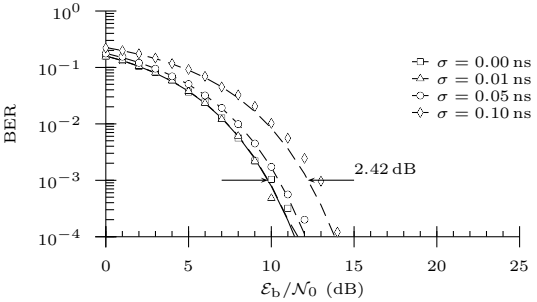

Figure 5.14: BER as a function of the SNR in an AWGN transmission channel for TM in the presence of Gaussian jitter with standard deviation σ. Numerical results obtained for $N_\mathrm{f} = 10$. The dashed line represent the theoretical performance for $N_\mathrm{f} \to \infty$.

thus consider the following symmetric uniform probability density function for the error term ϵ_j without loss of generality

$$\epsilon_j \sim \mathrm{U}(t) = \begin{cases} 1/\Delta t & \text{for } -\Delta t/2 < t < \Delta t/2, \\ 0 & \text{otherwise.} \end{cases} \tag{5.39}$$

Again the result for a second derivative Gaussian pulse is calculated. Using (5.22c) and (5.25) it follows that the pulse combining gain $G_\mathrm{PC}^{(\mathrm{U})}$ is a function

of N_f and the ratio α/t_n,

$$G_\mathrm{PC}^{(\mathrm{U})} = \frac{4t_n^2}{3N_\mathrm{f}\alpha^2} + \left(\frac{2N_\mathrm{f}}{3} - \frac{4t_n^2}{3N_\mathrm{f}\alpha^2}\right)\exp\left(-\frac{1}{4}\frac{N_\mathrm{f}^2\alpha^2}{t_n^2}\right). \tag{5.40}$$

It is represented in figure 5.15 and it is noted that the pulse combining gain is limited, hence it has a maximal value. Combining beyond the maximum will even result in a decrease of the obtained gain, because the pulse combining becomes incoherent. The maximum achievable gain $G_\mathrm{max}^{(\mathrm{U})}$ can be found by solving $\partial G_\mathrm{PC}^{(\mathrm{U})}/\partial N_\mathrm{f} = 0$ and is related to the pulse duration

$$G_\mathrm{max}^{(\mathrm{U})} \approx 0.9564\frac{t_n}{\alpha} \tag{5.41}$$

obtained for

$$N_\mathrm{max}^{(\mathrm{U})} \approx 1.6102\frac{t_n}{\alpha}. \tag{5.42}$$

In the following, a numerical example is given. Let us assume $t_n = 200\,\mathrm{ps}$ and a required pulse combining gain of 20 dB. Using (5.41), the maximum value for α to achieve the required gain is $\alpha_\mathrm{max} \approx 2\,\mathrm{ps}$. For a frame duration $t_\mathrm{f} = 100\,\mathrm{ns}$, this corresponds to a required accuracy of 20 ppm. A standard quartz oscillator will thus be sufficiently accurate and stable for this scenario.

5.5 Unmatched Pulse Template

When the receiver uses a pulse template $\hat{q}(t)$ which is not matched to the received pulse $q(t)$, the elements of the observation vector are modified and the BER is altered. Moreover, a pulse template mismatch is likely for every realistic communication system. This can be due to an imperfect channel estimation, a pulse template containing some noise, or even be intentional to improve other characteristics or lower the implementation complexity of the receiver. In this section, the influence of a pulse template mismatch to the SNR of the signal at the input of the detector is estimated for an AWGN transmission channel. The results are compared to the SNR of a matched filter receiver, and expressed in terms of a (negative) gain in SNR. With the goal to lower implementation complexity, [Lee02] estimates the loss in performance by using a receiver with a sinusoidal pulse template to receive second derivate Gaussian pulses. In [Blá03], the SNR with a rectangular acquisition window to acquire rectangular, triangular, or Gaussian pulse shapes is presented. The BER performance of a receiver with an unmatched template

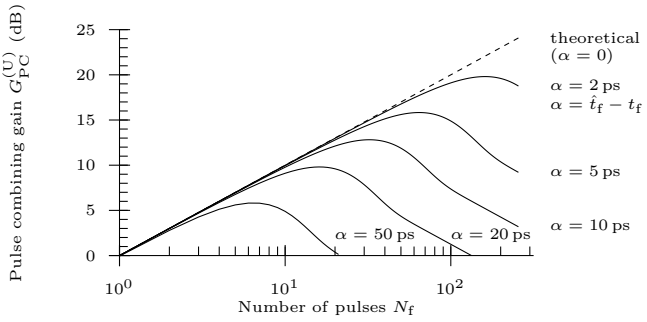

Figure 5.15: Pulse combining gain as a function of N_{f} in the presence of a frequency difference for a second derivative Gaussian pulse with duration $t_n = 200\,\mathrm{ps}$. The frequency difference is measured as the difference between the frame durations $\alpha = \hat{t}_{\mathrm{f}} - t_{\mathrm{f}}$.

is analyzed in [Kul04b, Kul04a] and the results are compared to the transmitted reference receiver. It is shown that a receiver with the unmatched template is capable to outperform a transmitted reference receiver at the cost of increased complexity. In this section, an approach is derived to generalize for any template and received pulse shape. Some of the results have been presented in [Mer04a].

5.5.1 Gain Definition

For the following performance analysis, we assume that the delay between two pulses of the received signal is larger than the channel excess delay and therefore that the inter pulse interference can be neglected. The analysis of the SNR can thus be performed by considering a single pulse. Let the received pulse of the user of interest be $q(t)$. The received signal energy is $\mathcal{E}_{\mathrm{b}}$. For a receiver with a matched template the SNR per bit is given by

$$\mathrm{SNR}_M = \frac{\mathcal{E}_{\mathrm{b}}}{\mathcal{N}_0}. \tag{5.43}$$

For a non matched template $\hat{q}(t) \neq q(t)$, the SNR per bit is

$$\mathrm{SNR}_{\mathrm{NM}} = \frac{\left(\int_{-t_{\mathrm{w}}/2}^{t_{\mathrm{w}}/2} q(t)\hat{q}(t)\,\mathrm{d}t \right)^2}{\mathcal{N}_0 \int_{t_{\mathrm{w}}/2}^{t_{\mathrm{w}}/2} |\hat{q}(t)|^2\,\mathrm{d}t}, \tag{5.44}$$

where t_{w} is the acquisition window duration. The gain is defined as the ratio between the SNR for a non-matched template and the one for a matched template, i.e., as $G_{\mathrm{NM}} = \mathrm{SNR}_{\mathrm{NM}}/\mathrm{SNR}_{\mathrm{M}}$. A possible approach to estimate the gain is represented in figure 5.16.

5.5.2 Pulse Template Models

The gain depends on the pulse template $\hat{q}(t)$. The template can also be considered as the impulse response of a filter applied to the input signal. In the following the gain is calculated for four typical templates and a second derivative Gaussian pulse shape. The templates are a second derivative Gaussian, a sinc (corresponding to an ideal low-pass filter), a template corresponding to a raised cosine filter, and a cosine (corresponding to a narrowband filter).

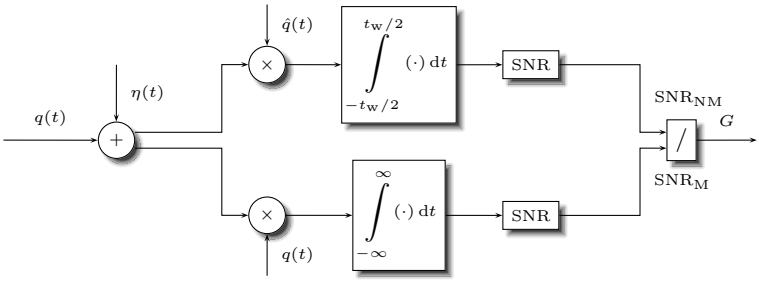

Figure 5.16: Estimation of the gain G as a function of the pulse template $\hat{q}(t)$.

Second derivative Gaussian: The template is given by

$$\hat{q}_2(t) = A\left(\frac{4\pi^2 t^2 f_o^2}{\ln(2)} - 1\right)\exp\left(-\frac{2\pi^2 t^2 f_o^2}{\ln(2)}\right) \tag{5.45}$$

with an arbitrary A. The multiplicative factor A can be used for normalization but the gain is independent of the normalization. In the case of an infinite acquisition window duration and an appropriate frequency f_o, the second derivative Gaussian becomes the matched template.

Ideal lowpass filter: The template corresponding to an ideal low pass filter with cut-off frequency f_o is given by

$$\hat{q}_{\mathrm{LP}}(t) = 2Af_o\frac{\sin(2\pi f_o t)}{2\pi f_o t} \tag{5.46}$$

and has an infinite duration.

Raised cosine filter: An equivalent to the raised cosine filter is obtained for a template

$$\hat{q}_{\mathrm{RC}}(t) = Af_o\frac{\sin(\pi t f_o)}{\pi t f_o}\frac{\cos(\pi R t f_o)}{1 - 4R^2 t^2 f_o^2} \tag{5.47}$$

where $0 \leq R \leq 1$ is the roll-of factor.

Narrowband filter: The template corresponding to a narrowband filter is

$$\hat{q}_{\mathrm{NB}}(t) = A\cos(2\pi f_o t) \tag{5.48}$$

where f_o indicates the center frequency. The bandwidth of the filter is defined by the acquisition window duration.

5.5.3 Application to the Second Derivative Gaussian Pulse

The gain G_{NM} is numerically estimated for a second derivative Gaussian pulse with duration $t_n = 0.1\,\mathrm{ns}$ as a function of the integration duration t_{w} and the frequency f_o of the filter. The outcomes are presented in figure 5.17. It is noted that the gain is relatively insensitive to a change of the integration time (as long as it is not shorter than about 1 ns) except for the narrowband

filter. This is due to a vanishing amplitude of the templates (5.45) to (5.47) for large t. For all the four proposed filters, the gain has a unique maximum. The values for t_w and f_o resulting in the maximal gain are listed in table 5.3. As expected, the maximal gain for a second derivative Gaussian filter is 0 dB. For illustration, the templates for the values given in table 5.3 are shown in figure 5.18.

5.6 Narrowband Interference

Wireless communication systems are ubiquitous nowadays. Several systems have emerged in addition to more traditional devices like radio and television broadcast. Today, widespread applications include among others wireless local area networks for computers, mobile phones, cordless home telephones, and personal area networks. An UWB system should not only cope with all of the above communication systems, but it should also work in the presence of many other possible—intentional or non-intentional—narrowband interferences up to reasonable interfering powers. On the other hand, the UWB system should not disturb or interrupt the narrowband communication systems. This issue is covered by the emission masks and not considered in this section. In the following, the robustness of UWB communications in the presence of a narrowband interference is evaluated based on an estimation of the variation of the elements of the observation vector. Other aspects, e.g., a narrowband interference that saturates the input amplifier which produces non-linearities are not considered. Corresponding to a worst case scenario the interference is first assumed to be synchronized with the UWB communication. The assumption of a synchronous interference is then removed and the resulting BER is calculated. The summed signal in the presence of a

Input Filter	f_o (GHz)	t_w (ns)	G_NM (dB)
second derivative Gaussian Filter	2.0	∞	0
Ideal LPF	0.9	2.2	−0.75
Narrow-band Filter	0.5	3.0	−0.76
Raised Cos ($R = 0.6$)	1.7	2.4	−1.11

Table 5.3: Maximal achievable gain for a second derivative Gaussian pulse shape depending on input filter.

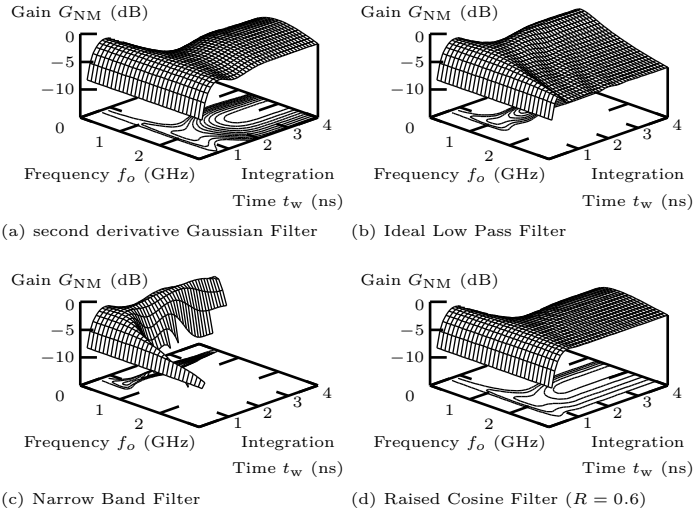

(a) second derivative Gaussian Filter (b) Ideal Low Pass Filter

(c) Narrow Band Filter (d) Raised Cosine Filter ($R = 0.6$)

Figure 5.17: Gain G_{NM} for various templates and a second derivative Gaussian pulse shape with $t_n = 0.5\,\mathrm{ns}$ as a function of filter frequency f_o and and acquisition window duration t_{w} for a synchronized system.

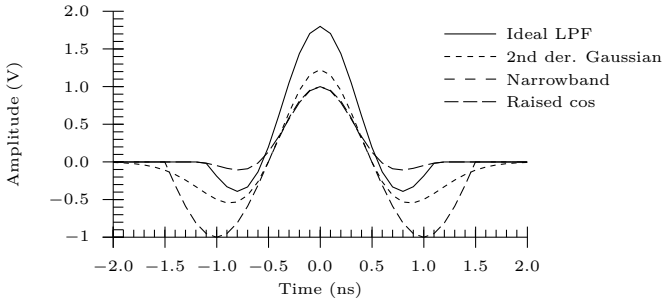

Figure 5.18: Shapes of the templates with the optimal values listed in table 5.3.

narrowband interference is

$$q_{\mathrm{sum}}(t) = \sum_{j=0}^{N_{\mathrm{f}}-1} \left[q(t) + A_{\mathrm{i}} \cos(\omega_{\mathrm{i}} t + \phi_j)\right] \tag{5.49a}$$

$$= N_{\mathrm{f}} q(t) + \sum_{j=0}^{N_{\mathrm{f}}-1} A_{\mathrm{i}} \cos(\omega_{\mathrm{i}} t + \phi_j), \tag{5.49b}$$

where A_{i} and ω_{i} are the amplitude and the frequency of the narrowband interference and ϕ_j is the phase modeling a delay.

5.6.1 Noiseless transmission

The receiver correlates the received summed signal with a local template. Without noise and interference, the nth element of the observation vector (normalized with the impedance R) is in the case of an antipodal AM and for the transmission of a data symbol $d_k \in \{0, 1\}$

$$\frac{\tilde{\boldsymbol{d}}_k[n]}{R} = \frac{1}{R} \int_{-t_{\mathrm{w}}/2}^{t_{\mathrm{w}}/2} \hat{q}_n(t) q_{\mathrm{sum}}(t)\, \mathrm{d}t = (2n-1)(2d_k - 1)\mathcal{E}_{\mathrm{b}}, \tag{5.50}$$

hence it takes the values $\pm\mathcal{E}_{\mathrm{b}}$. Because of the symmetry it is sufficient to calculate the outcome of a single receiver branch to obtain the BER. Without loss of generality the branch $n = 0$ and the data symbol $d_k = 1$ are considered and the corresponding element of the observation vector is $\tilde{\boldsymbol{d}}_k[0] = -\mathcal{E}_{\mathrm{b}} R$. In the presence of a narrowband interference, the element of the observation vector is altered. An error occurs, if the sign of the element $\tilde{\boldsymbol{d}}_k[0]$ changes due to the interference. In the following a lower bound is calculated below which a narrowband interference will not result in a transmission error. For narrowband interferences above the bound the BER is shown to be a function of the spreading code. To obtain a bound a worst case scenario is assumed, i.e., the narrowband interference has the largest possible impact on the element of the observation vector

$$\tilde{\boldsymbol{d}}_k[0] = -\mathcal{E}_{\mathrm{b}} R + \int_{-t_{\mathrm{w}}/2}^{t_{\mathrm{w}}/2} \hat{q}_0(t) \sum_{j=0}^{N_{\mathrm{f}}-1} A_{\mathrm{i}} \cos(\omega_{\mathrm{i}} t + \phi_j)\, \mathrm{d}t. \tag{5.51}$$

For real, symmetric templates $\hat{q}_0(t)$, it follows from (5.51) that in the worst case all the phase terms ϕ_j are zero. No error occurs when

$$\int_{-t_\mathrm{w}/2}^{t_\mathrm{w}/2} \hat{q}_0(t) \sum_{j=0}^{N_\mathrm{f}-1} A_\mathrm{i} \cos(\omega_\mathrm{i} t)\, \mathrm{d}t \leq \mathcal{E}_\mathrm{b} R. \tag{5.52}$$

For a matched template $\hat{q}_0(t) = q(t)$ and assuming that the pulse is received entirely inside the acquisition window, (5.52) becomes

$$\int_{-\infty}^{\infty} q(t) \cos(\omega_\mathrm{i} t)\, \mathrm{d}t \leq \frac{\mathcal{E}_\mathrm{b} R}{N_\mathrm{f} A_\mathrm{i}}. \tag{5.53}$$

In the following, a bound for the interference amplitude A_i is calculated such that the terms in (5.53) are equal, i.e.,

$$\int_{-\infty}^{\infty} q(t) \cos(\omega_\mathrm{i} t)\, \mathrm{d}t = \frac{\mathcal{E}_\mathrm{b} R}{N_\mathrm{f} A_\mathrm{i}}. \tag{5.54}$$

It is well known that the average value of a function $g(t)$ is equal to the Fourier transform evaluated at zero frequency, i.e., $\int_{-\infty}^{\infty} g(t)\, \mathrm{d}t = G(0)$. The Fourier transform of $q(t)\cos(\omega_i t)$ is

$$\frac{1}{2\pi} Q(\omega) * \pi(\delta(\omega - \omega_\mathrm{i}) + \delta(\omega + \omega_\mathrm{i})), \tag{5.55}$$

and (5.54) can be represented as

$$\frac{1}{2} Q(-\omega_\mathrm{i}) + \frac{1}{2} Q(+\omega_\mathrm{i}) = \frac{\mathcal{E}_\mathrm{b} R}{N_\mathrm{f} A_\mathrm{i}}. \tag{5.56}$$

Because of the assumption of a real, symmetric pulse, $Q(\omega)$ is also real and symmetric and (5.56) becomes

$$Q(\omega_\mathrm{i}) = \frac{\mathcal{E}_\mathrm{b} R}{N_\mathrm{f} A_\mathrm{i}}. \tag{5.57}$$

The amplitude of the narrowband interference A_i such that the bound for an error-free transmission is obtained is a function of the interference frequency and given by

$$A_\mathrm{i} = \frac{\mathcal{E}_\mathrm{b} R}{N_\mathrm{f} Q(\omega_\mathrm{i})}. \tag{5.58}$$

To obtain a performance estimation that is independent of the frame duration, a signal to interference ratio (SIR) is introduced by comparing the average UWB signal power $\mathcal{E}_\mathrm{b}/t_\mathrm{b}$ with the power of the narrowband interference P_i as

$$\mathrm{SIR} = \frac{\mathcal{E}_\mathrm{b}}{t_\mathrm{b} P_\mathrm{i}}. \tag{5.59}$$

Because the interference is assumed a sine wave, the SIR can also be written as a function of the interference amplitude as

$$\mathrm{SIR} = \frac{2R\mathcal{E}_\mathrm{b}}{t_\mathrm{b} A_\mathrm{i}^2}. \tag{5.60}$$

For a system with $50\,\Omega$, a bit duration $t_\mathrm{b} = 100\,\mathrm{ns}$, and a bit energy $\mathcal{E}_\mathrm{b} = 1\,\mathrm{pJ}$, (5.60) becomes in a decibel scale

$$\mathrm{SIR}\,(\mathrm{dB}) \approx 20\log_{10}(0.3162\,\mathrm{V}/A_\mathrm{i}). \tag{5.61}$$

Table 5.4 provides a conversion between the narrowband amplitude and the SIR for the above mentioned assumptions. As a reference, it is noted that a second derivative Gaussian pulse with duration $t_\mathrm{n} = 200\,\mathrm{ps}$ and a bit energy $\mathcal{E}_\mathrm{b} = 1\,\mathrm{pJ}$ and $N_\mathrm{f} = 1$ has a peak amplitude of about $0.43\,\mathrm{V}$. Combining (5.60) and (5.58), the bound for the SIR for which the BER is zero is found.

$$\mathrm{SIR}_0(\omega) = \frac{2}{t_\mathrm{b}\mathcal{E}_\mathrm{b}} N_\mathrm{f}^2 Q^2(\omega). \tag{5.62}$$

The bound is proportional to $N_\mathrm{f}^2 Q^2(\omega)$. For a given bit energy $\mathcal{E}_\mathrm{b}$, the pulse energy is divided by N_f or the signal amplitude is inversely proportional to

A_i (V)	SIR (dB)	A_i (V)	SIR (dB)
0.1	−10.00	1	−30.00
0.2	−16.02	2	−36.02
0.3	−19.54	3	−39.54
0.4	−22.04	4	−42.04
0.5	−23.98	5	−43.98
0.6	−25.56	6	−45.56
0.7	−26.90	7	−46.90
0.8	−28.06	8	−48.06
0.9	−29.08	9	−49.08

Table 5.4: Conversion between the amplitude of the interference and the SIR assuming a bit duration of 100 ns.

N_f. Using Parseval's theorem it follows that $Q(\omega)$ is also inversely proportional to N_f. Hence $N_\mathrm{f}^2 Q^2(\omega)$ is indeed independent of the number of pulses per symbol for a given bit energy. The bound SIR_0 depends on the spectrum and is represented in figure 5.19. For example for a narrowband interference with 500 MHz carrier frequency no transmission errors occur for a noiseless transmission when the SIR > -27 dB. For a SIR smaller than the bound, transmission errors are possible. To evaluate the BER in the presence of a narrowband interference a numerical simulation is made. The center frequency of the narrowband interference is 500 MHz and the phase is assumed to be random with an uniform distribution $\phi_j \sim \mathrm{U}[0, 2\pi[$. The outcomes of the numerical simulation are represented in figure 5.20. As expected the BER drops to zero for SIR $>$ SIR_0. For SIR $\to -\infty$, the BER approaches 0.5 independently of the code length. In the region $-\infty <$ SIR $<$ SIR_0 the BER performance can be improved with a longer spreading code as expected. This is due to the processing gain of the coherent addition. For increasing spreading code lengths the probability that all the contributions from the narrowband interference are combined coherently (i.e., that all phases ϕ_j are close to zero) decreases.

5.6.2 AWGN transmission

In this section, the transmission is not considered to be noiseless. The BER is evaluated for an AWGN transmission channel in the presence of a narrowband interfering signal. The phase of the interfering signal is again considered to be random with an uniform distribution $\phi_j \sim \mathrm{U}[0, 2\pi[$. The performance results shown in figure 5.20 are valid for the asymptotic behavior at high SNR. For a single pulse $N_\mathrm{f} = 1$ and a narrowband interference with center frequency 500 MHz the outcome of numerical simulations is represented in figure 5.21. As expected the BER tends toward the bounds for noiseless transmissions given in figure 5.20 for high SNR. The outcomes of numerical simulations for $N_\mathrm{f} = 8$ are represented in figure 5.22. It is noted that for SIR $\lesssim$ SIR_0 the performance is less degraded than for $N_\mathrm{f} = 1$. The bounds shown in figure 5.20 are again approached for high SNR.

5.7 Multiuser Interference

In this section the multiuser interference is considered under the assumption that the receiver is already synchronized with the user of interest. The synchronization in the presence of multiuser interference is considered in the

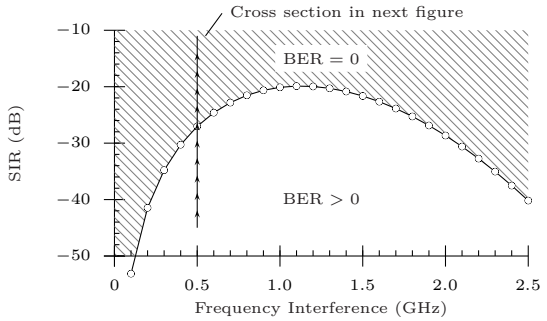

Figure 5.19: The domains for which a BER = 0 or a BER > 0 is obtained for a noiseless transmission with a narrowband interference. The bit duration is 100 ns.

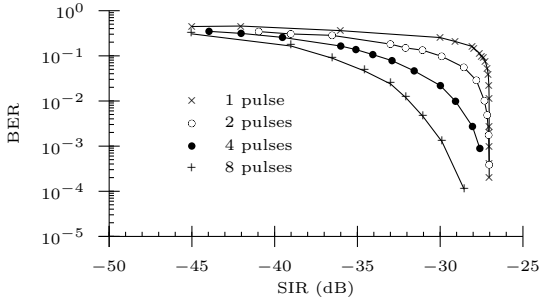

Figure 5.20: The BER as a function of the SIR in a noiseless transmission and a narrowband interference with 500 MHz and random phase and a bit duration of 100 ns.

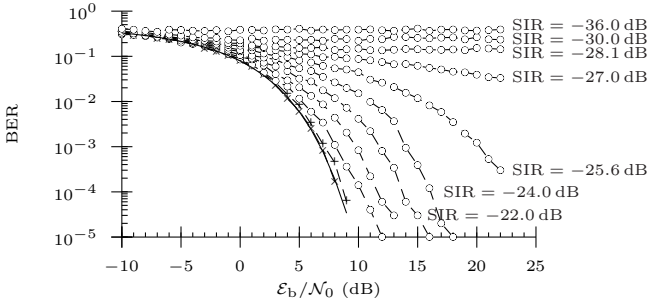

Figure 5.21: BER in the presence of a narrowband interference at 500 MHz and random phase for a UWB communication with $N_f = 1$and a bit duration of 100 ns

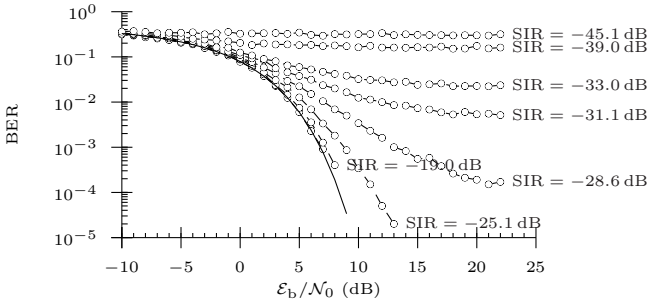

Figure 5.22: BER in the presence of a narrowband interference at 500 MHz with random phase for a UWB communication with $N_f = 8$ and a bit duration of 100 ns.

section 6.4. Multiple access and interference have always been one of the primary concern of wireless communications even since the very first wireless transmissions systems. Indeed, one of the reasons to forbid UWB signals as used in early spark-gap transmitters was the difficulty in discriminating the different transmissions at the receiver [Siw04]. With advances in signal processing effective methods for code discrimination in UWB communication systems have become applicable. Today, many extensive analyses of performance loss due to multiuser interference have been conducted, in general in terms of lowered signal to noise ratio (SNR) or increased BER. For example, an early contribution (see [Sch93]) discusses the SNR for asynchronous multiuser interference in an AWGN transmission channel, and introduces an approximation using a Gaussian noise to model a large number of interfering users. Same later contributions made by the same working team refine and generalize the results [Win97, Sch97, RM98b, RM98a, Win98]. These results are confirmed and generalized to BER in [Som02] and [Gez04]. Extensions to the above results are proposed in [Dur03] using Gaussian quadrature rules. With multiuser interference the distance estimation for positioning systems may be degraded [Maz04]. At the University of Oulu, a simulator has been developed to allow the numerical estimation of BER in various environments. In particular, AWGN and multipath propagation channels as well as narrowband and multiuser interference can be selected. Numerical results for multiuser interference in modified Saleh-Valenzuela channels are presented in [Tes04b] and [Tes04a]. Deterministic multiuser interference suppression is proposed in [LM00b] and [LM00a] and discussed in [LM02]. In [Yan02], the concept of deterministic multiuser interference suppression is extended

to uplink operation and block-spreading is applied to eliminate the inversion of large matrices. It is shown in [Yan04] that receivers based on deterministic multiuser interference suppression outperform Rake receivers with finite number of fingers, but rely on high sampling frequency and training sequences. Finally, in [Ers01] the ability of a receiver to recognize a single transmitting user in a non multipath propagation channel without assuming a synchronization with the user of interest is analyzed.

5.7.1 Models and Assumptions

When N_u transmitters are simultaneously active and the medium is linear, then the received signal is the superposition of all the individual signals

$$r(t) = \eta(t) + \sum_{u=0}^{N_\mathrm{u}-1} r^{(u)}(t). \tag{5.63}$$

From (2.15) it follows that the signal from the uth transmitter is

$$r^{(u)}(t) = \sum_{k=0}^{N_\mathrm{d}-1} \sum_{j=0}^{N_\mathrm{f}-1} d_{j,k}^{(\mathrm{a},u)} q^{(u)}(t - jt_\mathrm{f} - kt_\mathrm{s} - d_{j,k}^{(\mathrm{t},u)} t_\mathrm{c} + \phi_{j,k}^{(u)}), \tag{5.64}$$

where $\phi_{j,k}^{(u)}$ represents an arbitrary delay between the users. The received pulse shape $q^{(u)}(t)$ may be a function of the user u because a different propagation channel may be associated to each transmitter.

5.7.2 Multiuser Interference in AWGN

The signals from all users are assumed to be received with equal power and the receiver to be synchronized with the user of interest. As denoted in (5.64) the pulses from the interfering users are assumed to arrive at random instants. For the simulations, a uniform distribution during the frame $\phi_{j,k}^{(u)} \sim \mathrm{U}[0, t_\mathrm{f}[$ and nine interfering users ($N_\mathrm{u} = 10$) are assumed. The outcomes of the numerical simulations are given for a delay data modulation in figure 5.23 and for amplitude data modulation in figure 5.24. The AWGN performance without multiuser interference is shown as a solid line and it is noted that the BER performance at low SNR (SNR $< 5\,\mathrm{dB}$) is close to the AWGN limit. For high SNRs (SNR $> 20\,\mathrm{dB}$), the multiuser interference becomes the predominant source of transmission errors and the BER depends on the used code modulation. It is noted that TH8 modulation outperforms the

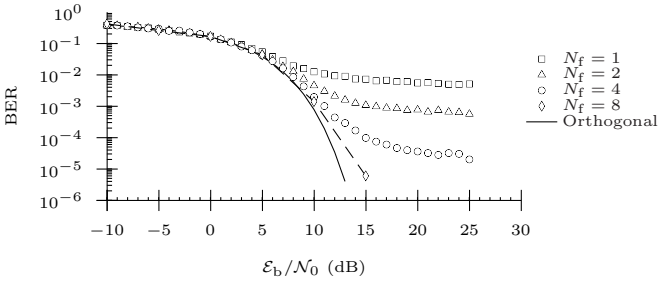

(a) TH8 TM

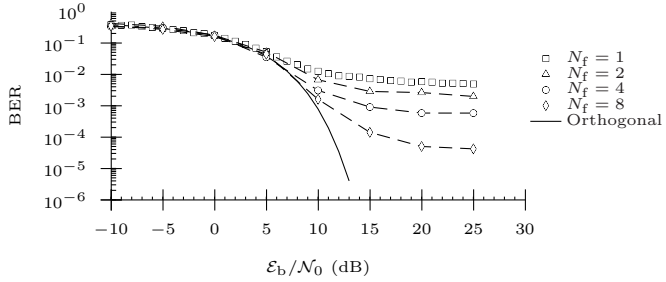

(b) AH TM

Figure 5.23: Comparison of the BER performance for TH8 TM and AH TM in AWGN in the presence of 9 interfering users.

AH one for code sequences $N_f \geq 2$. This can be explained by the larger set of admissible codes for TH8 than for AH.

5.7.3 Multiuser Interference in Multipath Propagation

All users are assumed to be received with equal power. The propagation channel is individual for each user and selected randomly for the simulations. The receiver uses the AWGN template and hence no a priori knowledge of the received signal shape from the user of interest is assumed. If such information is available it may improve the results in the presence of multiuser interference. The exploitation of the information concerning the channel impulse response from the user of interest is even proposed for secure communications and to detect intruders [Wil07]. The simulation results are shown in figure 5.25 for delay modulation and in figure 5.26 for amplitude modulation

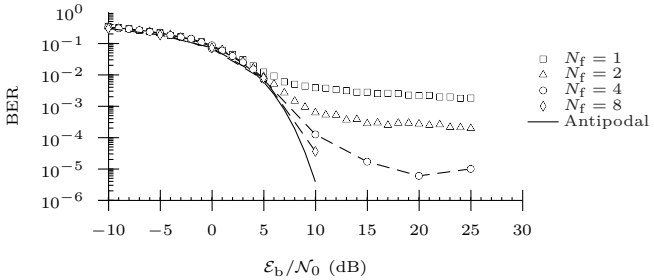

(a) TH8 AM

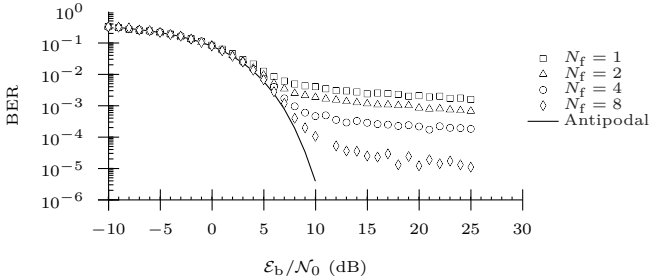

(b) AH AM

Figure 5.24: Comparison of the BER performance for TH8 AM and AH AM in AWGN in the presence of 9 interfering users.

in the presence of nine interfering users. As for the AWGN channel, the BER is close to the theoretical performance limit for small values of SNR (SNR $< 5\,\text{dB}$) and presents a lower bound for large SNRs (SNR $> 20\,\text{dB}$). Again, the TH8 modulation outperforms the AH one when more than one pulse per symbol is used ($N_f \geq 2$).

5.8 Summary

The theoretical BERs for transmissions over AWGN channels, expressed as functions of the SNR per bit, are also valid for UWB. They apply to both, AWGN and multipath channels[3]. Due to imperfections of the receiver, the

[3]However, the same SNR per bit may not correspond to the same communication range.

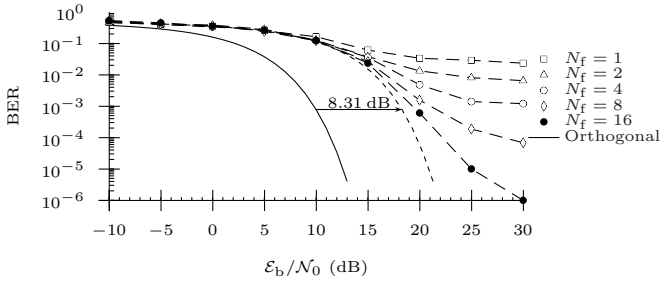

(a) TH8 TM

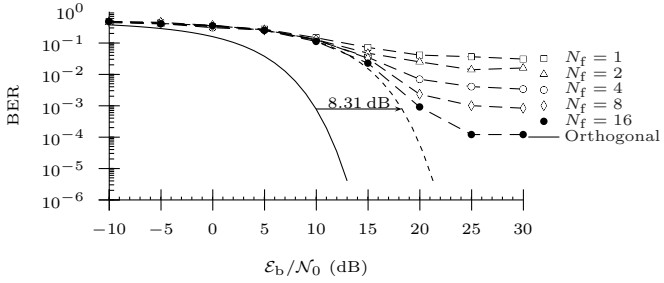

(b) AH TM

Figure 5.25: Comparison of the BER performance for TH8 TM and AH TM in CM3 in the presence of 9 interfering users.

processed energy per bit may be smaller than the received energy per bit, resulting in a loss of the SNR per bit. The losses due to selected imperfections are analyzed. When no channel estimation is performed and the receiver uses the transmitted pulse as a template, a degradation of the SNR by about 9 dB as compared with the SNR obtained with a matched template should be expected for a CM3 channel. Also for a CM3 channel, the received energy due to an acquisition window duration of 10 ns is shown to be lowered by about 3 dB as compared to an infinite acquisition window. The total processing gain is shown to be a function of the bandwidth and the data signaling rate. It can be decomposed into a duty cycle gain and a pulse combining gain. Without timing errors, the pulse combining gain increases linearly with the number of pulses per symbol. It is shown that the pulse combining gain is reduced in the presence of a Gaussian jitter or a frequency difference

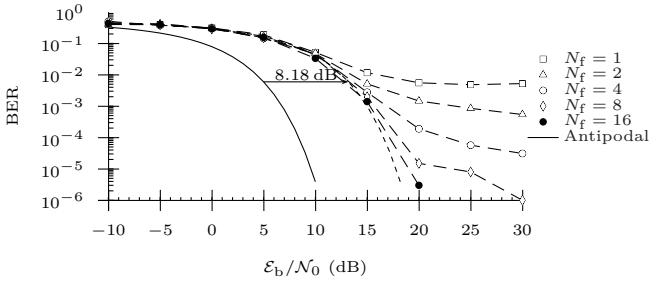

(a) TH8 AM

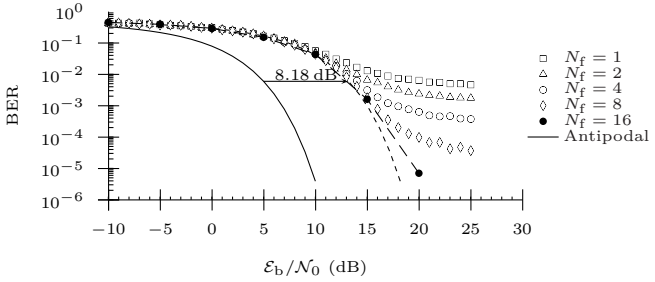

(b) AH AM

Figure 5.26: Comparison of the BER performance for TH8 AM and AH AM in CM3 in the presence of 9 interfering users.

between the receiver and the transmitter. Accepting a small degradation of the SNR, a non-matched template may be used by the receiver, for example to lower its implementation complexity. Finally the BER in the presence of narrowband and multiuser interference is shown. It is concluded that TH8 results in general in an improved robustness against multiuser interference as compared to AH.

Bibliography

[Blá03] R. Blázquez, P. P. Newaskar, and A. P. Chandrakasan. "Coarse Acquisition for Ultra Wideband Digital Receivers". *IEEE Conference on Acoustics, Speech, and Signal Processing*, vol. 4, pp. 137–140. Hong Kong, China, Apr. 2003.

[Dur03] G. Durisi and S. Benedetto. “Performance Evaluation of TH-PPM UWB Systems in the Presence of Multiuser Interference”. *IEEE Communications Letters*, 7(5):224–226, May 2003.

[Ers01] T. Erseghe. *Ultra Wide Band Pulse Communications*. Ph.D. thesis, Università Degli Studi Di Padova, 2001.

[Fis02] E. Fishler and H. V. Poor. “On The Tradeoff Between Two Types of Processing Gain”. *Conference on Communication, Control, and Computing*. Monticello, IL, USA, Oct. 2002.

[For03] J. Forgáč and P. Farkaš. “Analysis of Different UWB Systems with Timing Jitter and ISI in AWGN Channel”. *Joint IST Workshop on Mobile Future and Symposium on Trends in Communications*, pp. 51–54. Bratislava, Slovakia, Oct. 2003.

[Gez03] S. Gezici, H. Kobayashi, H. V. Poor, and A. F. Molisch. “Effect of Timing Jitter on the Trade-off Between Processing Gains”. MERL - A Mitsubishi Electric Research Laboratory, 2003.

[Gez04] S. Gezici, H. Kobayashi, H. V. Poor, and A. F. Molisch. “Performance Evaluation of Impulse Radio UWB Systems with Pulse-Based Polarity Randomization in Asynchronous Multiuser Environments”. *IEEE Wireless Communications and Networking Conference*, vol. 2, pp. 908–913. Atlanta, GA, USA, Mar. 2004.

[Güv03a] İ. Güvenç and H. Arslan. “On the Modulation Options for UWB Systems”. *Military Communications Conference*, vol. 2, pp. 892–897. Boston, MA, USA, Oct. 2003.

[Güv03b] İ. Güvenç and H. Arslan. “Performance Evaluation of UWB Systems in the Presence of Timing Jitter”. *IEEE Conference on Ultra Wideband Systems and Technologies*, pp. 136–141. Reston, VA, USA, Nov. 2003.

[Kul04a] B. Kull, J. Romme, H. Lüdiger, M. Mittelbach, S. Zeisberg, R. Moorfeld, and L. Piazzo. “Physical Layer Architecture and Performance”. Report for the European Project whyless.org, Jan. 2004.

[Kul04b] B. Kull and S. Zeisberg. "UWB Receiver Performance Comparison". *International Workshop on Ultra Wideband Systems Joint with Conference on Ultra Wideband Systems and Technologies*. Kyoto, Japan, May 2004.

[Lee02] S. Lee. *Design and Analysis of Ultra-Wide Bandwidth Impulse Radio Receiver*. Ph.D. thesis, University of Southern California, Aug. 2002.

[Lin03] S.-C. Lin and T.-D. Chiueh. "Performance Analysis of Impulse Radio Under Timing Jitter Using M-ary Bipolar Pulse Waveform and Position Modulation". *IEEE Conference on Ultra Wideband Systems and Technologies*, pp. 121–125. Reston, VA, USA, Nov. 2003.

[LM00a] C. J. Le Martret and G. B. Giannakis. "All-Digital Impulse Radio for MUI/ISI-Resilient Multiuser Communications Over Frequency-Selective Multipath Channels". *Military Communications Conference*, pp. 655–659. Los Angeles, CA, USA, Oct. 2000.

[LM00b] C. J. Le Martret and G. B. Giannakis. "All-Digital PAM Impulse Radio for Multiple-Access through Frequency-Selective Multipath". *IEEE Conference on Global Telecommunications*, vol. 1, pp. 77–81. San Francisco, CA, USA, 2000.

[LM02] C. J. Le Martret and G. B. Giannakis. "All-Digital Impulse Radio With Multiuser Detection for Wireless Cellular System". *IEEE Transactions on Communications*, 50(9):1440–1450, Sep. 2002.

[Lov02] W. M. Lovelace and J. K. Townsend. "The Effects on Timing Jitter and Tracking on the Performance of Impulse Radio". *IEEE Journal on Selected Areas in Communications*, 20(9), Dec. 2002.

[Maz04] C. Mazzucco, U. Spagnolini, and G. Mulas. "A Ranging Technique for UWB Indoor Channel Based on Power Delay Profile Analysis". *IEEE Vehicular Technology Conference*. Milan, Italy, May 2004.

[Mer04a] R. Merz, C. Botteron, and P.-A. Farine. "Characterization of Input Filters in UWB Receivers". *Atelier d'Arc et Senans du Laboratoire Européen Associé en Microtechnique*. Arc et Senans, France, Sep. 2004.

[Mer04b] R. Merz, C. Botteron, P.-A. Farine, and J. Farserotu. "Asymptotical Analysis of Timing Imperfections in UWB Receivers". *IEEE Conference on Circuits and Systems for Communications*. Moscow, Russia, Jul. 2004.

[Mer07] R. Merz, C. Botteron, and P.-A. Farine. "Performance of an Impulse Radio Communication System in the Presence of Gaussian Jitter". *IEEE International Conference on Ultra-Wideband*. Singapore, Sep. 2007.

[Mic01] L. B. Michael, M. Ghavami, and R. Kohno. "Effect of Timing Jitter on Hermite Function Based Orthogonal Pulses for Ultra Wideband Communication". *Wireless Personal Multimedia Communications, 4th International Symposium on*. Aalborg, Denmark, 2001.

[Opp04] I. Oppermann, M. Hämäläinen, and J. Iinatti (editors). *UWB Theory and Applications*. John Wiley & Sons, Ltd., 2004.

[Pel03] M. Pelissier, B. Denis, and D. Morche. "A Methodology to Investigate UWB Digital Receiver Sensitivity to Clock Jitter". *IEEE Conference on Ultra Wideband Systems and Technologies*, pp. 126–130. Reston, VA, USA, Nov. 2003.

[Pro01] J. G. Proakis. *Digital Communications*. McGraw-Hill Higher Education, 4 ed., 2001.

[RM98a] F. Ramírez-Mireles and R. A. Scholtz. "Multiple-Access Performance Limits with Time Hopping and Pulse Position Modulation". *Military Communications Conference*, vol. 2, pp. 529–533. McLean, VA, USA, Oct. 1998.

[RM98b] F. Ramírez-Mireles and R. A. Scholtz. "Wireless Multiple-Access Using SS Time-Hopping and Block Waveform Pulse Position Modulation Part 2: System Performance". *International Symposium on Information Theory and Its Applications*. Mexico City, Mexico, Oct. 1998.

[Sch93] R. A. Scholtz. "Multiple Access with Time-Hopping Impulse Modulation". *Military Communications Conference*, vol. 2, pp. 447–450. Boston, MA, USA. Invited Paper, Oct. 1993.

[Sch97] R. A. Scholtz and M. Z. Win. "Impulse Radio". *IEEE Symposium on Personal, Indoor and Mobile Radio Communications*, pp. 245–267. Helsinki, Finland. Invited Paper, Sep. 1997.

[Siw04] K. Siwiak and D. McKeown. *Ultra-Wideband Radio Technology*. John Wiley & Sons, Ltd., 2004.

[Som02] V. S. Somayazulu. "Multiple Access Performance in UWB Systems using Time Hopping vs. Direct Sequence Spreading". *IEEE Wireless Communications and Networking Conference*, vol. 2, pp. 522–525. Orlando, FL, USA, Mar. 2002.

[Tes04a] R. Tesi. "Ultra Wideband System Performance in the Presence of Interference". Licentiate Thesis, May 2004.

[Tes04b] R. Tesi, M. Hämäläinen, J. Iinatti, I. Oppermann, and V. Hovinen. "On the Multi-User Interference Study for Ultra Wideband Communication System in AWGN and Modified Saleh-Valenzuela Channel". *International Workshop on Ultra Wideband Systems Joint with Conference on Ultra Wideband Systems and Technologies*. Kyoto, Japan, May 2004.

[Vin97] Y. Viniotis. *Probability and Random Processses for Electrical Engineers*. McGraw-Hill, 1997.

[Wil07] R. Wilson, D. Tse, and R. A. Scholtz. "Channel Identification: Secret Sharing using Reciprocity in Ultrawideband Channels". *IEEE International Conference on Ultra-Wideband*. Singapore, Sep. 2007.

[Win97] M. Z. Win and R. A. Scholtz. "Comparisons of Analog and Digital Impulse Radio for Wireless Multiple-Access Communications". *IEEE Conference on Communications*, pp. 91–94. Montreal, QC, Canada, Jun. 1997.

[Win98] M. Z. Win and R. A. Scholtz. "Impulse Radio: How It Works?" *IEEE Communications Letters*, 2(2):36–38, Feb. 1998.

[Win99] M. Z. Win. "Spectral Density of Random Time-Hopping Spread-Spectrum UWB Signals with Uniform Timing Jitter". *Military Communications Conference*, vol. 2, pp. 1196–1200. Atlantic City, NJ, USA, Nov. 1999.

[Win02] M. Z. Win. "A Unified Spectral Analysis of Generalized Time-Hopping Spread-Spectrum Signals in the Presence of Timing Jitter". *IEEE Journal on Selected Areas in Communications*, 20(9):1664–1676, Dec. 2002.

[Yan02] L. Yang and G. B. Giannakis. "Multistage Block-Spreading for Impulse Radio Multiple Access Through ISI Channels". *IEEE Journal on Selected Areas in Communications*, 20(9), Dec. 2002.

[Yan04] L. Yang and G. B. Giannakis. "Ultra-Wideband Communications. An Idea Whose Time Has Come". *IEEE Signal Processing Magazine*, 21(6):26–54, Nov. 2004.

Chapter 6

Synchronization

For the performance estimations in chapter 5 it has been assumed that the receiver is already synchronized with the transmitter of interest. This assumption is valid during data transmission, but objectionable during the initial synchronization phase. In fact, during synchronization, the receiver aims to estimate the frequency and the delay of the received signal to establish a reliable communication for the consecutive data transmission. In this chapter, some aspects of the initial synchronization are considered. The most important terms are defined in section 6.1. In sections 6.2 and 6.3 two synchronization algorithms are presented. For each one, the required synchronization time is estimated. Finally, in section 6.4, the probability that an erroneous acquisition can be distinguished from the correct acquisition is calculated. In particular, the probability measures the ability of the receiver to reject an interfering transmitter during the synchronization phase.

6.1 Nomenclature

The initial synchronization after a cold start is composed of the frequency synchronization, the frame synchronization, and the data synchronization.

Frequency synchronization: During the frequency synchronization, the frame duration t_f of the transmitter is searched by the receiver. The frequency synchronization is a prerequisite for the coherent combining of the received pulses. A difference in the frame durations between the devices occurs because of the finite accuracy of the used clocks and depends among

others on the temperature and the aging of the clocks.

Time synchronization (frame and data synchronization): The frame synchronization and the data synchronization are both representatives of time synchronization. During the time synchronization, a possible delay between the transmitter of interest and the receiver is compensated. The frame synchronization compensates delays shorter than t_f, while the data synchronization applies delays that are multiples of t_f. The frame synchronization is successful when the instant of the pulse reception is known, i.e., the pulses are received within the acquisition windows. There may still be an ambiguity in which pulse corresponds to the first one during the transmission of the symbol. This ambiguity is removed by the data synchronization. Assuming that the length of the spreading code is identical to the number of pulses per symbol N_f, the search for the first pulse of the symbol (data synchronization) is equal to the search for the beginning of the spreading code (code synchronization). The data synchronization is in general based on the code sequence. However, it will be called data synchronization to avoid a confusion with a code selection, i.e., with a search for the code sequence used by the user of interest.

6.2 Intentional Frequency Difference

6.2.1 Working Principle

The synchronization compensates a potential frequency offset and delay between the transmitter and the receiver. However, the frequency and the delay are interdependent. For example, a constant frequency difference between the transmitter and the receiver results in a linearly increasing delay between the devices. Using this effect, it is possible to "scan" all the possible delays by applying intentionally a frequency difference. An illustration of the synchronization using an intentional frequency difference is illustrated in figure 6.1. Initially the delay between the clocks is δ_0. After a duration corresponding to k symbol acquisitions, the delay between the clocks is denoted as δ_k. In the following the synchronization time, i.e., the expected duration until the receiver is synchronized with the transmitter of interest, is calculated. Finally, a frequency selection scheme for the receiver is proposed to minimize the synchronization time. The selection scheme should be independent of the transmitter's frequency, because the receiver cannot estimate it before the synchronization phase ends.

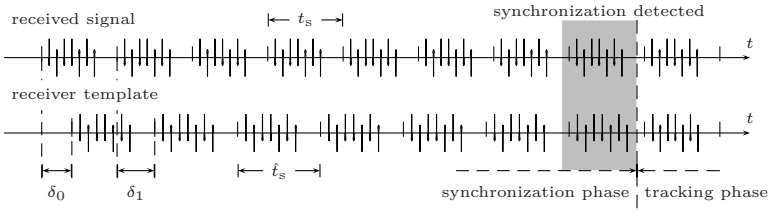

Figure 6.1: Illustration of the working principle of the synchronization using an intentional frequency difference. Due to the difference between $\hat{t}_s$ and t_s, the template may become aligned with the received signal.

6.2.2 Scan time

Is t_s the symbol duration at the transmitter and $\hat{t}_s$ the one at the receiver. The delay between the transmitter and the receiver is initially δ_0. Due to the difference of the clock frequency, the delay δ_k for the kth symbol is

$$\delta_k = \delta_0 + k(\hat{t}_s - t_s) \tag{6.1}$$

as represented in figure 6.1. One symbol duration is "scanned" when $\delta_k - \delta_0$ equals the symbol duration. From (6.1) it follows that one scan is finished for a k such that

$$\delta_k - \delta_0 = k|\hat{t}_s - t_s| = t_s. \tag{6.2}$$

Each one of the k symbol acquisitions requires a duration $\hat{t}_s$ to terminate. The time required to test for all possible delays, called scan time t_{scan}, is thus

$$t_{scan} = k\hat{t}_s = \frac{t_s\hat{t}_s}{|\hat{t}_s - t_s|}. \tag{6.3}$$

It follows from (6.3) that the scan time is reduced when the frequency difference and hence $|\hat{t}_s - t_s|$ is increased. However the coherent addition of the pulses decreases with an increasing frequency difference and it may happen that the pulse combining gain is not sufficient to detect the time synchronization. In the next section a strategy to minimize not the scan time but the synchronization time is deduced.

6.2.3 Synchronization time

The synchronization time is calculated for two scenarios. First, the receiver is assumed to know the frequency of the transmitter and the symbol duration t_s. This assumption is removed in the second scenario. For both assumption a synchronization scheme is proposed that minimizes the synchronization time.

KNOWN FREQUENCY: It is assumed that the receiver knows the symbol duration t_s and is able to tune its symbol duration $\hat{t}_\mathrm{s}$ to obtain any requested difference $\hat{t}_\mathrm{s} - t_\mathrm{s}$. As seen in (6.3), the difference should be selected as large as possible but is limited by the pulse combining gain. For the second derivative Gaussian pulse, it has been shown in (5.41) that the maximum achievable gain is limited to approximately $G_\mathrm{max} \approx 0.9564 t_n/\alpha$, where α is the difference between the frame durations. For a pulse duration $t_\mathrm{n} = 200\,\mathrm{ps}$ and a required pulse combining gain of 9.5 dB, the maximal value of α such that the gain can still be achieved is

$$\alpha \approx 0.9564 \cdot 200\,\mathrm{ps}/10^{9.5/10} \approx 20.13\,\mathrm{ps} \tag{6.4}$$

and is obtained for $N_\mathrm{max} \approx 15.99$ pulses. Taking $N_\mathrm{f} = 16$ and a frame duration of $t_\mathrm{f} = 100\,\mathrm{ns}$, the symbol duration is $t_\mathrm{s} = 1.6\,\mu\mathrm{s}$. Due to the frequency difference, the symbol duration at the receiver is $\hat{t}_\mathrm{s} = t_\mathrm{s} + N_\mathrm{f}\alpha \approx 1.6\,\mu\mathrm{s} + 322\,\mathrm{ps}$ and the scan time is

$$t_\mathrm{scan} = \frac{t_\mathrm{s}\hat{t}_\mathrm{s}}{|\hat{t}_\mathrm{s} - t_\mathrm{s}|} \approx 8.5\,\mathrm{ms}. \tag{6.5}$$

The expected synchronization time is half the scan time and is $\langle t_\mathrm{sync} \rangle \approx 4.25\,\mathrm{ms}$.

UNKNOWN FREQUENCY: Normally, the transmitter's frequency is not known by the receiver. However it can be assumed that the frequency difference is within given limits. This assumption is in general true because the accuracy of a clock, defined in first approximation by the temperature and the aging coefficients, is provided in the specifications of the used oscillators. If $\tilde{t}_\mathrm{s}$ is the initial symbol duration at the receiver after enabling the device without tuning the frequency, then the transmitter's symbol duration can be assumed to be within $\tilde{t}_\mathrm{s} \pm t_\mathrm{off}$. Figure 6.2 illustrates the situation. During the synchronization phase the receiver selects one symbol duration $\hat{t}_\mathrm{s}$ within the given

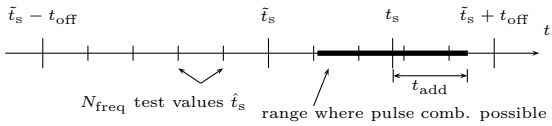

Figure 6.2: Illustration of the synchronization procedure for imprecise clocks.

range and "scans" the delays as described in the previous section. Either the synchronization phase stops successfully because the signal of interest is found or the search using the symbol duration $\hat{t}_\mathrm{s}$ is interrupted after a timeout and a new symbol duration $\hat{t}_\mathrm{s}$ is selected. A failure to synchronize can occur for two reasons. The difference between t_s and $\hat{t}_\mathrm{s}$ may be too large and the required pulse combining gain cannot be achieved. Another possible source of failure is that the difference may be too small. In this case, it may happen that the scan is interrupted before the receiver has a chance to become time synchronized with the transmitter.

In the following the minimal synchronization and the corresponding strategy to select $\hat{t}_\mathrm{s}$ are derived. The range within which the required pulse combining gain can be obtained is denoted as $[t_\mathrm{s} - t_\mathrm{add}, t_\mathrm{s} + t_\mathrm{add}]$. The receiver divides the interval $[\hat{t}_\mathrm{s} - t_\mathrm{off}, \hat{t}_\mathrm{s} + t_\mathrm{off}]$ into $(N_\mathrm{freq} - 1)$ intervals selecting N_freq symbol durations $\hat{t}_\mathrm{s}$. In the example shown in figure 6.2 three out of eleven symbol durations may potentially lead to a successful synchronization. In the following, the expected duration until synchronization $\langle t_\mathrm{sync} \rangle$ is minimized. Is is

$$\langle t_\mathrm{sync} \rangle = \frac{1}{2} N_\mathrm{freq} t_\mathrm{scan}. \tag{6.6}$$

It is noted that t_scan is also a function of N_freq. The scan time t_scan should be selected such that at least one selection of $\hat{t}_\mathrm{s}$ leads to a synchronization before the timeout. The longest duration for the scan is obtained for $\hat{t}_\mathrm{s} = t_\mathrm{s} + t_\mathrm{add} - 2t_\mathrm{off}/N_\mathrm{freq}$ and the scan time should be selected to be at least

$$t_\mathrm{scan} = \frac{t_\mathrm{s}(t_\mathrm{s} + t_\mathrm{add} - 2t_\mathrm{off}/N_\mathrm{freq})}{t_\mathrm{add} - 2t_\mathrm{off}/N_\mathrm{freq}}. \tag{6.7}$$

Inserting (6.7) in (6.6) it follows that

$$\langle t_\mathrm{sync} \rangle = \frac{1}{2} \frac{N_\mathrm{freq}^2 t_\mathrm{s}^2 + N_\mathrm{freq}^2 t_\mathrm{s} t_\mathrm{add} - 2N_\mathrm{freq} t_\mathrm{s} t_\mathrm{off}}{N_\mathrm{freq} t_\mathrm{add} - 2t_\mathrm{off}}. \tag{6.8}$$

The synchronization time is a function of N_{freq} as expected. It is noted that the validity of (6.8) is restricted to strictly positive values of the denominator. This corresponds to an assumption that the difference of two neighboring values of $\hat{t}_{\text{s}}$, obtained by $2t_{\text{off}}/N_{\text{freq}}$, is smaller than the zone for which the required processing gain can be achieved t_{add}.

The value N_{freq} for which the synchronization time is minimized is

$$\frac{\partial \langle t_{\text{sync}} \rangle}{\partial N_{\text{freq}}} = 0 \tag{6.9}$$

and is

$$N_{\text{freq,min}} = \frac{2t_{\text{off}}(t_{\text{s}} + t_{\text{add}} + \sqrt{t_{\text{s}}^2 + t_{\text{s}}t_{\text{add}}})}{t_{\text{add}}(t_{\text{s}} + t_{\text{add}})}, \tag{6.10}$$

obtained for

$$\langle t_{\text{sync}} \rangle = \frac{t_{\text{off}}t_{\text{s}}(t_{\text{s}} + t_{\text{add}} + \sqrt{t_{\text{s}}^2 + t_{\text{s}}t_{\text{add}}})(t_{\text{s}} + \sqrt{t_{\text{s}}^2 + t_{\text{s}}t_{\text{add}}})}{t_{\text{add}}^2\sqrt{t_{\text{s}}^2 + t_{\text{s}}t_{\text{add}}}} \tag{6.11}$$

The synchronization time as a function of the number of test frequencies N_{freq} is illustrated for $t_{\text{s}} = 100\,\text{ns}$ and $t_{\text{add}} = 1\,\text{ns}$ in figure 6.3. The validity of (6.10) and (6.11) is restricted to $N_{\text{freq}} \gg 1$. For example $t_{\text{s}} = 100\,\text{ns}$, $t_{\text{off}} = 2.5\,\text{ns}$, and $t_{\text{add}} = 1\,\text{ns}$, has a minimum of 201 µs for the synchronization time in the absence of a spreading code. The minimum is obtained for $N_{\text{freq}} = 9.975 \approx 10$. In the presence of a spreading code sequence with length 16, the symbol duration is $t_{\text{s}} = 1.6\,\mu\text{s}$ and the synchronization time is approximately 25.6 ms.

In general it is noted that $t_{\text{s}} \gg t_{\text{add}}$ and hence $t_{\text{s}} \approx t_{\text{s}} + t_{\text{add}}$. Inserting this approximation in (6.10) and (6.11), we obtain

$$N_{\text{freq,min}} \approx 4\frac{t_{\text{off}}}{t_{\text{add}}}, \tag{6.12}$$

obtained for

$$\langle t_{\text{sync}} \rangle \approx 4\frac{t_{\text{off}}}{t_{\text{add}}^2}t_{\text{s}}^2 = 4\frac{t_{\text{off}}}{t_{\text{add}}^2}N_{\text{f}}^2t_{\text{f}}^2. \tag{6.13}$$

The synchronization time is proportional to the squared symbol duration $N_{\text{f}}t_{\text{f}}$.

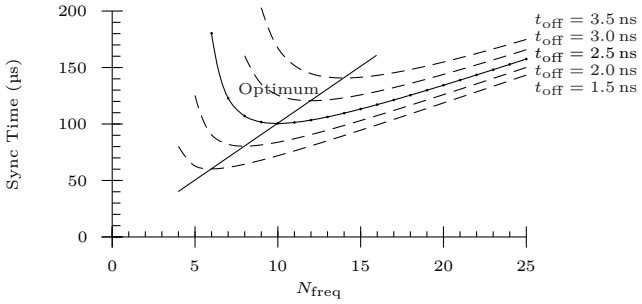

Figure 6.3: Expected synchronization time when using an intentional frequency offset. The pulse repetition period is 100 ns, t_{add} is 1 ns and no spreading code is assumed.

6.3 Bin Hopping Algorithm

The search through bin hopping is a trial and error approach. A set of parameters, consisting of a code sequence, a delay, and a frequency, is selected. When the signal from the transmitter of interest is detected using the current set of parameters, the set is stored and the synchronization is successfully terminated. When the signal is not detected, another set of parameters is selected and the process is repeated. In figure 6.4 each set of parameters is visualized as a bin. The intensity of the gray shading for each bin represents the probability that the synchronization stops because the signal of interest is detected. The bins framed with a bold black line are considered to lead to a correct acquisition. There may be several successive bins leading to a correct acquisition due to a multipath propagation channel. The synchronization procedure can be considered as an optimization problem in a two-dimensional space (when the spreading code sequence is known) or in a three-dimensional space (including the search for the correct spreading code sequence). In the following, we will assume that the spreading code sequence is known. First, the synchronization time is calculated for scenarios where the probability to terminate the search is either 0 or 1. It is then shown that the synchronization time depends on the search order for the bins, called the synchronization scheme. Finally, the estimation of the synchronization time is generalized to non-binary probabilities.

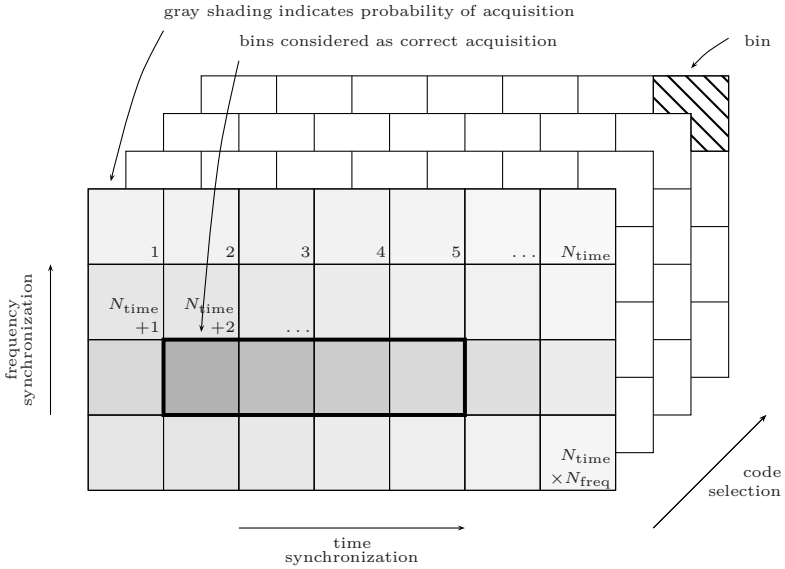

Figure 6.4: Model to decompose the three-dimensional search into bins that can be tested individually in a serial or parallel manner. The gray shading indicates the probability of acquisition for a given bin.

6.3.1 Single shot acquisition

First, the receiver is assumed to be able to capture the signal during the symbol duration t_s. The search for the frequency and time synchronization can be made entirely based on the acquired signal. Therefore, a single acquisition is required until the receiver is synchronized. If the processing time is negligible compared to the symbol duration, the synchronization time is t_s. Such a receiver requires large memories to store the signal and important processing power to test all the bins rapidly.

6.3.2 Single bin, binary probability

The next scenario assumes that exactly one bin leads to a correct acquisition and that the probability to terminate the synchronization is 1 for that bin and 0 for all others. The synchronization time depends on the duration for each test and the number of bins to be tested. The duration for each test

is at least t_s, when no additional processing time is required. The total number of bins is $N = N_\mathrm{time} N_\mathrm{freq}$ where N_time denotes the number of bins due to the search for the delay and N_freq the number of bins due to the frequency synchronization. N_freq depends on the clock accuracy, the pulse width, and the pulse repetition frequency. For the RSD receiver presented in section 3.4, only a short duration of the signal can be captured. The corresponding interval is called the acquisition window and has a duration t_w. For the time synchronization, it is required to place the acquisition windows at every possible instant during the symbol duration t_s. For non-overlapping acquisition windows, $N_\mathrm{time} = t_\mathrm{s}/t_\mathrm{w} = N_\mathrm{f} t_\mathrm{f}/t_\mathrm{w}$. The expected number of bins to be tested until synchronization is

$$\frac{\langle t_\mathrm{sync} \rangle}{t_\mathrm{s}} = \frac{1}{N} \sum_{n=1}^{N} n = \frac{N+1}{2}. \tag{6.14}$$

For $N \gg 1$, the expected synchronization time is hence

$$\langle t_\mathrm{sync} \rangle \approx \frac{1}{2} N_\mathrm{freq} N_\mathrm{time} N_\mathrm{f} t_\mathrm{f} = \frac{N_\mathrm{freq}}{2 t_\mathrm{w}} N_\mathrm{f}^2 t_\mathrm{f}^2. \tag{6.15a}$$

The synchronization time is proportional to the squared symbol duration, similar to (6.13) for the synchronization using an intentional frequency offset. To reduce the symbol duration, the code length N_f may be selected as short as possible. The result (6.15a) is independent of the search order. It is hence not possible to find a better search strategy to reduce the synchronization time.

For a numerical example, we assume $N_\mathrm{freq} = 3$, $t_\mathrm{f} = 100\,\mathrm{ns}$, and $t_\mathrm{w} = 10\,\mathrm{ns}$. For $N_\mathrm{f} = 1$ ($N = 3 \cdot 10 = 30$) $\langle t_\mathrm{sync} \rangle = 1.55\,\mu\mathrm{s}$ and for $N_\mathrm{f} = 16$, ($N = 3 \cdot 16 \cdot 10 = 480$) $\langle t_\mathrm{sync} \rangle \approx 385\,\mu\mathrm{s}$.

6.3.3 Consecutive bins, binary probability

When more than one bin leads to a correct acquisition, the search strategy, i.e., the order to test the bins, becomes important. For a serial synchronization algorithms, the bins are successively tested. In this section, it is assumed that K consecutive bins lead to a successful and correct synchronization with a probability 1. All other bins have a zero probability to terminate the synchronization. This model is an approximation for a multipath propagation channel that spreads the energy of the received pulse over several consecutive acquisition windows. The total number of bins is again denoted as

$N = N_{\text{freq}} N_{\text{time}}$. In the following, several search orders are proposed and discussed. The results for $N = 64$ are represented in figure 6.5.

LINEAR SEARCH: The linear search tests for all admissible bins in a strictly increasing order, i.e., in the order indicated by the bin number in figure 6.4. If no synchronization has been obtained, a new set of parameters is selected and the process starts over.

Because no information about the initial delay and the frequency difference is given, the selection of the first bin is random and it is assumed that all bins are equiprobable. The probability to terminate the synchronization after the first test is hence K/N. For all the following tests, the probability to successfully terminate the synchronization is only $1/N$. The expected number of bins to be tested is thus

$$\frac{\langle t_{\text{sync}} \rangle}{t_{\text{s}}} = \sum_{L=1}^{N-K+1} Lp(L) = \frac{K}{N} + \frac{1}{N} \sum_{L=2}^{N-K+1} L = \frac{3N - K + (N-K)^2}{2N} \tag{6.16}$$

where $p(L)$ is the probability that the acquisition successfully ends after L tests. The expected number of bins to be tested are illustrated in figure 6.5.

RANDOM SEARCH: For the random search, the probability that the acquisitions successfully ends after the Lth test is function of the probability that the $L-1$ previous tests are not successful and the Lth test is successful

$$p(L) = \left(1 - \frac{K}{N}\right)^{L-1} \left(\frac{K}{N}\right) \tag{6.17}$$

and hence

$$\frac{\langle t_{\text{sync}} \rangle}{t_{\text{s}}} = \sum_{L=1}^{\infty} Lp(L) = \frac{N}{K}. \tag{6.18}$$

For $K = 1$, the result is N and hence is worse than for every other synchronization scheme. From figure 6.5, we conclude that the random search should not be used when K is small.

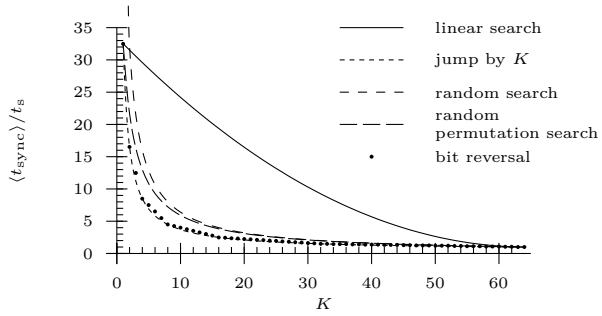

Figure 6.5: Comparison of the synchronization times for different synchronization schemes.

JUMP BY K: If K is known this synchronization scheme results in a minimal synchronization time. When the test for a bin k is not successful the next test is made for bin $k+K$. The probability for the Lth tests to be successful is K/N independently of L. The maximum number of tests is N/K. The expected number of bins to be tested is

$$\frac{\langle t_{\mathrm{sync}} \rangle}{t_{\mathrm{s}}} = \frac{N}{K} \sum_{L=1}^{N/K} L = \frac{1}{2} \left(1 + \frac{N}{K} \right). \tag{6.19}$$

It can be seen in figure 6.5 that the "jump by K" has the smallest synchronization time of all presented schemes. However the "jump by K" requires an a priori knowledge of K

RANDOM PERMUTATION SEARCH: The random permutation search is similar to the random search, but the already tested bins are excluded from all further tests. The synchronization time for the random permutation search is given in [Hom02] as

$$\frac{\langle t_{\mathrm{sync}} \rangle}{t_{\mathrm{s}}} = \frac{N+1}{K+1}. \tag{6.20}$$

The random permutation search results in nearly as low synchronization times as the "jump by K" but does not require a priori knowledge.

Bit reversal: The search order for the bit reversal scheme is calculated using the following algorithm. The bin number n is written as a binary number. The order of the bits is reversed and the resulting number provides the search order of the corresponding bins. For example for $N = 8$ the search order would be given by the sequence $\varepsilon(n)$

$$\begin{aligned} n \text{ decimal:} &\quad \{0, 1, 2, 3, 4, 5, 6, 7\} \\ n \text{ binary:} &\quad \{000, 001, 010, 011, 100, 101, 110, 110\} \\ \varepsilon(n) \text{ binary:} &\quad \{000, 100, 010, 110, 001, 101, 011, 111\} \\ \varepsilon(n) \text{ decimal:} &\quad \{0, 4, 2, 6, 1, 5, 3, 7\}, \end{aligned}$$

which means that bin 0 is tested before bin 4 followed by bin 2 and so on. From figure 6.5 it follows that the expected synchronization time for a bit reversal search is identical to the "jump by K" for K and N being powers of 2. The bit reversal search does not require an a priori knowledge and has a low implementation complexity.

Numerical Example: In the following the synchronization times for a typical scenario are calculated. It is assumed that the frame duration is $t_\mathrm{f} = 100\,\mathrm{ns}$ and that the number of pulses per symbol is either 1 or 16. The resulting symbol durations are 100 ns or 1.6 µs, respectively.

Because of the limited acquisition duration ($t_\mathrm{w} < t_\mathrm{s}$), only a part of the received signal can be stored. We assume $t_\mathrm{w} = 10\,\mathrm{ns}$. Further, it is assumed that due to the multipath the signal can be received during 40 ns, i.e., that $K = 4$ consecutive bins lead to a successful synchronization. Finally we assume $N_\mathrm{freq} = 3$ and $N_\mathrm{time} = t_\mathrm{s}/t_\mathrm{w}$. The total number of bins are $N = 10$ for $N_\mathrm{f} = 1$ or $N = 480$ for $N_\mathrm{f} = 16$. The synchronization times are listed in the following table.

	$N_\mathrm{f} = 1$		$N_\mathrm{f} = 16$	
Method	Number of Acquisitions	Synchronization time (µs)	Number of Acquisitions	Synchronization time (µs)
linear search	3.1	0.310	237.5	380
jump by K	1.75	0.175	60.5	97
random search	2.5	0.250	120.0	192
rand perm search	2.2	0.220	96.2	154

It is noted that the expected synchronization times for the bin hopping are significantly smaller than the ones for the intentional frequency difference algorithm.

6.3.4 Generalized synchronization time

In this section a generalized approach to calculate the expected synchronization time for the bin hopping algorithm is presented. The serial search is visualized with a flow graph [Hom03a, Hom03b, Suw05] as shown in figure 6.6. The search scheme is defined by a map $n \rightarrow \varepsilon(n)$ where n is the index of the bin and $\varepsilon(n)$ defines the search order. For each bin three probabilities are associated. $\pi_{\varepsilon(n)}$ is the probability that the search starts with bin n, $H_{\varepsilon(n)}(z)$ defines the probability that the synchronization is successfully terminated after having tested bin n and finally $G_{\varepsilon(n)}(z)$ defines the probability that the synchronization continues with the next bin. These probabilities can be written in the z-Domain to include also a processing time. The expected synchronization time is given by

$$\langle t_{\mathrm{sync}} \rangle = t_{\mathrm{s}} \left. \frac{\partial}{\partial z} P_{\mathrm{sync}} \right|_{z=1}, \tag{6.21}$$

where the generating function is given by [Hom03a]

$$P_{\mathrm{sync}} = \frac{\sum_{k=0}^{N-1} \pi_{\varepsilon(k)} \sum_{i=0}^{N-1} H_{\varepsilon(i \oplus_N k)}(z) \prod_{j=0}^{i-1} G_{\varepsilon(j \oplus_N k)}(z)}{1 - \prod_{i=0}^{N-1} G_{\varepsilon(i)}(z)} \tag{6.22}$$

Equations (6.21) and (6.22) can be used to calculate the expected synchronization times for any probabilities $\pi_{\varepsilon(n)}$, $G_{\varepsilon(n)}(z)$, and $H_{\varepsilon(n)}(z)$. A particular case is given when at least one of the probabilities $G_{\varepsilon(n)}(z)$ is zero, i.e., at least one bin leads to a synchronization with certainty. For this assumption (6.21) is simply given by the derivative of the numerator of (6.22) and is

$$\langle t_{\mathrm{sync}} \rangle = t_{\mathrm{s}} \sum_{k=0}^{N-1} \pi_{\varepsilon(k)} \sum_{i=0}^{N-1} \left(\prod_{j=0}^{i-1} G_{\varepsilon(j \oplus_N k)}(z) \right) \cdot \left[(i+1) H_{\varepsilon(i \oplus_N k)}(z) \right] \Bigg|_{z=1}. \tag{6.23}$$

6.4 Synchronization Probability

In this section, the receiver's ability to differentiate between the user of interest and the interfering users during synchronization phase is analyzed for the CM3 indoor multipath model and the case when the received pulse shape equals the transmitted one (denoted as AWGN). As a benchmark, a

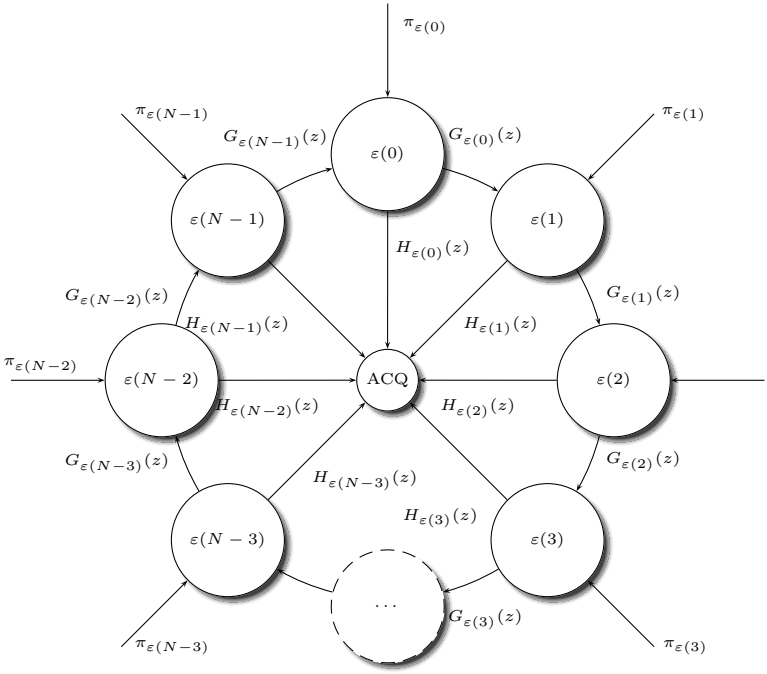

Figure 6.6: Generalized flow graph to calculate the synchronization time.

distinction coefficient related to the probability of successful termination of the initial synchronization is used. The distinction coefficient is defined in section 5.1.2 and is (5.6)

$$\mathcal{D} = \mathcal{W}_{(\mathrm{a})}/\mathcal{W}_{(\mathrm{b})}, \tag{6.24}$$

where $\mathcal{W}_{(\mathrm{a})}$ and $\mathcal{W}_{(\mathrm{b})}$ are the maximum values of the absolute received signals in scenarios (a) and (b) respectively. In all the examples, scenario (a) corresponds to the favored one and scenario (b) should be rejected. As such, a distinction coefficient above 1 would be sufficient for the identification in a noiseless scenario. However in practical applications, a distinction coefficient above 2 may be required. Another application of the distinction coefficient is to estimate the maximum tolerable difference of the received

powers due to near-far effect. Parts of the results in this section have been published [Mer05a, Mer05b].

6.4.1 Unique Transmitter

Scenario: In this section, it is assumed that a unique transmitter exists within the communication range of the receiver, i.e., no multiuser interference is assumed. Thus, two scenarios may happen during the synchronization phase.

(a) The receiver is synchronized with the user of interest. This scenario serves as a reference.
(b) The transmission from the user of interest is captured, but the receiver is not synchronized.

It is important that the receiver can differentiate between the scenarios (a) and (b) for a successful synchronization. Both scenarios are illustrated in figure 6.7. For (a), the summed signal w_k has a maximum amplitude that is N_f times larger than the maximum amplitude of an individual received pulse. For (b), the maximum amplitude is expected to be smaller than for (a) and to depend among others on the frequency and time difference between the transmitter and the receiver, the code sequence, and the modulation. In the following, the distinction coefficient is calculated for amplitude and delay modulations.

Description for TH: As only the user of interest $u = 0$ is assumed to transmit, the received summed signal is

$$w_k(t) = \sum_{j=0}^{N_\mathrm{f}-1} w_{j,k}(t) = \sum_{j=0}^{N_\mathrm{f}-1} q^{(0)}(t - \tau_j^{(0)} + \hat{\tau}_j^{(0)}) \tag{6.25}$$

and the delays are

$$\hat{\tau}_j^{(0)} - \tau_j^{(0)} = c_j^{(0)} t_\mathrm{c} - \hat{c}_j^{(0)} \hat{t}_\mathrm{c} + \phi^{(0)}. \tag{6.26}$$

It is assumed that the chip durations are sufficiently similar such that a coherent addition of the pulses is possible, $\hat{t}_\mathrm{c} = t_\mathrm{c}$ and that the receiver knows the spreading code sequence but not its beginning $\hat{c}^{(0)} = c^{(0)}_{j \oplus_N \Delta j}$. The additional delay $\phi^{(0)}$ may be used to model a timing error. During the whole chapter, $\phi^{(0)}$ is assumed to be independent of j, i.e., the delay between the

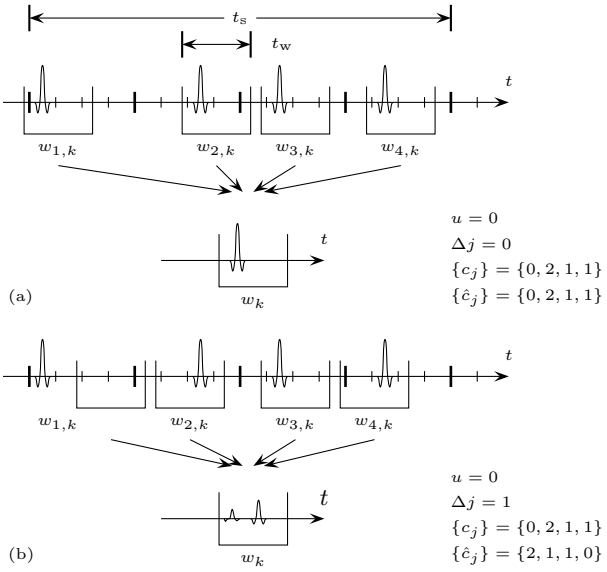

Figure 6.7: Coherent (a) and partially coherent (b) addition of limited duration windows for the user of interest $u = 0$. In scenario (a) the applied spreading code for the pulse delays is $\{0, 2, 1, 1\}$ and the same code is used to place the acquisition windows $w_{j,k}$. In scenario (b) the applied spreading code is again $\{0, 2, 1, 1\}$. The receiver applies the correct code, but shifted by one position ($\Delta j = 1$) and the code becomes $\{2, 1, 1, 0\}$. The distinction coefficient is $\mathcal{D} = 4/2$ for the given example.

transmitter and the receiver does not change significantly during one symbol acquisition. For scenario (a) the receiver is assumed to be synchronized. It follows from the data synchronization that $\Delta j = 0$ and from the frame synchronization that $\phi^{(0)} = 0$. Without noise the maximum for scenario (a) is

$$\mathcal{W}_{(\mathrm{a})} = N_\mathrm{f} \max_t \left| q^{(0)}(t) \right| . \tag{6.27}$$

For scenario (b), the receiver is not synchronized (not simultaneously $\Delta j = 0$ and $\phi^{(0)} = 0$) and the maximum value is calculated using

$$\mathcal{W}_{(\mathrm{b})} = \max_{\substack{\Delta j \neq 0 \\ \phi^{(0)}}} \max_t \left| \sum_{j=0}^{N_\mathrm{f}-1} q^{(0)}(t + (c_j^{(0)} - c_{j \oplus_N \Delta j}^{(0)}) t_\mathrm{c} + \phi^{(0)}) \right| . \tag{6.28}$$

The maximum for scenario (b) is obtained when the pulses are received within the acquisition windows. Without loss of generality, we can hence assume frame synchronization ($\phi^{(0)} = 0$). As the receiver is not synchronized for scenario (b), it follows that $\Delta j = \{1, \ldots, N_\mathrm{f} - 1\}$. If the shifted pulses do not overlap, i.e., the duration of $q^{(0)}(t)$ is smaller than t_c, (6.28) becomes

$$\mathcal{W}_{(\mathrm{b})} = \mathfrak{W}_{(\mathrm{b})} \left| \max_t q^{(0)}(t) \right| \tag{6.29}$$

where $\mathfrak{W}_{(\mathrm{b})}$ denotes the maximum number of solutions in j to

$$c_j^{(0)} - c_{j \oplus_N \Delta j}^{(0)} = l \tag{6.30}$$

for any admissible Δj and l [Ers01]. $\mathfrak{W}_{(\mathrm{b})}$ is referred to as the maximum number of hits between the two delayed TH codes and is studied extensively in [Ers01]. By definition, $\mathfrak{W}_{(\mathrm{b})}$ is a positive integer. The calculation of $\mathfrak{W}_{(\mathrm{b})}$ can be done with the following algorithm.

```
for Δj = 1 to N_f − 1
  Initialize a[l] with zero values
  for j = 0 to N_f − 1
    Increment the element a[c_j^(0) − c_{j⊕_N Δj}^(0)].
  end j
  store b[Δj] = max_l(a[l])
end Δj
store 𝔚_(b) = max_{Δ j} b[Δj].
```

The distinction coefficient

$$\mathcal{D} = \frac{\mathcal{W}_{(\mathrm{a})}}{\mathcal{W}_{(\mathrm{b})}} = \frac{N_\mathrm{f}}{\mathfrak{W}_{(\mathrm{b})}} \frac{\max_t |q^{(0)}(t)|}{\max_t |q^{(0)}(t)|} = \frac{N_\mathrm{f}}{\mathfrak{W}_{(\mathrm{b})}} \tag{6.31}$$

becomes independent of the pulse shape.

Theoretical bound for TH: The spreading code sequence has a length N_f and each value is M-ary and denoted as $c_j^{(0)} \in \{0, \ldots, M-1\}$. The $2M-1$ possible outcomes of the difference $c_j - \hat{c}_j$ are given by the set $\{-M-1, \ldots, M-1\}$. Again, for the scenario (a), all pulses are coherently added and $\mathcal{W}_{(\mathrm{a})} = N_\mathrm{f} \max_t |q^{(0)}(t)|$. From (6.30) it follows, that $\mathcal{W}_{(\mathrm{b})}$ is minimal when the $c_j^{(0)} - c_{j \oplus_N \Delta j}^{(0)}$ is uniformly distributed over the $2M-1$ admissible values of l. In this case

$$\mathcal{W}_{(\mathrm{b})} = \left\lceil \frac{N_\mathrm{f}}{2M-1} \right\rceil \max_t |q^{(0)}(t)| \tag{6.32}$$

and hence the distinction coefficient is

$$\mathcal{D} = \frac{N_\mathrm{f}}{\left\lceil \dfrac{N_\mathrm{f}}{2M-1} \right\rceil}. \tag{6.33}$$

Figure 6.8 represents the distinction coefficient as a function of N_f and M. As expected, an increase of M may result in a better distinction coefficient. The maximal value of the distinction coefficient for a given M is $\mathcal{D}_\mathrm{max} = 2M-1$ and is obtained whenever N_f is an integer multiple of $2M-1$. It follows that the best distinction coefficient may be obtained for a limited length of the code sequence and that a code length equal to a power of 2 does not necessarily result in the best performance.

Description for AH: For the antipodal amplitude modulation, the summed signal is for $\hat{t}_\mathrm{f} = t_\mathrm{f}$

$$w_k(t) = \sum_{j=0}^{N_\mathrm{f}-1} w_{j,k}(t) = \sum_{j=0}^{N_\mathrm{f}-1} c_j^{(0)} \hat{c}_j^{(0)} q^{(0)}(t + \phi^{(0)}) \tag{6.34}$$

Again, the worst case of scenario (b) occurs when the pulses are received within the acquisition window and a frame synchronization is thus assumed ($\phi^{(0)} = 0$). The outcomes are for scenario (a)

$$\mathcal{W}_\mathrm{(a)} = N_\mathrm{f} \max_t \left| q^{(0)}(t) \right|. \tag{6.35}$$

and scenario (b)

$$\mathcal{W}_\mathrm{(b)} = \mathfrak{W}_\mathrm{(b)} \max_t \left| q^{(0)}(t) \right|, \tag{6.36}$$

where

$$\mathfrak{W}_\mathrm{(b)} = \max_{\Delta j \neq 0} \left| \sum_{j=0}^{N_\mathrm{f}-1} c_j^{(0)} c_{j \oplus_N \Delta j}^{(0)} \right|. \tag{6.37}$$

Due to the absolute value $\mathfrak{W}_\mathrm{(b)}$ is a non-negative integer. The distinction coefficient

$$\mathcal{D} = \frac{N_\mathrm{f}}{\mathfrak{W}_\mathrm{(b)}} \tag{6.38}$$

is again independent of the pulse shape.

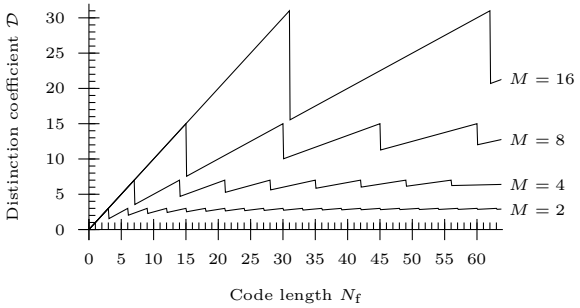

Figure 6.8: Best distinction coefficient for TH with an M-ary code with length N_f.

Theoretical bound for AH: A theoretical bound for the distinction coefficient is given by $\mathcal{D} = N_\mathrm{f}$ and is obtained when $\mathfrak{W}_{(\mathrm{b})} = 1$. Unfortunately, a code that achieves this bound does only exist for some code lengths N_f. An example of such a code sequence for $N_\mathrm{f} = 7$ is $c_j = \{1, -1, 1, -1, -1, -1, 1\}$ for which the autocorrelation function is $C_{\Delta j} = \{7, -1, -1, -1, -1, -1, -1\}$. An extensive search for the best code with respect to the distinction coefficient has been performed for code lengths $N_\mathrm{f} \leq 32$. The results of this search are illustrated in figure 6.9. It is noted that the performance depends on N_f and that a power for N_f does not necessarily results in the highest possible distinction coefficient.

Numerical evaluation for TH using (6.30) and AH using (6.37): A random spreading code is assumed to calculate distinction coefficients that can be expected in a realistic system. The distribution of the code symbol c_j is assumed to be uniform in the interval $[0, \ldots, M-1]$. Hence, $c_j - c_{j \oplus_N \Delta j}$ is not uniformly distributed, but has a triangular probability distribution in the interval $[-M-1, \ldots, M-1]$. The outcomes are illustrated in figure 6.10. For the delay modulation, the distinction coefficient depends on the number of admissible delays M. TH8 has a performance that is comparable with the one obtained for AH.

Numerical simulation for TH using (6.28): The results from a numerical simulation using second derivative Gaussian pulses are shown in figure 6.11. The outcomes using (6.28) are shown using dashed lines. They are compared to the results from the former section based on (6.30) represented

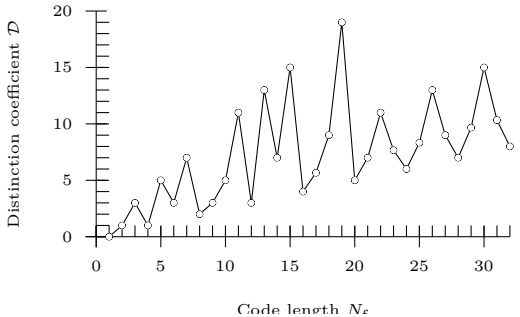

Figure 6.9: Best distinction coefficient that can be obtained for AH for a binary code with length N_f.

with solid lines. The number of iterations for the numerical simulation is limited to obtain admissible simulation durations. For this reason, the numerical values have a large variance and only trends should be deduced from them. In particular the variance is high for a small number of combined pulses. In figure 6.11 it can be seen that for a sufficiently high number of pulses, $N_\mathrm{f} \geq 32$, the numerical simulations are close to the predictions.

6.4.2 A Single Active Transmitter

Only one transmitter is assumed to be active at any time. However, several transmitters may be within the range of communication. The number of transmitters is denoted as N_u, and the uth transmitter is supposed to be active. Without loss of generality, the transmitter of interest is $u = 0$. The received summed signal is for TH

$$w_k(t) = \sum_{j=0}^{N_\mathrm{f}-1} w_{j,k}(t) = \sum_{j=0}^{N_\mathrm{f}-1} q^{(u)}(t - \tau_j^{(u)} + \hat{\tau}_j^{(0)}) \tag{6.39}$$

and the delays are

$$\hat{\tau}_j^{(0)} - \tau_j^{(u)} = (c_j^{(0)} - c_{j \oplus_N \Delta_j}^{(u)}) t_\mathrm{c} + \phi^{(u)}. \tag{6.40}$$

Scenario: The following scenarios may happen during the synchronization phase.

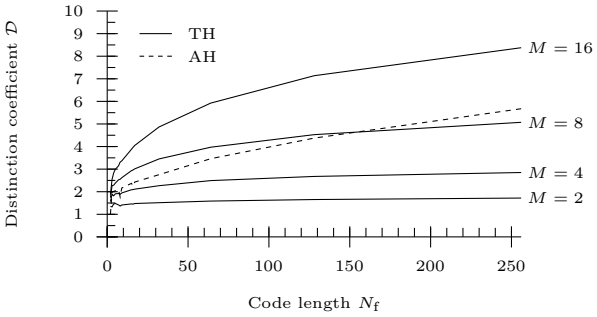

(a) linear representation

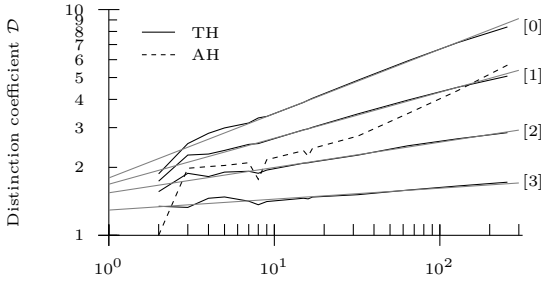

[0] $M = 16$ $\log_{10}(\mathcal{D}) \approx 0.2850 \log_{10}(N_\mathrm{f}) + 0.2542$
[1] $M = 8$ $\log_{10}(\mathcal{D}) \approx 0.2037 \log_{10}(N_\mathrm{f}) + 0.2264$
[2] $M = 4$ $\log_{10}(\mathcal{D}) \approx 0.1121 \log_{10}(N_\mathrm{f}) + 0.1884$
[3] $M = 2$ $\log_{10}(\mathcal{D}) \approx 0.0485 \log_{10}(N_\mathrm{f}) + 0.1118$

(b) double-logarithmic representation

Figure 6.10: Linear (a) and double-logarithmic (b) representation of the expected distinction coefficient for a unique transmitter with a white, uniform code sequence with length N_f.

(a) The transmission from the user of interest is captured ($u = 0$) and the receiver is synchronized ($\phi^{(0)} = 0$, $\Delta j = 0$). This scenario serves as a reference.

(b1) The transmission from the user of interest is captured ($u = 0$), but the receiver is not synchronized ($\phi^{(0)} \neq 0$ or $\Delta j \neq 0$).

(b2) The user of interest is not transmitting and the transmission from an interfering user $u \neq 0$ is captured.

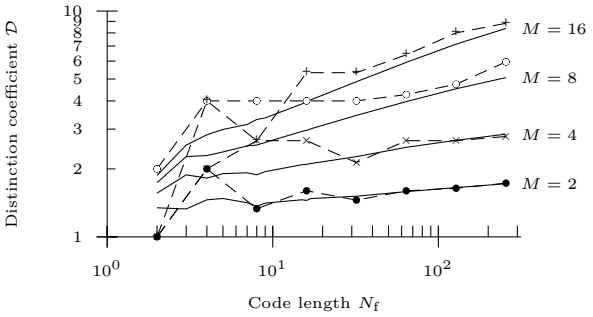

Figure 6.11: Distinction coefficient for random spreading codes and a unique transmitter. The dashed lines are the outcomes of numerical simulations using second derivative Gaussian pulses. The solid line represent the predictions from figure 6.10.

It is important that the receiver can differentiate between the case (a) and the cases (b1) and (b2) for a successful termination of the search phase. For the estimations, a perfect power control is assumed, i.e., the received power from each transmitter is identical.

Numerical evaluation based on the codes: The maximum for all configurations belonging to scenario (b) is obtained when the pulses from the uth transmitter are received within the acquisition window ($\phi^{(u)} = 0$). By analogy to (6.30), the maximum for

$$c_j^{(0)} - c_{j \oplus_N \Delta j}^{(u)} = l \tag{6.41}$$

for any admissible Δj, l, and u is calculated to find the distinction coefficient. The results for a random code are given in figure 6.12. For each value of M the results for 0, 1, 3, 7, and 15 interfering users are shown. For each additional interfering user the distinction coefficient is reduced. The reduction of the distinction coefficient in a linear scale is relatively independent of the code length N_f.

Numerical simulation based on the UWB signal: Again, numerical simulations are made for a second derivative Gaussian pulse with a duration $t_n = 200\,\mathrm{ps}$, a frame duration 100 ns, and a chip duration of 1 ns. The outcomes of the simulations are shown in figure 6.13 for TH8 using an AWGN and a CM3 channel. As expected the distinction coefficient increases with

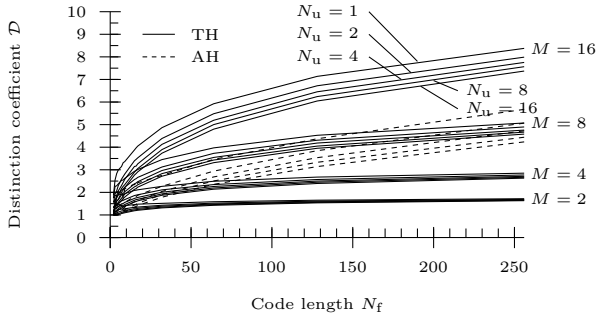

(a) linear representation

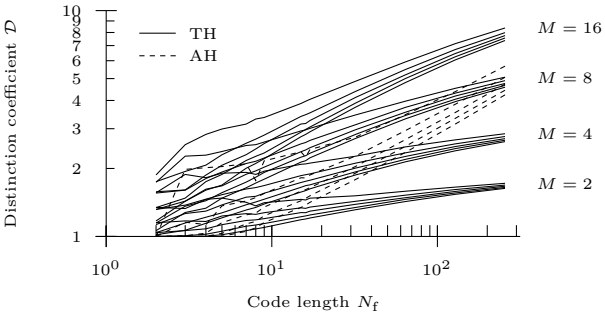

(b) double logarithmic representation

Figure 6.12: Linear (a) and double logarithmic (b) representation of the distinction coefficients obtained with random codes and $N_u \in \{1, 2, 4, 8, 16\}$ transmitters and M-ary code modulation. It is assumed that exactly one transmitter is active at any time.

the code length N_f and decreases with the number of users N_u. For scenario (b), the receiver is not synchronized and the maximum value is calculated using

$$\mathcal{W}_{(b)} = \max_{(b)} \max_{t} \left| \sum_{j=0}^{N_f-1} q^{(u)}(t + (c_j^{(u)} - c_{j \oplus_N \Delta j}^{(0)})t_c + \phi^{(u)}) \right|, \qquad (6.42)$$

where $\max_{(b)}$ denotes the search for the maximum of all configurations belonging to scenario (b), among others testing for all admissible users u.

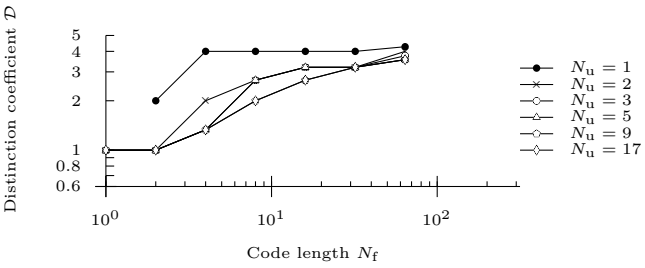

(a) AWGN

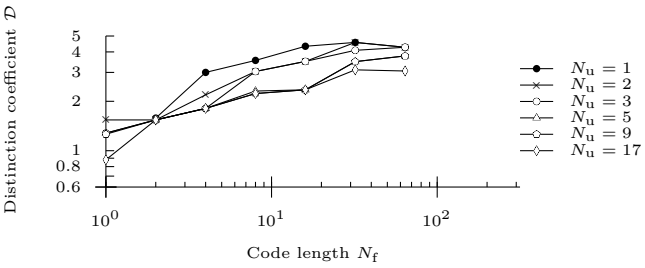

(b) CM3

Figure 6.13: Distinction coefficient for a random code and TH8. A single transmitter out of N_u is active at any time.

6.4.3 Several Active, Frame Synchronized Transmitters

The distinction coefficient is now estimated under the assumption that the signals from N_u transmitters are simultaneously received. The pulses from the transmitters are again assumed to be received with the same power. The received summed signal is for THM

$$w_k(t) = \sum_{u=0}^{N_\mathrm{u}-1} \sum_{j=0}^{N_\mathrm{f}-1} q^{(u)}(t + (c_j^{(0)} - c_{j \oplus_N \Delta j}^{(u)})t_\mathrm{c} + \phi^{(u)}) \tag{6.43}$$

In this section the transmitters are assumed to be chip synchronized. As a worst case scenario it is again assumed that the transmitters are frame synchronized ($\phi^{(u)} = 0$). Because of this assumption the probability that many interfering pulses are received within the acquisition window is high.

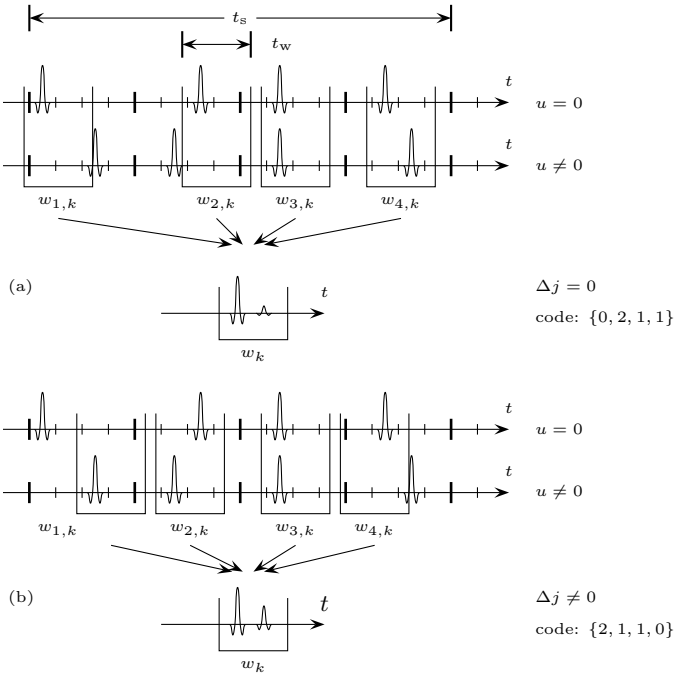

Figure 6.14: Coherent (a) and partially coherent (b) addition of limited duration windows. The spreading code from the user of interest is $\{0, 2, 1, 1\}$. In the illustrated example for scenario (b), the receiver applies the correct code, but shifted by one position $\{2, 1, 1, 0\}$. The distinction coefficient is $\mathcal{D} = 5/4$.

Scenarios: The possible scenarios, illustrated in figure 6.14, are the following.

(a) The receiver is synchronized with the user of interest. This results in a coherent addition of the N_f pulses from the user of interest and in a incoherent addition of the $(N_u - 1)N_f$ interfering pulses.
(b) The receiver is not synchronized with the transmitter of interest, i.e., $\Delta j \neq 0$.

Numerical evaluation based on the codes: Again the distinction coefficient is calculated for random spreading codes and represented in figure 6.15. It is noted that the degradation due to multiuser interference is severe for

frame synchronized transmitters. The assumption of frame synchronized transmitters is pessimistic. A more realistic assumption are asynchronous transmitters. The outcomes for that scenario are presented in the next section.

Numerical simulation based on the UWB signal: This synchronous case is modeled with

$$\mathcal{W}_{(\mathrm{b})} = \max_{(\mathrm{b})} \max_{t} \left| \sum_{u=0}^{N_\mathrm{u}-1} \sum_{j=0}^{N_\mathrm{f}-1} q^{(u)}(t + (c_j^{(u)} - c_{j \oplus_N \Delta j}^{(0)}) t_\mathrm{c} + \phi^{(u)}) \right|, \quad (6.44)$$

where all the phases $\phi^{(u)}$ are equal (and can be considered as 0). The outcomes of numerical simulations using radio frequency signals are shown in figure 6.16. For both the AWGN and the CM3 channel the numerical simulation results are slightly improved compared to the numerical evaluations obtained above.

6.4.4 Several Active, Asynchronous Transmitters

The signals from N_u transmitters are assumed to be received simultaneously. In contrast to the previous sections, all the interfering transmitters are assumed to be asynchronous, modeled by an uniform distribution for the delays $\phi^{(u)} \sim \mathrm{U}[0, t_\mathrm{f}[$. The frame duration is 100 ns.

Numerical simulation based on the UWB signal: The asynchronous case is modeled with

$$\mathcal{W}_{(\mathrm{b})} = \max_{(\mathrm{b})} \max_{t} \left| \sum_{u=0}^{N_\mathrm{u}-1} \sum_{j=0}^{N_\mathrm{f}-1} q^{(u)}(t + (c_j^{(u)} - c_{j \oplus_N \Delta j}^{(0)}) t_\mathrm{c} + \phi^{(u)}) \right|, \quad (6.45)$$

with random phases $\phi^{(u)}$. The outcomes from numerical simulations using radio frequency signals are represented in figure 6.17 for AWGN and CM3. It can be seen that the distinction coefficient is improved as compared to frame synchronized transmitters and that a distinction coefficient of 2 can be obtained for $N_\mathrm{f} = 16$ up to about 10 simultaneously active transmitters.

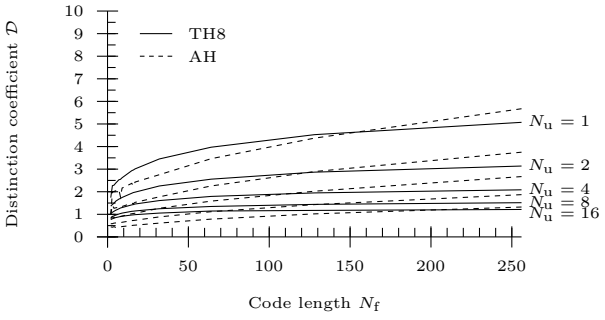

(a) linear representation

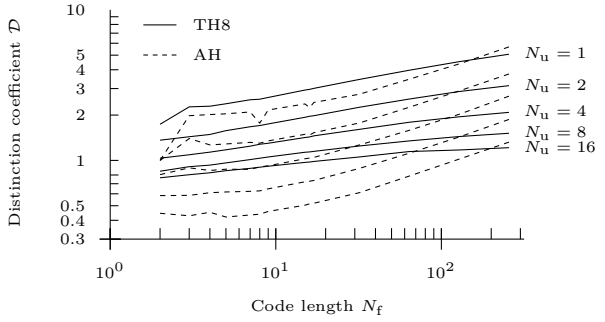

(b) double logarithmic representation

Figure 6.15: Distinction coefficient for $N_u \in \{1, 2, 4, 8, 16\}$ synchronized, simultaneously active transmitters.

6.5 Summary

Two synchronization algorithms are presented. It is shown that the "bin hopping algorithm" results in general in shorter synchronization times than the "intentional frequency difference" algorithm and should thus be preferred. The search order can have an impact on the synchronization time. The "bit reversal search" results in nearly minimal synchronization times, does not require any a priori knowledge, and low complexity implementations are feasible.

A distinction coefficient is introduced to benchmark the probability that the receiver correctly terminates the synchronization. It is shown to be

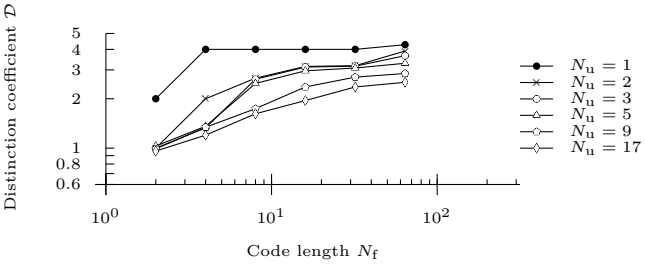

(a) AWGN

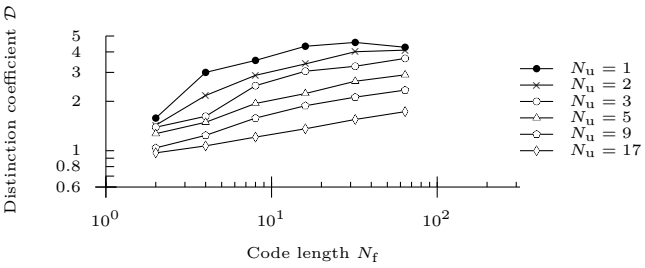

(b) CM3

Figure 6.16: Distinction coefficient for a random code and TH8 in the presence of N_u synchronized, simultaneously active transmitters.

a function of the spreading code length, the modulation, and the number of interfering users. In general, TH8 offers similar or improved distinction coefficients as compared to AH. Without multiuser interference, a distinction coefficient larger than 2 can be obtained even for short spreading codes. In an indoor propagation channel and for a random spreading code with length $N_\mathrm{f} = 16$, the receiver may be capable to synchronize with the transmitter of interest in the presence of up to about 10 simultaneously active, interfering transmitters.

Bibliography

[Ers01] T. Erseghe. *Ultra Wide Band Pulse Communications*. Ph.D. thesis, Università Degli Studi Di Padova, 2001.

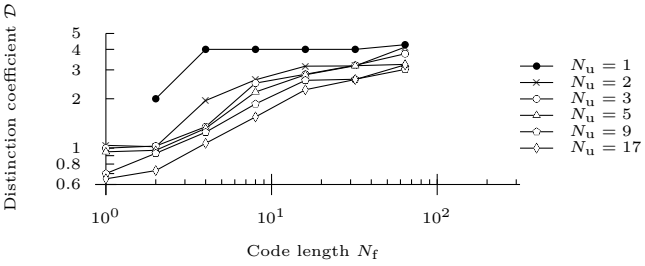

(a) AWGN

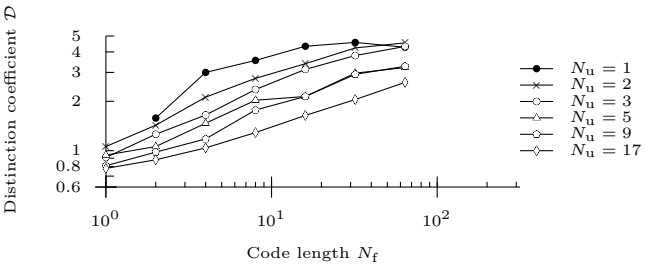

(b) CM3

Figure 6.17: Distinction coefficient for a random code and TH8 in the presence of N_u unsynchronized, simultaneously active transmitters.

[Hom02] E. A. Homier and R. A. Scholtz. "Rapid Acquisition of UWB Signals in the Dense Multipath Channel". *IEEE Conference on Ultra Wideband Systems and Technologies*, pp. 105–109. Baltimore, MD, USA, May 2002.

[Hom03a] E. A. Homier and R. A. Scholtz. "A Generalized Signal Flow Graph Approach for Hybrid Acquisition of Ultra-Wideband Signals". *International Journal on Wireless Information Networks*, 10(4):179–191, Oct. 2003.

[Hom03b] E. A. Homier and R. A. Scholtz. "Hybrid Fixed-Dwell-Time Search Techniques for Rapid Acquisition of Ultra-Wideband Signals". *International Workshop on Ultra Wideband Systems*. Oulu, Finland, Jun. 2003.

[Mer05a] R. Merz, C. Botteron, and P.-A. Farine. “Multiuser Interference during Synchronization Phase in UWB Impulse Radio”. *IEEE International Conference on Ultra-Wideband*, pp. 661–666. Zürich, Switzerland, Sep. 2005.

[Mer05b] R. Merz, C. Botteron, and P.-A. Farine. “Multiuser Interference in TH-UWB”. Presentation at the Workshop on UWB for Sensor Networks. Lausanne, Switzerland, Nov. 2005.

[Suw05] W. Suwansantisuk and M. Z. Win. “Optimal Search Strategies for Ultrawide Bandwidth Signal Acquisition”. *IEEE International Conference on Ultra-Wideband*, pp. 349–354. Zürich, Switzerland, Sep. 2005.

Chapter 7

Conclusion and Outlook

7.1 Conclusion

Impulse radio UWB relies on the generation and transmission of a signal composed of short duration pulses and is promising for positioning and low power communications. UWB has gained a lot of interest for civil applications, in particular during the last decade. It can be used for high data rate communications, for indoor positioning and location systems, or for low power communication devices.

The spectral masks for Europe, the United States of America, and some Asian countries are settled and the power spectrum density can be up to $-41.3\,\mathrm{dBm/MHz}$ in selected frequency bands. The occupied bandwidth is mainly defined by the pulse shape, which is often assumed Gaussian. Among others, amplitude and delay modulations can be applied to UWB. A spreading code unique for each user may be used and repeated for the transmission of each data symbol. The spreading code improves the robustness against multiuser and other interferences. A multipath model combined with an additive white Gaussian noise can be used to provide accurate predictions for indoor propagation channels.

A fast pulse generator is required for the implementation of a transmitter. For typical average output power used for communications, a pulse generator may be implemented using a standard CMOS process resulting in low cost and low power devices.

The receiver architectures can be classified into incoherent and coherent ones. An incoherent receiver may result in a simplification of the synchroniza-

tion and tracking algorithms, but may typically not achieve a bit error rate as low as the one of a coherent receiver. In this thesis, a receiver architecture based on a modified redundant signed digit (RSD) ADC with a near optimal BER in AWGN is presented. It is tailored for low power consumption communications when implemented in a CMOS process. A receiver based on this architecture is currently designed and will be fabricated in a 0.18 µm CMOS process.

For baseband signals with limited bandwidth the sampling at the Nyquist rate is shown to be sufficient. Undersampling is shown to be possible for passband signals with limited bandwidth and also for repetitive signals when the repetition period is known. Finally, a lower bound on the sampling frequency is shown to be related to the rate of innovation and not to the bandwidth of the signal. A typical link budget for UWB communications shows the feasibility of a data communication for ranges up to 100 m for an AWGN channel and about 50 m for a typical indoor channel.

The theoretical BERs for transmissions over AWGN channels, expressed as functions of the SNR per bit, are also valid for UWB. They apply to both, AWGN and multipath channels[1]. Due to imperfections of the receiver, the processed energy per bit may be lower than the received energy per bit, resulting in a loss of the SNR per bit. The losses due to selected imperfections are analyzed. When no channel estimation is performed and the receiver uses the transmitted pulse as a template, a degradation of the SNR by about 9 dB as compared with the SNR obtained with a matched template should be expected for a CM3 channel. Also for a CM3 channel, the received energy due to an acquisition window duration of 10 ns is shown to be lowered by about 3 dB as compared to an infinite acquisition window. The total processing gain is shown to be a function of the bandwidth and the data signaling rate. It can be decomposed into a duty cycle gain and a pulse combining gain. Without timing errors, the pulse combining gain increases linearly with the number of pulses per symbol. It is shown that the pulse combining gain is reduced in the presence of a Gaussian jitter or a frequency difference between the receiver and the transmitter. Accepting a small degradation of the SNR, a non-matched template may be used by the receiver, for example to lower its implementation complexity. Finally the BER in the presence of narrowband and multiuser interference is shown. It is concluded that TH8 results in general in an improved robustness against multiuser interference

[1] However, the same SNR per bit may not correspond to the same communication range.

as compared to AH.

Two synchronization algorithms are presented. It is shown that the "bin hopping algorithm" results in general in shorter synchronization times than the "intentional frequency difference" algorithm and should thus be preferred. The search order can have an impact on the synchronization time. The "bit reversal search" results in nearly minimal synchronization times, does not require any a priori knowledge, and low complexity implementations are feasible.

A distinction coefficient is introduced to benchmark the probability that the receiver correctly terminates the synchronization. It is shown to be a function of the spreading code length, the modulation, and the number of interfering users. In general, TH8 offers similar or improved distinction coefficients as compared to AH. Without multiuser interference, a distinction coefficient larger than 2 can be obtained even for short spreading codes. In an indoor propagation channel and for a random spreading code with length $N_\mathrm{f} = 16$, the receiver may be capable to synchronize with the transmitter of interest in the presence of up to about 10 simultaneously active, interfering transmitters.

7.2 Possible Extensions

In this section, a non-exhaustive list of potential extensions to this research is given.

- All the performed analyses are restricted to baseband signaling, i.e., to signals for which the lower bound of the spectrum is much smaller than the bandwidth. An adaptation of the theoretical and numerical performance estimations to passband signals would be a useful extension.
- The impact of the multiuser interference on synchronized communications is shown based on numerical simulations. The outcomes could also be compared to the results from analytical or semi-analytical approaches.
- For the multiuser interference after and during the synchronization phase, it has been assumed that all the interfering signals are received with equal power. It would be interesting to consider scenarios that include also a near-far effect.

7.3 Future Development for UWB

During the last years, many market forecasts have announced a stunning increase of both the number of available UWB products and the UWB chip market. While a number of products have appeared indeed, the market forecast expectations are by far not yet met. Hence, is UWB doomed to remain a future technology forever?

In my opinion, the optimistic market forecast are partially due to excessive expectations from UWB technology. UWB may have been considered as a technology that solves several challenges simultaneously: high data rate, accurate distance measurement, robustness against interference, simple architecture – all in a single low power integrated circuit. Unfortunately, some of these expectations may be mutually exclusive. Currently, there seem to be a phase of disillusionment. This should be considered as a chance to review the potential for UWB and focus the further product developments to the most promising applications. In the following, some applications are listed, for which I expect UWB to be used in the near future.

- Accurate indoor localization and positioning systems will be based on UWB. To achieve a high accuracy, it is important to resolve the multipaths and to identify the signal received from the most direct propagation path. The capability for high time resolution requires a large bandwidth. First products for indoor localization and positioning using UWB have appeared on the market. Currently, localization systems are relatively costly and no common standard has been adopted yet. I expect more systems to appear and the price to decrease. However, in the near future, the applications may still remain limited to industrial and professional purposes due to prohibitive costs of equipment.
- To transfer the ever increasing amounts of data rapidly, the bandwidth used during the transmission may be increased. An imaginable application is for example a wireless video transmission between a laptop and an overhead projector. However, devices using UWB should not try to replace but to complement the existing wireless networks. I expect UWB, e.g., based on orthogonal frequency-division multiplexing to be widely used in high data rate applications in the near future.
- I expect many of the approaches and technologies developed for today's UWB systems to be integrated in future millimeter-wave communications.
- Finally, UWB will remain the technology of choice for applications like material characterization or through wall radar.

Acknowledgments

I would like to express my sincere gratitude to Prof. Dr. Fausto Pellandini for offering the opportunity to join his group as a PhD student and to Prof. Dr. Pierre-André Farine for ensuring a seamless continuation of my studies. My deepest thanks also go to Dr. Cyril Botteron, who supervised most of my professional activities. Since he started his work at IMT, he always believed in a future for UWB systems. Thanks to his efforts, an UWB team could be formed and financed by several academic and industrial projects. Thanks to the team, it then became possible to complement the performance evaluations with numerical simulations, prototype developments, integrated circuit designs, and laboratory experiments. Furthermore, his continuous support helped me to strengthen the aptitude for exact and accurate work. I also thank Dr. Alexander Heubi for accepting to be part of my thesis jury.

I thank the members of the IMT's UWB team, Cyril Botteron, Frédéric Chastellain, Narumol Kiatwarin, Christian Robert, Paul Saad, Uroschanit Yodprasit, for the countless contributions, discussions, and exchanges and all the members of the laboratory for the friendly atmosphere.

I'm grateful for the support and contributions from CSEM, CTI and ON Semiconductor (grant number 8427.2 NMPP-NM), SNSF (grant numbers 200021-105401 and 200020-113472), and PX Group.

I would like to express my deepest gratitude to my parents for their constant encouragement and their huge confidence.

Finally, my warmest thanks also go to all my friends, especially Guido, Kristina, and Thomas.

Curriculum Vitae

Roman Merz
University of Neuchâtel
Rue A.-L. Breguet 2
2000 Neuchâtel
roman.merz@unine.ch

Place of citizenship: Leimbach AG, Switzerland
Place of residence: Neuchâtel, Switzerland

Education

1990–1995	Kantonsschule Wattwil, 9630 Wattwil Maturität Typus C.
1995–2000	University of Neuchâtel, 2000 Neuchâtel Diploma in physical electronics.

Work Experience

1998 Hewlett Packard (Internship)

- Planning and implementation of the migration from HPUX to Windows based servers.

1998–1999 University of Neuchâtel (Undergraduate Teaching Assistant)

- Teaching assistant for the lectures “introduction to electronics”.

1999 FSRM (Scientific Collaborator)

- Contributions to the compilation of texts and illustrations for the multimedia CD “World of Microsystems”.

2000 MicroChemical SA (Programmer)

- Assembler programming of a microcontroller for automotive applications.

Since 2000 University of Neuchâtel (Scientific Collaborator)

- Implementation of distance measurement units using Xemics radio modules at 433 MHz.
- Development of data acquisition boards with 3 GS/s ADCs and FPGAs for real-time data processing.
- Realization if a first indoor positioning demonstrator based on a pulse generator and an oscilloscope. Implementation of a second demonstrator using the above mentioned data acquisition boards containing an ADC and a FPGA. Developed and implemented novel algorithms for synchronization, calibrations, and data demodulation.
- High level modeling and simulation of UWB receiver architectures.
- Development of an improved method for the estimation of the apex position in a root channel of a tooth based on an extensive measurement campaign.
- Development of low-level routines for a communication system used in the SwissCube satellite.
- Assistant of the IT administrator for a heterogeneous network composed of Solaris, Linux, and Windows based computers

Publications

Patent

- C. Botteron, R. Merz, P.-A. Farine, *Procédé et dispositif récepteur pour communication de données sans fil par des signaux codés temporellement et à ultra-large bande*, EP 1 553 426 A1, 2004.
- C. Botteron, R. Merz, P.-A. Farine, *Method and Receiver Device for Wireless Data Communication Through Temporally Coded Ultra Wideband Signals*, WO 2005/076032 A1, 2005.
- R. Merz, C. Botteron, P.-A. Farine, *Wireless Data Communication Method via Ultra-Wide Band Encoded Signals, And Receiver Device for Implementing the Same*, US 2007/0147476 A1, 2007.
- C. Botteron, R. Merz, P.-A. Farine, *Procédé d'identification d'une donnée codée par modulation PPM, récepteur pour ce procédé*, EP 08102940, 2008.

Journal

- A. Schilling, R. Merz, C. Ossmann, H.P. Herzig, *Surface Profiles of Reflow-Microlenses under the Influence of Surface Tension and Gravity*, Opt. Eng. 39(8), August 2000, 2171-2176.
- R. Merz, C. Botteron, F. Chastellain, P.-A. Farine, *A Programmable Receiver for Communication Systems and its Application to Impulse Radio*, Accepted for publication in Hindawi Research Letters for Communications, 2009.

Conference

- A. Schilling, R. Merz, C. Ossmann, H.P. Herzig, *Optimale Oberflächenprofile von Schmelzlack-Mikrolinsen unter dem Einfluss von Oberflächenspannung und Gravitation*, DGaO Jahrestagung 2000.
- R. Merz, C. Botteron, P.-A. Farine, J. Farserotu, *Asymptotical Analysis of Timing Imperfections in UWB Receivers*, 2nd IEEE International Conference on Circuits and Systems for Communications, Moscow, 2004.
- R. Merz, C. Botteron, P.-A. Farine, *Characterization of Input Filters in UWB Receivers*, Laboratoire Européen Associé en Microtechnique, Atelier d'Arc et Senans, 2004.
- R. Merz, C. Botteron, P.-A. Farine, *Multiuser Interference during Synchronization Phase in UWB Impulse Radio*, IEEE International Conference on Ultra-Wideband, Zürich, 2005.
- R. Merz, *Multiuser Interference in TH-UWB*, Ultra-Wideband for Sensor Networks, Lausanne, 2005.
- P. Saad, C. Botteron, F. Chastellain, R. Merz, C. Robert, U. Yodprasit, P.-A. Farine, *Systèmes de communications à Ultra Large Bande*, Laboratoire Européen Associé en Microtechnique, Atelier d'Arc et Senans, 2007.
- R. Merz, C. Botteron, P.-A. Farine, *Performance of an Impulse Radio Communication System in the Presence of Gaussian Jitter*, IEEE International Conference on Ultra-Wideband, Singapore, 2007.
- P. Saad, C. Botteron, R. Merz, P.-A. Farine, *Performance Comparison of UWB Impulse-Based Multiple Access Schemes in Indoor Multipath Channels*, Workshop on Positioning, Navigation and Communication, Hannover, 2008.
- R. Merz, F. Chastellain, C. Botteron, P.-A. Farine, *An Experimental*

Platform for an Indoor Location and Tracking System, European Navigation Conference, ENC-GNSS, Toulouse, 2008.

- P. Saad, R. Merz, F. Chastellain, C. Robert, U. Yodprasit, C. Botteron, P.-A. Farine, R. Caillet, A. Heubi, N. Senouci, *A Low-Power, Low Data-Rate, Ultra-Wideband Receiver Architecture for Indoor Wireless Systems*, IEEE International Conference on Ultra-Wideband, Hannover, 2008.

Appendix A

Modulations

A general notation for the possible modulations of impulse radio is proposed in this appendix. The well known modulation AH AM, TH AM, AH TM, and TH TM are derived from the general notation as particular cases. The nomenclature used in this appendix does not figure in the nomenclature list.

Pulse Shape Modulation

It is assumed that the data symbol d_k is an element of the set $\mathscr{D}$ and that for each admissible data symbol one sequence $\{d_{j,k}^{(\mathrm{p})}\}$ with length N_f is associated. Each value $d_{j,k}^{(\mathrm{p})}$ is an element of the set $\mathscr{P}$. The association is hence given by a map $f^{(\mathrm{p})}$,

$$f^{(\mathrm{p})} : \mathscr{D} \to \mathscr{P}^{N_\mathrm{f}}, \qquad d_k \mapsto \{d_{j,k}^{(\mathrm{p})}\}. \tag{A.1}$$

The cardinality of the set $\mathscr{P}$ is denoted as $|\mathscr{P}|$ and it is assumed that $|\mathscr{P}|$ pulses shapes are defined and can be addressed by $p_{d_{j,k}^{(\mathrm{p})}}(t)$. The generated UWB signal is then given by

$$s(t) = \sum_{k=0}^{N_\mathrm{s}-1} \sum_{j=0}^{N_\mathrm{f}-1} p_{d_{j,k}^{(\mathrm{p})}}(t - jt_\mathrm{f} - kt_\mathrm{s} + \epsilon_{j,k}). \tag{A.2}$$

where $\epsilon_{j,k}$ can be used to model any timing errors.

Amplitude and Delay Modulation

Two cases are of particular interest. First, if $p_d(t) = \zeta_d p_0(t)$ for all $d \in \mathscr{P}$, the signal is said amplitude modulated. Second, if $p_d(t) = p(t - dt_c)$, it is called delay modulated. Using both AM and TM the generated signal can be written as a function of the amplitude spreading sequence $\{d^{(a)}_{j,k}\}$, the delay spreading sequence $\{d^{(t)}_{j,k}\}$, and a generic pulse shape $p(t)$ as

$$s(t) = \sum_{k=0}^{N_s-1} \sum_{j=0}^{N_f-1} d^{(a)}_{j,k} p(t - jT_f - kT_s - d^{(t)}_{j,k} T_c + \epsilon_{j,k}). \tag{A.3}$$

Writing the sets for the amplitude and the time modulation as $\mathscr{A}$ and $\mathscr{T}$ respectively, the signal is defined by two maps

$$f^{(a)} : \mathscr{D} \to \mathscr{A}^{N_f}, \qquad d_k \mapsto \{d^{(a)}_{j,k}\} \tag{A.4a}$$

$$f^{(t)} : \mathscr{D} \to \mathscr{T}^{N_f}, \qquad d_k \mapsto \{d^{(t)}_{j,k}\} \tag{A.4b}$$

and a pulse shape $p(t)$. It is noted that the cardinalities $|\mathscr{A}|$ and $|\mathscr{T}|$ can be between 1 (no modulation) and the cardinality of the continuum $\mathfrak{c} = 2^{\aleph_0}$. The modulation is said to be binary for cardinality 2 and fluid for cardinality $\mathfrak{c}$ [Gia06]. It is noted that the fluid modulation is identical to a classic analog modulation.

Time-Invariant, Separable Modulations

An important subset of all the imaginable modulations has the following two properties.

1. A code sequence $\{c_j\}$ with length N_f exists and the sequences $\{d^{(a)}_{j,k}\}$ and $\{d^{(t)}_{j,k}\}$ is a time-invariant function of the data symbol d_k and the code sequence $\{c_j\}$.
2. The demodulation of the data d_k and the code sequence $\{c_j\}$ are independent and can be separated.

In the following, the modulations having the required properties are listed. For the notation, the code functions $f^{(a)}_c(c_j)$ and $f^{(t)}_c(c_j)$ as well as the data functions $f^{(a)}_d(d_k)$ and $f^{(t)}_d(d_k)$ are introduced. Selected code and data functions are considered in the next section. First, some potentially[1] separable

[1] The resulting modulations are separable for appropriate selections of the code and data functions.

modulations are listed. The following four separable modulations have been considered throughout the thesis.

- AH TM: $d_{j,k}^{(\mathrm{t})} = f_d^{(\mathrm{t})}(d_k), \quad d_{j,k}^{(\mathrm{a})} = f_c^{(\mathrm{a})}(c_j)$.
- TH AM: $d_{j,k}^{(\mathrm{t})} = f_c^{(\mathrm{t})}(c_j), \quad d_{j,k}^{(\mathrm{a})} = f_d^{(\mathrm{a})}(d_k)$.
- TH TM: $d_{j,k}^{(\mathrm{t})} = f_d^{(\mathrm{t})}(d_k) + f_c^{(\mathrm{t})}(c_j), \quad d_{j,k}^{(\mathrm{a})} = \text{const}$.
- AH AM: $d_{j,k}^{(\mathrm{t})} = \text{const.}, \quad d_{j,k}^{(\mathrm{a})} = f_c^{(\mathrm{a})}(c_j) f_d^{(\mathrm{a})}(d_k)$.

Other separable modulations exists but they do not have practical significance because they would result in increased complexity of the receiver.

- $d_{j,k}^{(\mathrm{t})} = f_d^{(\mathrm{t})}(d_k) + f_c^{(\mathrm{t})}(c_j), \quad d_{j,k}^{(\mathrm{a})} = f_c^{(\mathrm{a})}(c_j)$.
- $d_{j,k}^{(\mathrm{t})} = f_d^{(\mathrm{t})}(d_k) + f_c^{(\mathrm{t})}(c_j), \quad d_{j,k}^{(\mathrm{a})} = f_d^{(\mathrm{a})}(d_k)$.
- $d_{j,k}^{(\mathrm{t})} = f_d^{(\mathrm{t})}(d_k) + f_c^{(\mathrm{t})}(c_j), \quad d_{j,k}^{(\mathrm{a})} = f_c^{(\mathrm{a})}(c_j) f_d^{(\mathrm{a})}(d_k)$.
- $d_{j,k}^{(\mathrm{t})} = f_d^{(\mathrm{t})}(d_k), \quad d_{j,k}^{(\mathrm{a})} = f_c^{(\mathrm{a})}(c_j) f_d^{(\mathrm{a})}(d_k)$.
- $d_{j,k}^{(\mathrm{t})} = f_c^{(\mathrm{t})}(c_j), \quad d_{j,k}^{(\mathrm{a})} = f_c^{(\mathrm{a})}(c_j) f_d^{(\mathrm{a})}(d_k)$.

The subset of the separable modulations allows a receiver to use its knowledge of $\{c_j\}$ independently of the transmitted data d_k. Therefore in general only separable modulations are of practical interest.

Selected Code and Data Functions

The selection of the code and data functions is one factor that define the performance of the communication system. The functions need to be adjusted accordingly to the receiver architecture. For example, for an energy detection receiver, an orthogonal amplitude modulation (e.g., on-off-keying) is more appropriate than an antipodal amplitude modulation.

Amplitude Modulation

M-ary amplitude modulations are sensitive to variations of the received signal energy, and hence to effects like fading. The discussion is therefore restricted to binary amplitude modulation. It can be orthogonal ($\mathscr{A} = \{0, 1\}$) or antipodal ($\mathscr{A} = \{-1, 1\}$). Sometimes the antipodal amplitude modulation is called binary phase shift keying (BPSK) in analogy to narrowband systems, where the inversion of the amplitude corresponds to a phase shift of π of the carrier. The antipodal amplitude modulation cannot be applied with energy detection receivers but offers a good performance for coherent receivers. For binary values $d_k \in \{0, 1\}$ and $c_j \in \{0, 1\}$, an orthogonal amplitude modulation can be obtained with

- AH: $d_{j,k}^{(\mathrm{a})} = c_j$,
- AM: $d_{j,k}^{(\mathrm{a})} = d_k$, and
- AH AM: $d_{j,k}^{(\mathrm{a})} = d_k c_j$.

An antipodal amplitude modulation can for example be obtained with

- AH: $d_{j,k}^{(\mathrm{a})} = 2c_j - 1$,
- AM: $d_{j,k}^{(\mathrm{a})} = 2d_k - 1$, and
- AH AM: $d_{j,k}^{(\mathrm{a})} = (2d_k - 1)(2c_j - 1)$.

Delay Modulation

For the delay modulation, the instant when the pulse is emitted is delayed with respect to the average pulse repetition interval. For the delay modulation, the most simple data and code functions are given by

- TM: $d_{j,k}^{(\mathrm{t})} = d_k$,
- TH: $d_{j,k}^{(\mathrm{t})} = c_j$, and
- TH TM: $d_{j,k}^{(\mathrm{t})} = d_k + c_j$.

Recommended Modulations

It is recommended to apply an antipodal amplitude modulation if the value is a binary and delay modulation if the symbol is M-ary. This general rule is valid for the data value d_k and the code value c_j. Considering the improved performance of antipodal AM compared to TM, it is recommended to transmit binary data. Seen the improved robustness against multiuser interference it is proposed to use TH8 for the code modulation. The code length N_f may typically be between 1 and 32 depending on the application, the required robustness of the communication link against interferences, the maximum synchronization time, and the required data rate.

Bibliography

[Gia06] G. Giancola, D. Domenicali, and M.-G. Di Benedetto. "Application of Fluid Time Hopping Coding to Multiple Access in Ultra Wide Band Sensor Networks". *IEEE Symposium on Circuits and Systems*. Island of Kos, Greece, May 2006.